INSIGHT INTO NUCLEATION OF MICROTUBULES TO REALIZE NOVEL DRUG TARGETS

A THESIS SUBMITTED IN FULFILLMENT OF THE REQUIREMENTS OF
THE DEGREE OF DOCTOR OF PHILOSOPHY

IN

BIOINFORMATICS

BY

CHARU SURI

Enrolment No. 116503

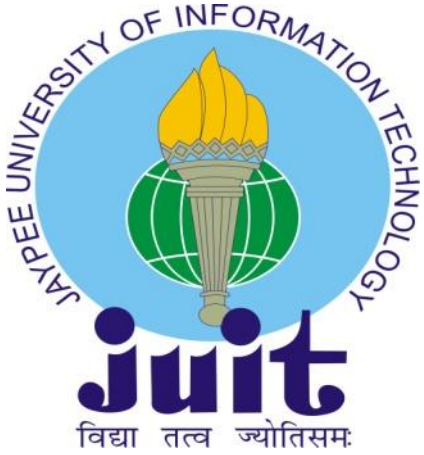

UNDER THE GUIDANCE OF
DR. PRADEEP KUMAR NAIK

DEPARTMENT OF BIOTECHNOLOGY & BIOINFORMATICS
JAYPEE UNIVERSITY OF INFORMATION TECHNOLOGY
WAKNAGHAT, SOLAN-173234, HP, INDIA

OCTOBER 2014

Dedicated to my loving parents

DECLARATION

I certify that

a. The work contained in this thesis is original and has been done by me under the guidance of my supervisor.
b. The work has not been submitted to any other organisation for any degree or diploma.
c. Whenever, I have used materials (data, analysis, figures or text), I have given due credit by citing them in the text of the thesis.

Charu Suri **Date:**

(Enrollment No. 116503)

Department of Biotechnology and Bioinformatics

Jaypee University of Information Technology, Waknaghat, India

Email: charu.juit@gmail.com

CERTIFICATE

This is to certify that the thesis entitled, **"Insight into nucleation of microtubules to realize novel drug targets"** which is being submitted by Charu Suri for the award of degree of Doctor of Philosophy in Bioinformatics by the Jaypee University of Information Technology at Waknaghat, is a record of the candidate's own work, carried out by her under my supervision. This work has not been submitted partially or wholly to any other University or Institute for the award of this or any other degree or diploma.

Dr. Pradeep Kumar Naik
Associate Professor
Department of Biotechnology and Bioinformatics
Jaypee University of Information Technology
Waknaghat, Solan, H.P. India- 173234

Date: 20.10.2014

ACKNOWLEDGEMENTS

If we supply the willingness, GOD supplies the power

I deem it my privilege and honour to place and record my gratitude and indebtedness to the following without whose guidance, support and concern I would not have been able to complete my Ph. D thesis.

I feel privileged to express my deep sense of reverence and gratitude to my revered mentor, ***Dr. Pradeep Kumar Naik****, for his unconditional support, immaculate guidance, constructive criticism, constant encouragement and providing requisite facilities to carry on my research which otherwise would have remained incomplete. I also appreciate his untiring efforts during the entire tenure of my research work and patience during writing of this thesis. I thank him from bottom of my heart.*

I emphatically express my loyal and venerable thanks to ***Brig. (Retd.) Balbir Singh*** *(Director, JUIT),* ***Dr. S.K. Kak*** *(Vice Chancellor, JUIT) and* ***Prof. T. S. Lamba*** *(Dean, JUIT) for providing opportunity to pursue my research work at Jaypee University of Information Technology, Waknaghat, India. I am very much grateful to them for their valuable guidance.*

I can never thank enough ***Dr. Y. Medury*** *(former COO, Jaypee Education System), for showing me this path and encouraging me to take up this journey.*

I gratefully acknowledge the help rendered by ***Prof. R. S. Chauhan*** *(HOD, Dept. of BT & BI) for his encouragement, timely help and cooperation throughout my research work. His criticism and his discerning advice always encouraged me to stretch my boundaries.*

I feel indebted to Dr Harish C. Joshi (Emory School of Medicine) for his valuable advice, unconditional support and providing me the research scientific advises as and when required. I also thank Dr B. Jayram and staff especially Mr. Ashutosh and Mr Shashank, at IIT Delhi for allowing me to use their super-computing facility for running molecular dynamic simulations. I would extend thanks to Dr Subba Rao for his support throughout. Without their support, this work would have taken many more years to complete.

This work would have remained an infant had it not received its necessary 'diet' in the form of comments, suggestions etc. by ***Dr. Harvinder Singh, Dr. Hemant Sood*** *and* ***Dr. Dipankar Sengupta****.*

I wish to convey my sincere thanks to all the faculty members of Department of Biotechnology and Bioinformatics, for their help and guidance at the various stages of this study.

*I am also thankful to all the members of technical and non-technical staff of the department, especially **Mrs. Somlata Sharma** for her assistance and valuable contributions.*

*It was indeed my good luck to have seniors like **Bharti Negi, Varun Jaiswal and Krishna Sir** who extended their support in all possible ways. I thank them for always being there to guide and encourage me whenever the journey got tough.*

*I am fortunate to have friends who have always stood beside me. I extend my heartfelt thanks to my colleagues and friends **Seneha, Tamanna, Manika, Tarun and Kritika** for their sustained support and ever needed cooperation. This journey would have been so memorable if my roommates – **Parul, Arunima, Anandita, Abhilasha and Versha** were not a part of it. I also thanks to **Jyotsana, Laxmi, Ankit, Aditya, Akansha, Anuj, Shruti, Ambuj, Jassi, Ashish, Malika** for sincere friendship.*

*This work would have never taken shape sans the moral support and encouragement rendered by my **family** and my husband **Ankur**. I can never express enough love to my sweet niece **"Risha"** whose innocence refreshed me during my difficult times. I can never thank enough my brothers-**Harsh** and **Ashish**, and bhabhi-**Dora** for supporting my decision to take up research and always being there. The successful culmination of this thesis could not have been possible without the blessing of **my loving parents**. Without their help I would have been greatly incapacitated.*

All may not be mentioned, but no one is forgotten.

Charu Suri

TABLE OF CONTENTS

LIST OF FIGURES

LIST OF TABLES

ABSTRACT OF THE DISSERTATION

Microtubules are highly dynamic cytosketal polymers that are built up of heterodimers of α- and β-tubulin proteins that self assembles in a head to tail fashion to make long protofilaments. Generally, thirteen of these protofilaments then assemble laterally to form a sheet which then folds into a hollow cylinder to form microtubule. The linear arrangement of α/β tubulin also gives a polarity to resulting microtubules that display dynamic instability in that they continually undergo lengthening and shortening at both ends—more rapidly at one end, named the plus end, than the other slower minus end. Microtubules are key component of mitotic spindle apparatus that is necessary for the alignment and subsequent segregation of duplicated chromosomes into daughter cells during cell division. They play a vital role in many other cellular functions including cell polarity, cell motility, transport of intracellular organelles and maintenance of the overall cellular morphology. Such a myriad of roles calls for a very rapid reorganization of microtubules.

γ-tubulin is essential for the nucleation and organization of mitotic microtubules in dividing cells. It is localized at the microtubule organizing centre and experimentally observed to interact with the minus end of microtubules. The most well accepted hypothesis for the initiation of microtubule polymerization is that α/β-tubulin dimers add onto a γ-tubulin ring complex (γTuRC), in which adjacent γ-tubulin subunits bind to the underlying non-tubulin components of the γTuRC. This template thus determines the resulting microtubule lattice. In this study we have used molecular modelling and molecular dynamics simulations, combined with computational MM-PBSA/MM-GBSA methods, to determine the extent of the lateral atomic interaction between two adjacent γ-tubulins. Towards this end we simulated γ-γ homodimer complex for 10 ns and calculated the ensemble average of binding free energy of -107.76 kcal/mol by the MM-PBSA method and -87.12 kcal/mol by the MM-GBSA method. These highly favourable binding free energy values revealed robust lateral interactions between γ-tubulin subunits in addition to their end-interactions longitudinally with other proteins of γTuRC and γ-tubulin of the tubulin dimer. Furthermore, we identified the hot spot amino acids that play key role in the γ-γ interactions by computational alanine scanning mutagenesis and free energy decomposition per residue. Experimental mutagenesis validated these hot spot amino acids. The results from the experimental findings were consistent with the theoretical calculations and offer important insights on the mechanism of interaction between the γ-tubulin homodimers.

γ-tubulin plays crucial role in the nucleation and organization of microtubules during cell division and recent studies have also indicated their role in the regulation of microtubule dynamics at the plus end of the microtubules. Moreover, γ-tubulin has been found to be over-expressed in many cancer types like carcinomas of the breast and glioblastoma multiforme. These studies have led to immense interest in the identification of chemical leads that might interact with γ-tubulin and disrupt its function in order to explore γ-tubulin as potential chemotherapeutic target. Recently a colchicine-interacting cavity was identified on γ-tubulin that might also interact with other similar compounds. In the same direction we found a class of compounds, noscapinoids (noscapine and its derivatives) that fits well in a cavity close to the interface of γ-tubulin dimer. Molecular interaction of noscapine and two of its derivatives, amino-noscapine and bromo-noscapine was investigated by molecular docking, molecular dynamics simulation and binding free energy calculation. All noscapinoids displayed stable interaction throughout simulation of 10 ns. The predictive binding free energy (ΔG_{bind}) indicates that noscapinoids bind strongly with γ-tubulin dimer. However, bromo-noscapine showed the best binding affinity (ΔG_{bind} -37.6 kcal/mol) followed by noscapine (ΔG_{bind} -29.85 kcal/mol) and amino noscapine (ΔG_{bind} -23.99 kcal/mol) using the MM-PBSA method. Similarly using the MM-GBSA method also, bromo-noscapine showed highest binding affinity with ΔG_{bind} value of -43.64 kcal/mol followed by amino-noscapine with ΔG_{bind} value of -37.56 kcal/mol and noscapine with ΔG_{bind} value of -34.57 kcal/mol. The results thus generate compelling evidence that these noscapinoids indicate a great potential for preclinical and clinical evaluation.

The initiation of microtubule assembly within cells is guided by a cone shaped multi-protein complex containing γ-tubulin and atleast five other γ-tubulin-complex proteins (GCPs) i.e., GCP2, GCP3, GCP4, GCP5, and GCP6. The rim of complex is a ring of γ-tubulin molecules that interacts, via one of its longitudinal interfaces, with GCP2, GCP3 or GCP4 of γ-tubulin ring complex (γTuRC) and, via other interface, with αβ-tubulin dimer recruited for the microtubule lattice formation. These interactions however, are not well understood. Therefore, in this study we used molecular modelling and MD simulations, combined with MM-PBSA and MM-GBSA computational methods to understand atomic interactions between γ-tubulin and GCP4. We simulated two conformations of γ-tubulin-GCP4 complex for 10 ns and calculated the binding free energy of -172.7 kcal/mol and -188.5 kcal/mol using MM-PBSA and MM-GBSA methods respectively, for dimer1 and -124.6 kcal/mol and -93.58

kcal/mol by MM-PBSA and MM-GBSA methods for dimer2. These values points to very robust interactions between GCP4 and γ-tubulin. We also identified amino acids crucial for the interaction of γ-tubulin with GCP4, called hot spots, by computational alanine-scanning mutagenesis.

In recent years, there has been immense interest in the identification of chemical leads that might interact with the interface of γ-tubulin-GCP4 complex and disrupt its function. Therefore, in the endeavour to identify chemical leads we found a class of compound, noscapinoids that fits well in a cavity close to γ-tubulin-GCP4 interface. All noscapinoids displayed stable interaction throughout the simulation. However, most robust interaction was observed for bromo-noscapine followed by noscapine and amino-noscapine with binding free energy of -46.73 kcal/mol, -41.69 kcal/mol and -35.40 kcal/mol respectively, using the MM-GBSA method and -31.86 kcal/mol, -23.60 kcal/mol and -20.50 kcal/mol respectively, using the MM-PBSA method in one conformation of γ-tubulin-GCP4 complex. Similarly for the other conformation also the most robust interaction with the γ-tubulin-GCP4 dimer was observed for bromo-noscapine with the binding affinity of -40 kcal/mol followed by noscapine with -32.82 kcal/mol and -21.84 kcal/mol for amino-noscapine, using MM-GBSA method. This offers a novel chemical scaffold that binds at the γ-tubulin-GCP4 interface and disrupts its function.

As already discussed, γ-tubulin is indispensible for the microtubule spindle function in mitosis and its absence causes cell death. According to the template model γ-tubulin directly interacts, via one of its longitudinal interfaces, with the GCP2, GCP3 or GCP4 and, via its other interface, with the αβ-tubulin dimer. We therefore, elucidated the mode and mechanism of interaction of γ-tubulin with αβ-tubulin. The binding interface of γ-tubulin with αβ-tubulin was identified using molecular modeling calculations. Residues playing crucial role in the interaction were also identified as hot spot amino acids. To further reinforce the hot spots, computational alanine scanning mutagenesis was performed. The results were further verified using the experimental alanine scanning mutagenesis. For three of the mutants- M1, M2 and M4 the binding affinity was lesser as compared to the wild type as observed after MM-GBSA analysis. Computationally identified interface was well verified by the experimental results.

Collectively, the study reported here the molecular insight of the association between various proteins involve in the initiation of microtubule formation from MTOC. We have also identified the key interfaces onto which chemical lead molecules could be develop to deform

the microtubule nucleation pertaining to induction of apoptosis cell death to cancer cells at concentration much lower than currently using dose of regimen. Taken together, my study provides a proof-of-concept for the identification of novel chemical leads, noscapinoids as the potential candidate for inhibiting the microtubule nucleation and demands further preclinical and clinical evaluation.

CHAPTER 1

INTRODUCTION

1.1 Microtubule structure, function and dynamic

Microtubules are filamentous polymers that constitute an essential part of the cytoskeleton in all eukaryotes. Most prominently, microtubules are visible during cell division, as the main structural elements of the spindle apparatus. They are critically important for the spatial and temporal organization of eukaryotic cells, playing a central part in functions as diverse as intracellular transport, organelle positioning, motility, signalling, development and maintenance of cell shape and cell division. The ability to play this range of parts requires microtubules to be arranged in complex arrays that are capable of rapid reorganization. The microtubule cytoskeleton is essential for proper cell cycle progression. These functions are highly conserved from humans to yeast. The cell cycle can be divided into two basic components, interphase and mitosis. The cell spends the majority of its time in interphase. Interphase can be subdivided into three phases: gap 1 (G1-phase) when the cell is metabolically active and continuously growing, synthetic (S-phase) when DNA replication takes place and gap 2 (G2-phase) when the cell continues to grow and prepares to enter into mitosis. Mitosis is the most dramatic stage since it is the shortest phase in the cell cycle, and it is during this phase that the duplicated chromosomes are segregated into two genetically equivalent daughter cells. Microtubule function is critical during both interphase and mitosis. During interphase, microtubules function to maintain cell polarity and to organize the cytoplasmic milieu [1-6]. At the transition between G2 of interphase and mitosis, cytoplasmic microtubules undergo a dramatic reorganization [7-9]. Interphase microtubules disassemble and reassemble to form a short, bipolar mitotic spindle [6, 10]. During mitosis, the mitotic spindle functions to segregate the duplicated chromosomes before the cell undergoes cytokinesis, resulting in two genetically equivalent cells at the end of mitosis [6, 10].

Microtubules are intrinsically dynamic polymers and they grow and shorten by the reversible non-covalent addition and loss of tubulin dimer at their ends [7, 11-13]. GTP binds to free tubulin in an exchangeable fashion and becomes irreversibly hydrolyzed to guanosine diphosphate (GDP) during the addition of tubulin dimer to the ends of microtubules [14, 15]. This gives rise to two unusual dynamic behaviors. Dynamic instability describes the abrupt and stochastic alternation of microtubules between periods of growth and shortening and treadmilling describes the net growth of microtubules at one end and the net shortening at the other end [16-18]. Several parameters have been used to characterize the dynamics of microtubule assembly [19, 20]. These include growth rate, shortening rate, frequency of

transitions from growth to shortening (catastrophe frequency), frequency of transition from shortening to growth or an attenuated (pause) state (rescue frequency) and the duration of the attenuated state when neither microtubule growth nor shortening can be detected (Figure 1.1). Overall microtubule dynamics due to dynamic instability is described as dynamicity, which measures the sum of visually detectable tubulin dimer exchange per unit time at the ends of microtubules [20]. The dynamic property is crucial for microtubules to carry out many of their cellular functions such as reorientation of the microtubule network when cells undergo migration or morphological changes and the dramatic microtubule rearrangement at the onset of mitosis. Mitotic microtubules are 10-100 times more dynamic than interphase microtubules; they exchange their tubulin with the soluble tubulin pool with half-times of ~15 s during mitosis as compared with 3 min to several hours in interphase [7, 12, 13]. The rapid microtubule dynamics in mitosis is thought to be critical for both the morphogenesis and activities of the mitotic spindle that directs chromosome congression to the equatorial plane (also called the metaphase plate) and their final segregation into the daughter cells.

Structurally microtubules are hollow tubes of about 250 Å in diameter that are assembled from α-tubulin–β-tubulin (αβ-tubulin) heterodimers in a GTP-dependent manner (Figure 1.2). The tubulin subunits make two types of filament contacts: longitudinal contacts run the length of the microtubule forming protofilaments, and lateral contacts between protofilaments (generally α-tubulin to α-tubulin and β-tubulin to β-tubulin) form the circumference of the microtubule (Figure 1.3a) [21, 22]. Microtubule geometry is not fixed, however; the more-flexible lateral contacts can accommodate between 11 and 16 protofilaments [23], yielding microtubules of different diameter when assembled *in vitro* from purified tubulin [24].

In vivo, though, almost all microtubules have 13 protofilaments [25-27], suggesting that one level of cellular control involves defining unique microtubule geometry. The 13-fold symmetry is probably preferred because it is the only geometry in which protofilaments run straight along the microtubule length, as opposed to twisting around the microtubule, which allows processively tracking motor proteins to always remain on the same face of the structure. An unusual feature of 13-protofilament microtubules is that, as a consequence of their helical symmetry, a ‘seam’ is formed from lateral α-tubulin–β-tubulin interactions [28, 29], which are generally presumed to be weaker than α-tubulin–α-tubulin or β-tubulin–β-

tubulin lateral contacts. The mechanism by which cells ensure 13-protofilament geometry has long been a mystery.

(A)

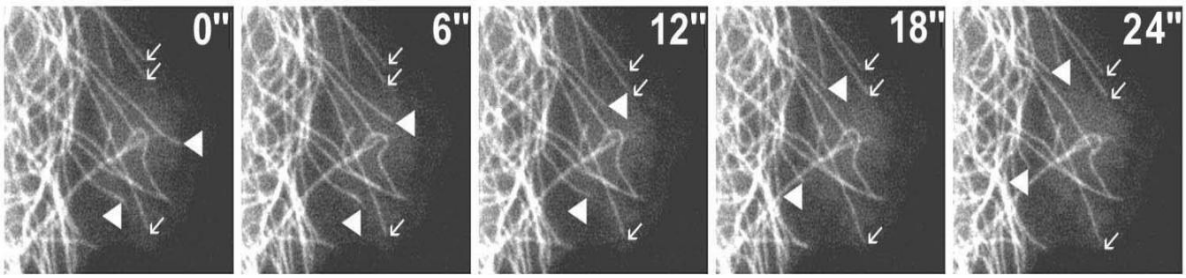

(B)

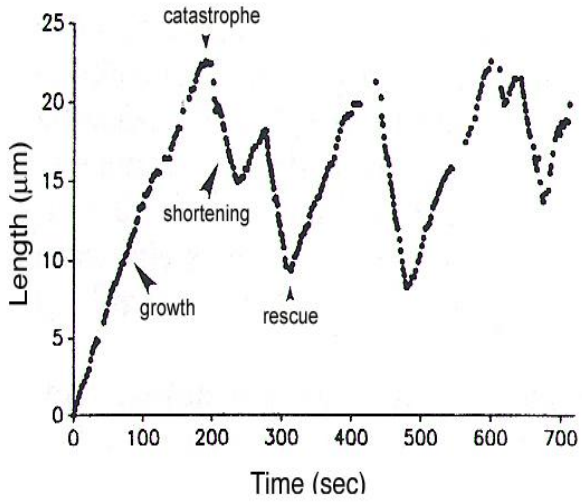

(C)

Dynamic parameters	74 MTs (n=20)
Growth	
Rate (mm/min)	9.15 ± 2.72
Distance (mm)	1.88 ± 0.44
Duration (sec)	14.33 ± 1.22
Shrink	
Rate (mm/min)	12.04 ± 3.63
Distance (mm)	1.99 ± 0.56
Duration (sec)	13.11 ± 1.45
Average pause duration	8.16 ± 2.42
Percentage time per phase	
Growth/ Shrink/ Pause	41.8/36.3/21.8
Rescue frequency (sec-1)	0.077 ± 0.015
Catastrophe frequency (sec-1)	0.086 ± 0.023
Dynamicity (mm/min)	6.61 ± 2.36

Figure 1.1: A gallery of microtubule dynamics and the measured dynamic parameters. (A) A gallery of video frames, 6 seconds apart, showing the plus ends of several microtubules. (B) One representative microtubule plus end behavior is shown. As time goes in seconds the microtubule plus end is growing and growing and all of a sudden the microtubule can revert into a phase of shortening and the shortening can be rescued by another growth phase. So it is continuously growing and shortening as you can see hardly any pausing between both the phases. (C) The measured dynamic parameters of microtubules (from Ye et al., 1998).

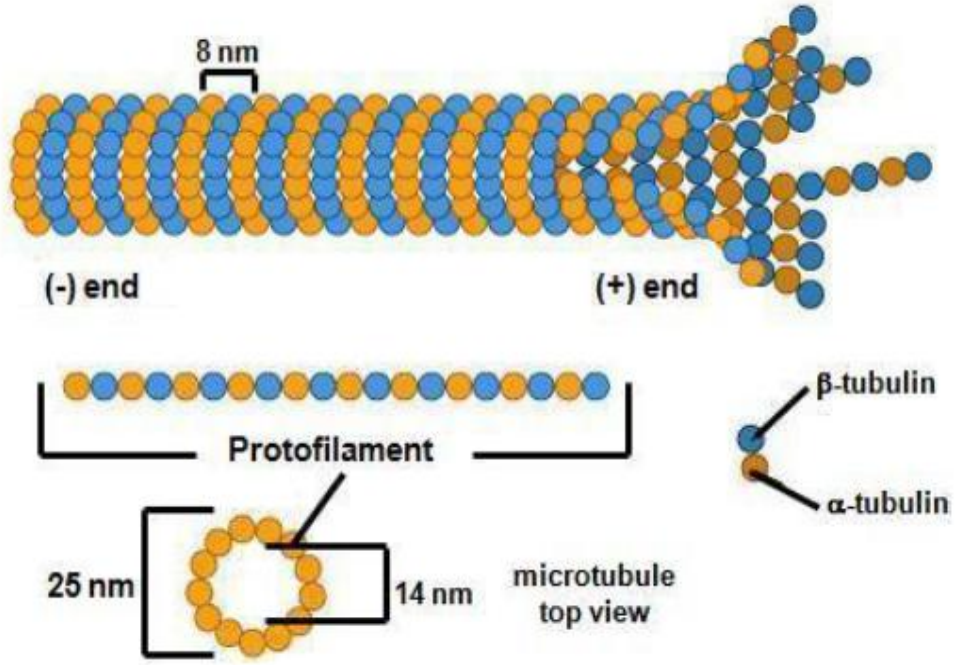

Figure 1.2: Schematic representation of the structure of microtubule. They are hollow tube like structures formed from oligomeric structures known as protofilaments. The protofilaments contain repeating units of α- and β-tubulin heterodimers that are assembled exclusively onto the plus (+) end of the microtubule (from Moore, 2008. Manual of Cellular and Molecular Functions).

Another key difference between microtubule assembly *in vivo* and *in vitro* is with regard to how new microtubules are initiated. *In vitro*, microtubule growth must proceed through small early assembly intermediates, for which disassembly is energetically favoured over assembly, resulting in slow initial growth [30]. After a sufficiently large oligomer has been achieved, microtubule growth becomes energetically favourable and the addition of tubulin heterodimers proceeds rapidly (Figure 1.3b). Significantly, rather than relying on the spontaneous initiation of new microtubules, cells have evolved specialized nucleation sites *in vivo* that bypass the early, slower growth phase. These nucleation sites are largely found at microtubule-organizing centres (MTOCs).

1.2 Microtubule-organizing center (MTOC)

Proper orientation and organization of microtubules are essential for cell structure and cellular functions. For example, development and maintenance of polarized cell structure depends upon microtubule distribution and polarity; correct distribution of cellular organelles for interphase functions requires the correct orientation of microtubules and accurate cell division requires the precise organization of microtubules in the mitotic spindle. Microtubules are organized into diverse structural arrays, each with distinct functions. Therefore, one

relevant question is: how does the cell ensure that microtubules are properly distributed and oriented? General principles have emerged which partially answer this question. Microtubules are dynamic and intrinsically polar filaments and in most cells, microtubule arrays are organized by a specialized organelle called the microtubule-organizing center, MTOC [31-33]. The MTOC is located at the minus end of microtubules and must play the major role in determining the orientation of cellular microtubules (Figure 1.4). The organization of microtubules allows for the movement of cellular organelles, powered by orientation-specific motor molecules, to move into or out of specific cytoplasmic locations. Therefore, to facilitate our understanding of microtubule function, it is important to establish the molecular identity of proteins found in the MTOC that initiate microtubule polymerization *in vivo* and that link microtubules to microtubule-organizing centers.

The MTOC, centrosome in mammals and spindle pole body (SPB) in yeast, is crucial for the precise organization of both interphase and spindle microtubules [34-37]. One known component of the MTOC is a highly conserved and essential protein, (Figure 1.5). γ-tubulin was originally discovered in a suppressor screen of a γ-tubulin mutant in the filamentous fungus, *Aspergillus nidulans* [38]. γ-tubulin localizes to where the microtubule minus-ends lie *in vivo* and it has been shown *in vitro* that γ-tubulin binds stoichometrically and specifically to the microtubule minus-ends [34, 39].

Furthermore, nucleation of microtubule assembly is thought to be mediated by γ-tubulin containing protein complexes at the MTOC [40-43]. γ-tubulin itself is thought to be crucial for the nucleation of the spindle microtubules [44-50]. The most striking of these complexes is a large lock washer-shaped spiral called the γ-tubulin ring complex (γ-TuRC) [49]. This complex contains 12–14 molecules of γ-tubulin and at least 6 other proteins of unknown stochiometry. Purified γ-TuRC complexes can stimulate microtubule nucleation and cap the minus-ends of microtubules *in vitro* [49, 51, 52]. Electron microscopic studies have shown that these complexes can be detected in the centrosome [53, 54]. γ-tubulin containing complexes of similar large size are being found in many species including in the fission yeast *S. pombe* [43]. Members of the *S. pombe* γ-tubulin complex (γ-TuC) include three γ-tubulin binding proteins: Alp4, Alp6, and Alp16 (Figure 1.5) [43, 55].

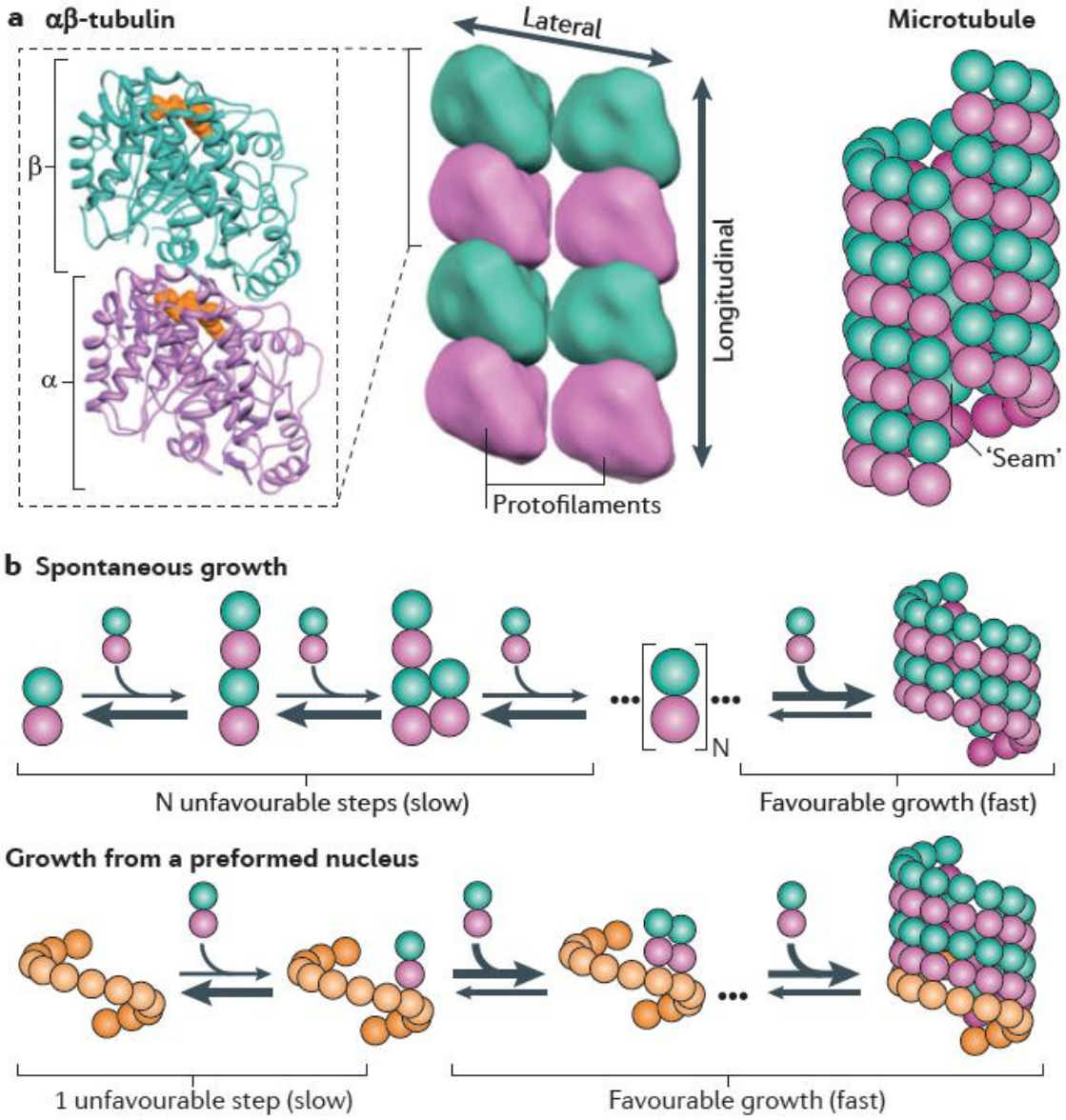

Figure 1.3**:** (a) The α-tubulin–β-tubulin (αβ-tubulin) heterodimer is the fundamental repeating subunit of microtubules. When bound to GTP (shown in orange in the left panel), heterodimers come together through two types of contacts (indicated by double-headed arrows): GTP-mediated longitudinal contacts between α-tubulin and β-tubulin that form protofilaments, and lateral α-tubulin–α-tubulin and β-tubulin–β-tubulin contacts that form between protofilaments. The addition of tubulin subunits to this lattice yields the hollow microtubule. In 13-protofilament microtubules, a 'seam' is formed as a result of lateral α-tubulin–β-tubulin interactions.(b)Spontaneous microtubule growth in vitro occurs in two stages: a relatively slow phase through unstable early assembly intermediates, and a rapid elongation phase. In early steps, the assembly energetics favour disassembly over assembly but, after a sufficiently large oligomer is formed by a variable number of steps (denoted here by N), assembly is energetically favoured and elongation proceeds rapidly. Whether disassembly or assembly is favoured by the assembly energetics is indicated by a bold arrow. In vivo, preformed nuclei allow microtubule growth to bypass the slow phase, providing spatial and temporal control over new microtubule growth.

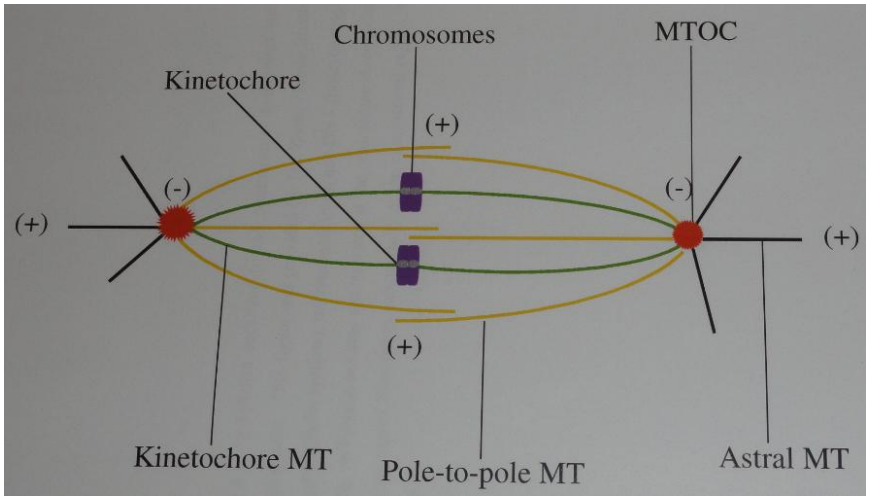

Figure 1.4: The mitotic apparatus in a metaphase mammalian cell. The mitotic apparatus is made up of three types of microtubules which all emanate from the microtubule-organizing center (MTOC). The kinetochore microtubules (green) extend from the MTOC (red) into the center of the cell where they attach to the sister chromatids (blue) at the kinetochores (grey). The pole-to-pole microtubules (yellow) overlap at the center of the cell and generate force by moving against each other with the aid of microtubule motors. Finally, the astral microtubules (black) extend toward the cell cortex where they serve to pull the MTOCs, thus contributing to the separation of sister chromatids. The microtubules are arranged with their minus end at the MTOC and plus ends distal to the MTOC.

Despite the variation in MTOC morphology, all MTOCs rely on γ-tubulin, a homologue of α-tubulin and β-tubulin, for nucleating microtubules. γ-tubulin was originally discovered in a suppressor screen of a γ-tubulin mutant in the filamentous fungus, *Aspergillus nidulans* and it was subsequently found localized at all MTOCs [56-61]. Purification of γ-tubulin from animal and yeast cells showed it to be part of larger complexes, which can directly nucleate microtubule growth *in vitro* [62-66]. γ-tubulin is essential for normal microtubule organization in every organism in which it has been studied, and it is nearly ubiquitous throughout the eukaryotes. Moreover, it is also involved in nucleation from non-MTOC sites within cells, such as nucleation that occurs through the chromosome-mediated nucleation pathway [67], and in plants [68], which lack centrosome-like structures, suggesting that it is critical for the initiation of all new microtubules *in vivo*.

1.2.1 γ-tubulin small complex (γTuSC) and γ-tubulin ring complex (γTuRC)

Nucleation of microtubule assembly is thought to be mediated by γ-tubulin containing protein complexes at the MTOC [40-43]. When γ-tubulin was purified from *Drosophila melanogaster* embryos or *Xenopus laevis* eggs, it was found to be part of a ~2.2 MDa complex with at least six other proteins: γ-tubulin complex protein 2 (GCP2), GCP3, GCP4, GCP5, GCP6 and NEDD1. The complex had a striking ring shape in electron micrographs,

leading to the name γTuRC24. The γTuRC dissociates under high salt conditions to yield a stable 300 kDa subcomplex of γ-tubulin associated with GCP2 and GCP3, which is dubbed the γTuSC [69] (Figure 1.6). Importantly, purified γTuSC has a much lower microtubule-nucleating activity than intact γTuRC [69], suggesting that the assembly state of γ-tubulin is important in determining its activity. Furthermore, *Saccharomyces cerevisiae* and closely related yeasts are unusual, as they appear to have lost all of the γTuRC-specific components, retaining only the γTuSC [65, 66, 70]. This supports the view that the γTuSC is the core of the nucleating machinery, sufficient in itself for proper microtubule organization.

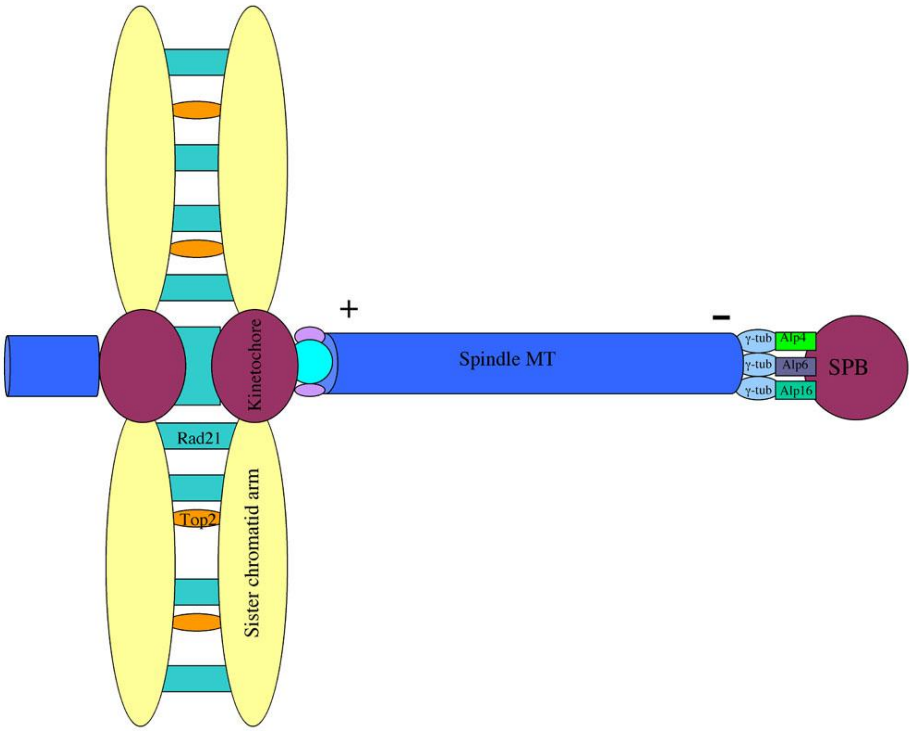

Figure 1.5: Secure microtubule attachment at both the microtubule plus- and minus-end might be required to generate appropriate tension to satisfy the SAC. Microtubules must be properly attached at both the microtubule plus-end to kinetochores and at the microtubule minus-end at the SPB. Microtubules are anchored at the SPB by the microtubule minus-end binding protein, γ-tubulin. γ-tubulin exists in a complex, γ-TuC, and interacts with non-tubulin proteins at the SPB. Three such proteins include the spindle pole component proteins, Alp4, Alp6, and Alp16, and these proteins have been shown to directly bind to γ-tubulin. Rad21 is a sister cohesin subunit that is cleaved at the onset of anaphase, resulting in sister chromatid separation. While Top2, topo II isomerase, helps to untangle the DNA.

1.2.3 The GCP family of γ-tubulin complex components

In addition to γ-tubulin, microtubule-nucleating complexes include five homologous GCPs [71–73] (Figure 1.6). The γTuSC consists of two copies of γ-tubulin and one each of GCP2 and GCP3. The γTuRC is composed of multiple copies of the γTuSC plus GCP4, GCP5 and GCP6. GCP2 and GCP3 are found in almost all eukaryotes and are essential for

proper microtubule organization, suggesting that they form the core of the nucleating machinery [74]. Most eukaryotes also possess GCP4 and GCP5, whereas GCP6 appears to be a recent addition in the animal and fungal lineages. Although they constitute a unique family of homologous proteins, the overall sequence identity between GCPs is quite low (less than 15% identity overall in most comparisons between GCP family members). Homology has only been confidently predicted in two short segments, the GRIP1 and GRIP2 motifs31, which are unique to the GCPs. The overall size of GCPs varies by more than twofold (ranging from ~70–210 kDa), as a result of numerous insertions and/or deletions, suggesting a different function for each family member. Outside of the GRIP1 and GRIP2 motifs that define the GCP family, no GCPs have other identifiable motifs conserved with other protein families. The precise stoichiometry of γTuRC components remains unclear. A study in human cells showed that the complex contains multiple copies of the γTuSC components and GCP4, but only a single copy of GCP5.

1.3 γTuRC assembly and action

It has been assumed that γ-tubulin nucleates by forming oligomers that mimic an early assembly intermediate of αβ-tubulin, with either lateral or longitudinal microtubule-like lattice contacts forming between γ-tubulins. Nucleation should then proceed through direct interactions of γ-tubulin with αβ-tubulin through lattice-like contacts. Electron microscopic studies of the γTuRC revealed a unique 'lock washer' shape, with repeating subunits around the circumference and a diameter and a helical pitch that are similar to those of a microtubule. γTuSCs were proposed to form the repeating wall of the ring. An apparent cap-like feature at the base of γTuRC, seen in the low-resolution structure, was thought to be formed from GCP4, GCP5 and GCP6. Given its position, the asymmetric cap was predicted to act as a scaffold for arranging γTuSCs into a defined ring shape (Figure 1.6).

In vitro, the γTuRC was shown to interact specifically with microtubule minus ends, at which it functions as a cap to prevent microtubule growth in the minus direction [75]. This was consistent with electron micrograph images showing closed structures at the ends of microtubules, whether nucleated by γTuRCs *in vitro* [74–76] or attached to MTOCs *in vivo* [77]. Synthesis of these data led to the 'template model', which suggests that the γ-tubulins in the γTuRC function as a microtubule template, making lateral contacts with each other around the ring and longitudinal contacts with α-tubulin (Figure 1.6b and c).

An alternative hypothesis — the 'protofilament model' — was proposed early on, in which γ-tubulins would make longitudinal contacts with each other around the ring [78, 79] (Figure 1.6d). This seemed reasonable, a priori, as longitudinal contacts are much stronger than lateral contacts, and rings of longitudinally-interacting tubulin and its bacterial homologue FtsZ, have been observed. Moreover, electron micrographs of γTuRCs indicated that the structure might be quite flexible, suggesting that it could potentially unfurl to present a single protofilament of γ-tubulins that would nucleate through lateral contacts with α-tubulin and β-tubulin. However, the weight of evidence now strongly supports the template model.

Although a template mechanism of nucleation has been the dominant model for γTuRC function for over a decade, it has remained unproven, and several important questions have persisted. What is the mode of interaction (lateral or longitudinal) between γ-tubulin and αβ-tubulin? Why is γ-tubulin nucleating capacity weaker in the γTuSC than in the γTuRC, and how does *S. cerevisiae*, which only has the γTuSC, efficiently nucleate microtubules? How are 13-protofilament microtubules nucleated when γ-tubulins enter the complex in pairs through the γTuSC? And, finally, what are the structural and functional roles of the non γ-tubulin components of the γTuRC?

1.4 Structural insight into γTuRC function

A thorough, mechanistic understanding of microtubule nucleation by γ-tubulin will require a high-resolution structural model of the γTuRC. However, this is not yet being possible. The availability of low resolution electron crystallography structure of γTuRC reveals the structural insight into the complex structure.

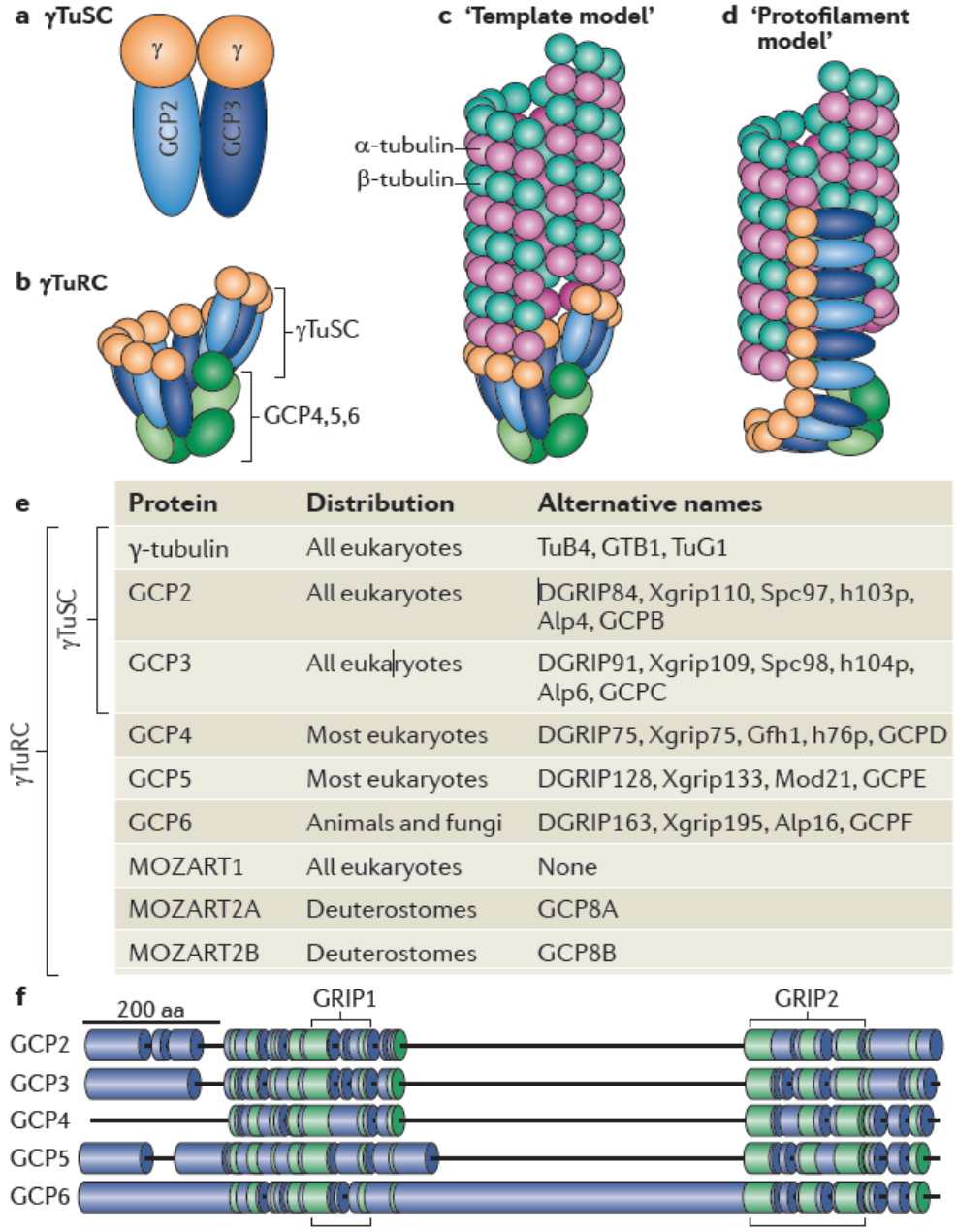

e

	Protein	Distribution	Alternative names
γTuSC	γ-tubulin	All eukaryotes	TuB4, GTB1, TuG1
γTuSC	GCP2	All eukaryotes	DGRIP84, Xgrip110, Spc97, h103p, Alp4, GCPB
γTuSC	GCP3	All eukaryotes	DGRIP91, Xgrip109, Spc98, h104p, Alp6, GCPC
γTuRC	GCP4	Most eukaryotes	DGRIP75, Xgrip75, Gfh1, h76p, GCPD
γTuRC	GCP5	Most eukaryotes	DGRIP128, Xgrip133, Mod21, GCPE
γTuRC	GCP6	Animals and fungi	DGRIP163, Xgrip195, Alp16, GCPF
γTuRC	MOZART1	All eukaryotes	None
γTuRC	MOZART2A	Deuterostomes	GCP8A
γTuRC	MOZART2B	Deuterostomes	GCP8B

Figure 1.6: The γ-tubulin small complex (γTuSC) is the conserved, essential core of the microtubule nucleating machinery, and it is found in nearly all eukaryotes. (a) The γTuSC has two copies of γ-tubulin and one each of γ-tubulin complex protein 2 (GCP2) and GCP3. (b) In many eukaryotes, multiple γTuSCs assemble with GCP4, GCP5 and GCP6 into the γ-tubulin ring complex (γTuRC). Previous models of γTuRC assembly suggested that GCP4, GCP5 and GCP6 together function as a cap-like scaffold for arranging multiple γTuSCs into a distinctive ring shape. This view depicts a model with six γTuSCs (12 γ-tubulins), which would leave a gap in the template, owing to the fact that microtubules are made up of 13 protofilaments. (c) The most widely accepted model for the mechanism of γTuRC-based nucleation, the 'template model', suggests that the γTuRC acts as a template, presenting a ring of γ-tubulins that make longitudinal contacts with α-tubulin–β-tubulin (αβ-tubulin). (d) By contrast, the 'protofilament model' suggests that the γTuRC unfurls to present a γ-tubulin protofilament, which would nucleate through lateral contacts with αβ-tubulin. (e) A complete list of proteins that are thought to be part of the γTuSC and the γTuRC. (f)The five GCPs share regions of homology, although with very low levels of sequence identity (as low as 15% identity between GCP family members). Two homologous regions of GCPs, GRIP1 and GRIP2, defined their homology. Regions of more-distant homology were shown to be more widely dispersed in the GCP sequences(green shading).

1.4.1 The γ-tubulin crystal structure.

The crystal structure of monomeric human γ-tubulin was determined bound to GTP and to GDP [30, 80]. γ-tubulin is very similar to α-tubulin and β-tubulin in its overall fold, which is consistent with the expectation that it is capable of making lattice-like contacts with the microtubule. Small differences on the microtubule lattice surfaces may give rise to differences in γ-tubulin interaction affinities at those sites, influencing the strength of γ-tubulin– γ-tubulin assembly interactions or γ-tubulin–microtubule interactions. Importantly, in the two γ-tubulin crystal forms, the individual γ-tubulins make lateral contacts with each other through the same contact region that αβ-tubulin use in microtubule lateral interactions, suggesting that this is their preferred mode of interaction. The crystal packing provided support for the template model of microtubule nucleation, which predicts lateral interactions between γ-tubulins and longitudinal interactions between γ-tubulin and αβ-tubulin.

1.4.2 The structure of the γTuSC

The structure of free *S. cerevisiae* γTuSC was initially determined at 25 Å by negative-stain single-particle electron microscopy (EM) [81] (its V-shaped structure was later confirmed at higher resolution by cryo-EM), and the subunit arrangement and the orientations of GCP2 and GCP3 in the structure were determined by direct labelling experiments [82].
The arms of the V-shaped structure are composed of GCP2 and GCP3, which have similar overall shapes and dimerize through their amino-terminal domains at the base of the V-shape. The tips of the V-shape contain γ-tubulin, which interacts with the carboxy-terminal domains of GCP2 and GCP3 (Figure 1.7a). Surprisingly, the two γ-tubulins in the structure are held apart from each other, not making the anticipated lateral contacts that are required to match the microtubule lattice. This mismatch provides a partial explanation for the weaker nucleating activity of free γTuSC — each γ-tubulin remains totally independent, rather than forming a microtubule-like assembly intermediate that could facilitate microtubule assembly. Thus, the structure of the γTuSC suggests that it is in an ‘off ’ state, which raises the possibility of regulation at the level of γTuSC conformation.

1.4.3 The γTuSC assembles with microtubule-like symmetry

Purified *S. cerevisiae* γTuSCs have a weak tendency to spontaneously assemble *in vitro* into ring-shaped structures that closely resemble the γTuRC [83]. The ring assemblies are only formed under a narrow range of buffer conditions, and their heterogeneity and insta-

bility made them an extremely challenging subject for structure determination. However, it was discovered that co-purification of the γTuSC with the N-terminal domain of the *S. cerevisiae* attachment factor spindle pole body component 110 (Spc110; which links the γTuSC to the core of the spindle pole body) dramatically stabilizes γTuSC assembly. So much so that, when associated with Spc110, γTuSC rings continue to grow, yielding extended helical filaments of laterally associated γTuSCs that are very well suited to cryo-EM reconstruction. The 8 Å structure of this γTuSC filament provided a breakthrough in our understanding of γTuSC assembly, with important implications for the mechanism of microtubule nucleation [83]. The most striking feature of the γTuSC oligomer structure is that there are six and a half γTuSCs per helical turn, owing to a half-subunit overlap between the first and seventh subunits (Figure 1.7b). This gives 13 γ-tubulins per turn, matching the *in vivo* microtubule protofilament number with a helical pitch that is very similar to that of a microtubule. There is remarkable similarity between a single ring of the γTuSC and the low-resolution structure of the γTuRC, strongly suggesting that γTuSC assemblies like these constitute the core of the γTuRC (Figure 1.7c). This finding also resolved the paradox of how budding yeast efficiently nucleate microtubules with only the γTuSC — they can form γTuRC-like structures from γTuSCs alone.

The increased resolution of the γTuSC subunit structure allowed the precise orientation of each γ-tubulin. The minus ends of both γ-tubulins are buried in the interaction surface with GCP2 or GCP3, and their lateral surfaces are facing adjacent γ-tubulins. Moreover, each γ-tubulin plus end is fully exposed, strongly suggesting that this surface interacts via longitudinal contacts with the minus ends of αβ-tubulin. The combination of the γ-tubulin geometry and its orientation provides the strongest evidence to date that γ-tubulin complexes function as microtubule templates. Indeed, the γTuSC rings are likely to provide the constraint that ensures the creation of 13-protofilament microtubules *in vivo*. It is important to note that the 13-fold architecture of the oligomer is defined almost entirely by the conformations of, and interactions between, GCP2 and GCP3, with only minor contacts between γ-tubulins within the ring.

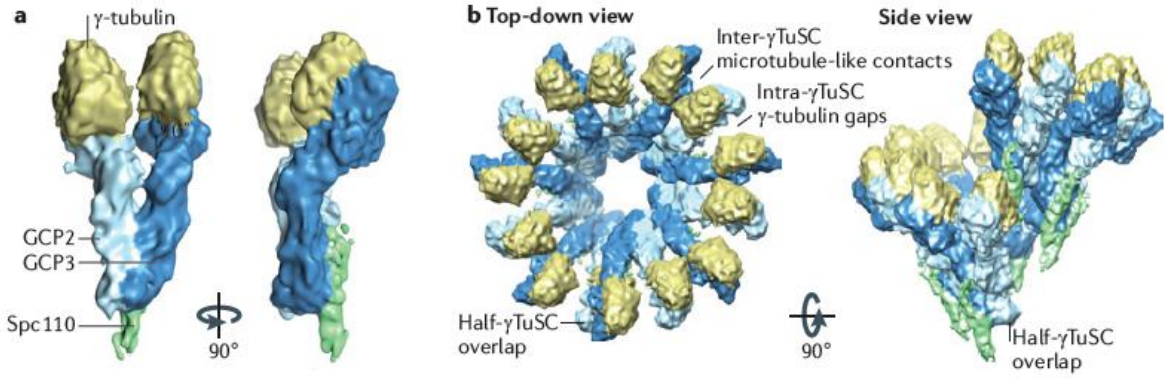

Figure 1.7: The structure of γTuSC. (a) The 8 Å cryo-electron microscopy (EM) structure of Saccharomyces cerevisiae γ-tubulin small complex (γTuSC) bound to the attachment factor spindle pole body component 110 (Spc110) is shown. In this view, the amino termini of γ-tubulin complex protein 2 (GCP2) and GCP3 are at the bottom, with their carboxy-terminal domains near the top interacting with γ-tubulin. In the structure, the two γ-tubulins are held apart from each other in a configuration that is incompatible with the microtubule lattice, which partially explains the relatively low nucleating capacity of free γTuSC relative to that of the γ-tubulin ring complex (γTuRC). (b) Top-down and side views of the γTuSC ring are shown. The ring has six and a half γTuSCs per turn, which arise owing to a half-γTuSC overlap between the first and seventh subunits in the ring. This yields 13 γ-tubulins per turn, matching the in vivo microtubule protofilament number. The conformation of the γTuSC is unchanged in the ring structure, such that the intra-γTuSC gap between γ-tubulins remains. However, microtubule-like lateral interactions are observed between γ-tubulins at the inter-γTuSC interface.

1.4.4 A pseudo-atomic model of the γTuSC

A major advance toward the full understanding of γ-tubulin complexes was achieved recently by the determination of the crystal structure of human GCP4 [83] (Figure 1.8a). Using the GCP4 crystal structure as a template, homology models of GCP2 and GCP3 were generated and fit into the γTuSC cryo-EM structure, along with the crystal structure of γ-tubulin, to create a pseudo-atomic model of the γTuSC50 (Figure 1.8b). The γTuSC model predicts the surfaces involved in γ-tubulin–GCP2 and γ-tubulin–GCP3 interactions. The model also reveals the positions of the GCP GRIP1 and GRIP2 motifs (Figure 1.8c). The GRIP2 motif is clearly part of the γ-tubulin-binding surface of GCPs, which is consistent with *in vitro* binding experiments using GCP4 and γ-tubulin. The role of GRIP1 is less clear; it forms part of the lateral interaction surfaces, suggesting that it has a role in γTuSC assembly. However, it also forms part of the surface of GCP2 and GCP3 that is exposed on the outer surface of the ring, suggesting that it may be a binding site for other proteins that interact with the γTuSC. The pseudo-atomic model of the γTuSC also provides insight into the nature of assembly contacts in γTuSC oligomers (Figure 1.8d). The intra-γTuSC and inter-γTuSC interactions between GCP2 and GCP3 are very similar: essentially, the interactions along the base of a γTuSC ring are the same all the way around and primarily involve contacts between helical bundles i and ii (Figure 1.8e). There appears to be a single assembly rule guiding

interactions between GCP2 and GCP3, whether within or between γTuSCs. Changes at these interaction surfaces seem to have tuned affinities to give very strong binding to hold together individual γTuSCs but weaker interactions that drive the reversible assembly of these γTuSCs into γTuSC rings.

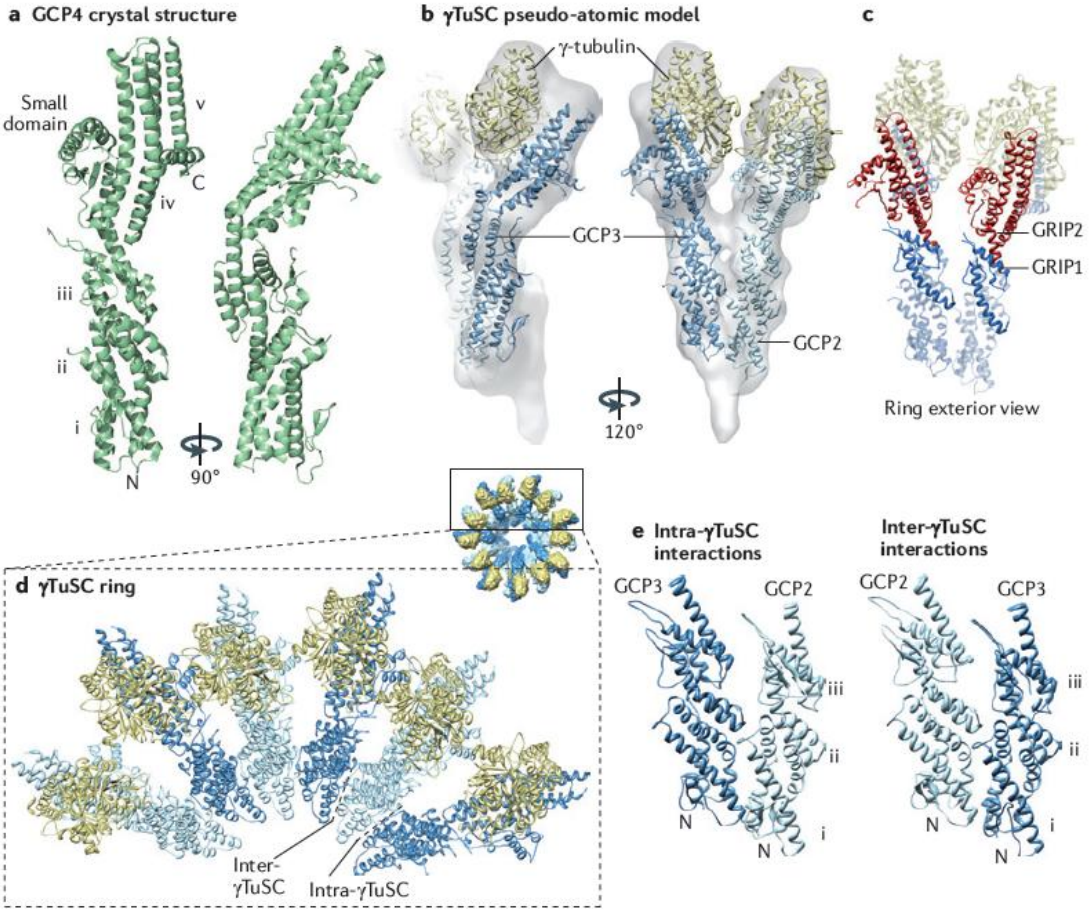

Figure 1.8: Pseudo-atomic model of the γ-tubulin small complex (γTuSC). (a) The γ-tubulin complex protein 4 (GCP4) crystal structure is shown in two orthogonal views. In the view on the left, the five α-helical bundles (i–v), small domain, amino terminus and carboxyl terminus are labelled. The C-terminal domain, consisting of bundle iv, bundle v and the small domain, was shown to directly bind γ-tubulin. (b) Two views of the pseudo-atomic model of the γ-tubulin small complex (γTuSC) are shown. The model was generated by fitting the γ-tubulin crystal structure (gold) and the GCP4 crystal structure (blue), as a stand-in for GCP2 and GCP3, into the cryo-electron microscopy (EM) reconstruction of the γTuSC (semi-transparent surface). The model reveals interaction surfaces between complex components. (c) The model also shows the positions of the conserved GRIP1 and GRIP2 domains in GCP2 and GCP3 in the context of the full γTuSC. GRIP2 is clearly involved in γ-tubulin binding. The role of GRIP1 is more ambiguous; it forms part of the lateral contact surfaces between γTuSCs, as well as part of the faces of GCP2 and GCP3 that are exposed on the outside of the γTuSC ring.(d) The surfaces of GCP2 and GCP3 that are important for oligomerization. γTuSCs interact with each other primarily through the sides of bundles i and ii. (e) The N-terminal domains of GCP2 and GCP3 are shown making intra-γTuSC and inter-γTuSC contacts, with helical bundles i–iii labelled. Equivalent surfaces of the N-terminal domains of GCP2 and GCP3 are involved in both intra-γTuSC and inter-γTuSC interactions, indicating that a single assembly rule determine the organization of the ring structure.

1.5 Targeting γ-Tubulin complex for inhibition of microtubule nucleation

The function of γTuRC is to nucleate the assembly of dynamic microtubules that coordinate the accurate segregation of duplicated chromosomes into two dividing cells. Thus the assembly and organization of microtubules also serve as excellent targets for cancer chemotherapy. Several drugs such as paclitaxel derivatives and vinca alkaloids are now routinely used in chemotherapy of cancer, affecting dynamics of microtubules and thus provoking errors in mitotic spindle assembly and ultimately cause apoptosis. The targets of these inhibitors are α- and β- tubulin [85]. In contrast, so far no chemotherapeutic agents have been developed against γ-tubulin or against any of its associated γ-tubulin complex proteins. Nevertheless, removal of γ-tubulin or of other γTuRC components from the cell induces changes in microtubule dynamics and spindle defects that resemble phenotypes obtained with microtubule drugs [86– 88]. Additionally, although tubulins (α/β) are abundant proteins constituting roughly 2.5% of the total protein in a cell, γ-tubulin makes up for less than 1% of the total tubulin content of the cell [89]. It will therefore be of major interest to investigate the assembly of γTuRCs, since these are crucial for microtubule assembly and may represent potential pharmacological targets. Earlier studies in this regard are very encouraging. Whitehurst et al. [90] have described proteins of the γTuRC as putative targets whose depletion by siRNA sensitizes a lung cancer cell line at 1000-fold reduced doses of paclitaxel. Moreover, it has been shown that small amounts of siRNA against the γTuRC component NEDD1 potentiate the anti-mitotic activity of low doses of a Plk1 inhibitor [88].

Advances in the crystal structures of alpha- beta- and gamma-tubulins yielded a realization that the overall structure of γ-tubulin was more similar to β-tubulin subunit than it is to the α-tubulin subunit [91-93]. Because β-tubulin has a very well characterized drug binding cavities, one straight approach for the future is to explore how well these cavities are conserved in γ-tubulin structure and whether they can be used to identify additional potential lead compounds that can bind these cavities. To this end, Friesen et al. (2012) performed a rigorous search for colchicine binding site within the structure of γ-tubulin [94]. The colchicine site also accommodates many structurally related compounds such as podophyllotoxin and combrestatin. Not only did they find that the colchicine site is conserved between β-tubulin and γ-tubulin, but they showed that bacterially expressed γ-tubulin binds colchicine with a dissociation constant of 13.9 μM compared to a dissociation constant of 1.1 μM with β-tubulin suggesting that this is a good lead [94]. Colchicine and podophyllotoxin

however, have been of limited use for cancer therapy because they are too toxic to animals at cancer therapeutic doses.

Based on the structures of colchicine, podophyllotoxin, combrestatin like compounds, Ye et al. (1998) identified a natural plant alkaloid noscapine [95]. Several higher affinity analogues (noscapinoids) were then developed and shown to compete with the colchicine [96]. These compounds modulate microtubule dynamics upon binding and induce apoptosis both during mitosis and during interphase of the cell cycle [97, 98]. More importantly, perhaps due to milder effect on the normal cells, they do not display major side effects due to the disruption of haematopoiesis, hair follicles, gastrointestinal lining and the axonal transport and integrity. For example, Phase I/II studies showed low toxicity even at high dose of 300 mg/kg body weight [99]. Therefore it is necessary to investigate whether this class of compounds can also form suitable lead-compounds for the development of γ-tubulin interacting agents. Another attraction of investigating this class of compounds as structural leads comes from the fact that this binding pocket within the γ-tubulin lies in a close vicinity to its interaction site with a component of the TuSC, GCP4. Since intact γTuRCs are essential for microtubule nucleation and mitosis, such drugs are expected to interfere with those mechanisms thus provoking mitotic spindle defects and arrest of the cell cycle.

In this study, we elucidated the molecular basis of interaction of γ-tubulin with microtubules and other components of the MTOC like adjacent γ-tubulin unit and GCP4 using molecular modelling and molecular dynamics simulations. In the second chapter, we elucidated the protein-protein interactions of γ-tubulin with adjacent γ-tubulin. In this endeavour, we found out the predicted binding affinity between two adjacent γ-tubulin proteins using both MM-PBSA and MM-GBSA methods. We also found the amino acids that contributed most to the stability of γ-tubulin-GCP4 complex. The hot spot amino acids were further verified based on alanine scanning mutagenesis using both experimental and computational methods. In the third chapter we tried to identify chemical compounds which can disrupt the binding between adjacent γ-tubulins. We performed docking studies with a promising new class of compounds called noscapinoids which include natural compound called noscapine and two of its derivatives, amino–noscapine and bromo-noscapine. We followed up the docking studies with molecular dynamics simulations and binding affinity analysis using MM-PBSA and MM-GBSA methods. We found that bromo-noscapine shows most robust interaction with the γ-tubulin dimer. In the fourth chapter, we used molecular

modelling and MD simulations, combined with MM-PBSA and MM-GBSA computational methods to understand atomic interactions between γ-tubulin and GCP4. We simulated two conformations of γ-tubulin-GCP4 complex for 10 ns and calculated the binding free energy of -172.7 kcal/mol and -188.5 kcal/mol using MM-PBSA and MM-GBSA method respectively, for dimer1 and -124.6 kcal/mol and -93.58 kcal/mol by MM-PBSA and MM-GBSA methods for dimer 2. These values points to very robust interactions between GCP4 and γ-tubulin. We also identified amino acids crucial for the interaction of γ-tubulin with GCP4, called hot spots, by computational alanine-scanning mutagenesis. In the fifth chapter, we reported chemical leads called noscapinoids that might fits well in a cavity close to γ-tubulin-GCP4 interface. All noscapinoids displayed stable interaction throughout simulation, however, most robust interaction was observed for bromo-noscapine followed by noscapine and amino-noscapine with binding free energy of -46.73 kcal/mol, -41.69 kcal/mol and -35.40 kcal/mol respectively, using the MM-GBSA method and -31.86 kcal/mol, -23.60 kcal/mol and -20.50 kcal/mol respectively, using the MM-PBSA method with dimer1 of γ-tubulin-GCP4 complex. Similarly with dimer2 of γ-tubulin-GCP4 complex the most robust interaction was observed for bromo-noscapine with the binding affinity of -40 kcal/mol followed by noscapine with -32.82 kcal/mol and -21.84 kcal/mol for amino-noscapine, using MM-GBSA method. This offers a novel chemical scaffold for γ-tubulin binding drugs near γ-tubulin-GCP4 interface. In the sixth chapter we explored the interaction between γ-tubulin and microtubules. We first obtained a molecular system consisting of γ-tubulin, αβ-tubulin and GCP4 using protein-protein docking. We simulated the molecular system for 10 ns and followed it up with binding affinity analysis using MM-GBSA and MM-PBSA approach. We identified the hot spot amino acids which were deemed most critical to the binding of γ-tubulin with the microtubules. These hot spot amino acids were then verified by means of alanine scanning mutagenesis using both experimental as well as the computational methods. I have summarized my results and discuss the future directions for research in the final chapter.

REFERENCES

[1] Gould, R.R., and Borisy, G.G. *The pericentriolar material in Chinese hamster ovary cells nucleates microtubule formation*. J. Cell Biol, 73 pp 601-615. 1977.

[2] Margolis, R.L. and Wilson, L. *Microtubule treadmilling: what goes around comes around. Bioessays*, 20 pp 830-6. 1998.

[3] Dabora, S.L., and Sheetz, M.P. *The microtubule-dependent formation of a tubulovesicular network with characteristics of the ER from cultured cell extracts*. Cell, 54, pp 27-35. 1988.

[4] Kreis, T.E. *Role of microtubules in the organisation of the golgi apparatus.* Cell Motil. Cytoskeleton, 15 pp 67-70. 1990.

[5] Terasaki, M. *Recent progress on structural interactions of the endoplasmic reticulum*. Cell Motil. Cytoskeleton, *15* pp 71-75. 1990.

[6] May, K.M., and Hyams, J.S. *The yeast cytoskeleton: The closer we look, the more we see*. Fungal Genet. Biol. *24* pp 110-122. 1998.

[7] Saxton, W.M., Stemple, D.L., Leslie, R.J., Salmon, E.D., Zavortink, M., and McIntosh, J.R. *Tubulin dynamics in cultured mammalian cells*. J. Cell Biol. *99* pp 2175-2186. 1984.

[8] Mandeville, E.C., and Rieder, C.L. *Keratin filaments restrict organelle migration into the forming spindle of newt pneumocytes*. Cell Motil. Cytoskeleton 15 pp 111-120. 1990.

[9] Ding, R., West, R.R., Morphew, D.M., Oakley, B.R., and McIntosh, J.R. *The spindle pole body of Schizosaccharomyces pombe enters and leaves the nuclear envelope as the cell cycle proceeds.* Mol. Biol. Cell, 8 pp 1461-1479. 1997.

[10] Brinkley, B.R. *Microtubule organizing centers*. Annu. Rev. Cell Biol. 1 pp 145-172. 1985.

[11] Margolis RL and Wilson L. *Opposite end assembly and disassembly of microtubules at steady state in vitro*. Cell, 13 pp 1-8. 1978.

[12] Schulze E and Kirschner M. *Microtubule dynamics in interphase cells*. Journal Cell Biology, 102 pp 1020-1031. 1986.

[13] Belmont LD, Hyman AA, Sawin KE and Mitchison TJ. *Real-time visualization of cell cycle-dependent changes in microtubule dynamics in cytoplasmic extracts.* Cell 62 pp 579-589. 1990.

[14] David-Pfeuty T, Erickson HP and Pantaloni D. *Guanosinetriphosphatase activity of tubulin associated with microtubule assembly*. Proceedings of the National Academic of Sciences USA, 74 pp 5372-5376. 1977.

[15] MacNeal RK and Purich DL. *Stoichiometry and role of GTP hydrolysis in bovine neurotubule assembly*. Journal of Biological Chemistry, 253 pp 4683-4687. 1978.

[16] Mitchison T and Kirschner M. *Microtubule assembly nucleated by isolated centrosomes. Nature*, 312 pp 232-237. 1984a

[17] Mitchison T and Kirschner M. *Dynamic instability of microtubule growth*. Nature, 312 pp 237-242. 1984b.

[18] Margolis RL and Wilson L (1978). Opposite end assembly and disassembly of microtubules at steady state in vitro. Cell 13: 1-8.

[19] Walker RA, O'Brien ET, Pryer NK, Soboeiro MF, Voter WA, Erickson HP and Salmon ED. *Dynamic instability of individual microtubules analyzed by video light microscopy: rate constants and transition frequencies*. Journal Cell Biology, 107 pp 1437-1448. 1988.

[20] Jordan, M.A. and Wilson, L. Microtubules as a target for anticancer drugs. Nat Rev Cancer, 4 pp 253-65. 2004.

[21] Nogales, E., Whittaker, M., Milligan, R. A. & Downing, K. H. *High-resolution model of the microtubule*. Cell, 96 pp 79–88. 1999.

[22] Nogales, E., Wolf, S.G. and Downing, K.H. Structure of the alpha beta tubulin dimer by electron crystallography. Nature, 391 pp 199-203. 1998.

[23] Chretien, D., Wade, R. H. *New data on the microtubule surface lattice*. Biol. Cell, 71 pp 161–174. 1991.

[24] Sui, H., Downing, K. H. *Structural basis of interprotofilament interaction and lateral deformation of microtubules*. Structure, 18 pp 1022–1031. 2010.

[25] Ledbetter, M. C., Porter, K. R. *Morphology of microtubules of plant cell.* Science, 144 pp 872–874. 1964.

[26] Tilney, L. G. *et al. Microtubules: evidence for 13 protofilaments*. J. Cell Biol., 59 pp 267–275. 1973.

[27] Evans, L., Mitchison, T., Kirschner, M. *Influence of the centrosome on the structure of nucleated microtubules.* J. Cell Biol. 100 pp 1185–1191. 1985.

[28] Mandelkow, E. M., Schultheiss, R., Rapp, R., Muller, M., Mandelkow, E. *On the surface lattice of microtubules: helix starts, protofilament number, seam, and handedness*. J. Cell Biol, 102 pp 1067–1073. 1986.

[29] McEwen, B., Edelstein, S. J. *Evidence for a mixed lattice in microtubules reassembled in vitro*. J. Mol. Biol, 139 pp 123–145. 1980.

[30] Rice, L. M., Montabana, E. A., Agard, D. A. *The lattice as allosteric effector: structural studies of αβ-and γ-tubulin clarify the role of GTP in microtubule assembly.* Proc. Natl Acad. Sci USA, 105 pp 5378–5383. 2008.

[31] Pickett-Heaps, J.D. *The evolution of the mitotic apparatus. An attempt at comparative ultrasound cytology in dividing plant cells*. Cytobios, 3 pp 2570-2580. 1969.

[32] Brinkley, B.R. Microtubule organizing centers. Annu. Rev. Cell Biol. 1, 145-172. 1985.

[33] Rose, M.D., Biggins, S. and Satterwhite L.L. *Unraveling the tangled web at the microtubule-organizing center*. Curr. Opin. Cell Biol, 5 pp 105-115. 1993.

[34] Li, Q and Joshi, H.C. *Gamma-tubulin is a minus end-specific microtubule binding protein.* J. Cell Biol, 131 pp 207-214. 1995.

[35] Shu, H.B., Li, Z., Palacios, M.J., Li, Q. and Joshi, H.C. *A transient association of gamma-tubulin at the midbody is required for the completion of cytokinesis during the mammalian cell division*. J. Cell Sci, 108 pp 2955-2962. 1995.

[36] Stearns, T. and Winey, M. The cell center at 100. Cell, 91 pp 303-309. 1997.

[37] Saunders, W.S. *Action at the ends of microtubules.* Curr. Opin. Cell Biol, 11 pp 129-133. 1999.

[38] Oakley, C.E., and Oakley, B.R. *Identification of gamma-tubulin, a new member of the tubulin superfamily encoded by the mipA gene in Aspergillus nidulans*. Nature, 338 pp 662-664. 1989.

[39] Leguy R., Melk, R., Pantaloni, D., and Carlier, M.F. Monomeric gamma-tubulin nucleates microtubules. J. Biol Chem. *275*, 21975-21980. 2000

[40] Jeng, R., and Stearns, T. *Gamma-tubulin complexes: Size does matter*. *Trends* Cell Biol, 9 pp 339-342. 1999.

[41] Wiese, C., and Zheng, Y. *Gamma-tubulin complexes and their interaction with microtubule organizing centers*. Curr. Opin. Struct. Biol. *9*, 250-259. 1999.

[42] Schiebel, E. *Gamma-tubulin complexes: Binding to the centrosome, regulation and microtubule nucleation.* Curr. Opin. Cell Biol, 12 pp 113-118. 2000.

[43] Vardy, L., and Toda, T. *The fission yeast gamma-tubulin complex is required in G1 phase and is a component of the spindle assembly checkpoint.* EMBO J, 19 pp 6098-6111. 2000.

[44] Oakley, B.R., Oakley, C.E., Yoon, Y., and Jung, M.K. *Gamma-tubulin is a component of the spindle pole body that is essential for microtubule function in Aspergillus nidulans.* Cell 61, 1289-1301. 1990.

[45] Horio, T., Uzawa, S., Jung, M.K., Oakley, B.R., Tanaka, K., and Yanagida, M. *The fission yeast γ-tubulin is essential for mitosis and is localized at microtubule organizing centers*. J. Cell Sci. 99 pp 693-700. 1991.

[46] Joshi, H.C., Palacios, M.J., McNamara, L., and Cleveland, D.W. *Gamma-tubulin is a centrosomal protein required for cell cycle-dependent microtubule nucleation.* Nature, 356 pp 80-83. 1992.

[47] Felix, M.A., Antony, C., Wright, M., and Maro, B. *Centrosome assembly in vitro: Role of gamma-tubulin recruitment in Xenopus sperm aster formation.* J. Cell Biol., 124 pp 19-31. 1994.

[48] Sobel, S.G., and Snyder, M. *A highly divergent gamma-tubulin gene is essential for cell growth and proper microtubule organization in Saccharomyces cerevisiae.* J. Cell Biol., 131 pp 1775-1788. 1995.

[49] Zheng, Y., Wong, M.L., Alberts, B., and Mitchison, T. *Nucleation of microtubule assembly by a gamma-tubulin-containing ring complex.* Nature, 378 pp 578-583. 1995.

[50] Schnackenberg, B.J., Khodjakov, A., Rieder, C.L., and Palazzo, R.E. *The disassembly and reassembly of functional centrosomes in vitro.* Proc. Natl. Acad. Sci. U.S.A., *95* pp 9295-9300. 1998.

[51] Oegema, K., Wiese, C., Martin, O.C., Milligan, R.A., Iwamatsu, A., Mitchison, T.J., and Zheng, *Y. Characterization of two related Drosophila gamma-tubulin complexes that differ in their ability to nucleate microtubules.* J. Cell Biol., 144 pp 721-733. 1999.

[52] Wiese, C., and Zheng, Y. *A new function for the gamma-tubulin ring complex as a microtubule minus-end cap*. Nat. Cell Biol., 2 pp 358-364. 2000.

[53] Moritz, M., Braunfeld, M.B., Sedat, J.W., Alberts, B., and Agard, D.A. *Microtubule nucleation by gamma-tubulin-containing rings in the centrosome.* Nature 378 pp 638-640. 1995a.

[54] Moritz, M., Braunfeld, M.B., Fung, J.C., Sedat, J.W., Alberts, B.M., and Agard, D.A. *Three-dimensional structural characterization of centrosomes from early Drosophila embryos.* J. Cell Biol., 130 pp 1149-1159. 1995b.

[55] Fujita, A., Vardy, L., Garcia, M.A., and Toda, T. *A fourth component of the fission yeast γ-tubulin complex, Alp16, is required for cytoplasmic microtubule integrity and becomes indispensable when γ-tubulin function is compromised.* Mol. Biol. Cell, 13 pp 2360-2373. 2002.

[56] Oakley, B. R., Oakley, C. E., Yoon, Y. & Jung, M. K. *γ-tubulin is a component of the spindle pole body that is essential for microtubule function in Aspergillus nidulans*. Cell 61 pp 1289–1301. 1990.

[57] Zheng, Y., Jung, M. K. & Oakley, B. R. *γ-tubulin is present in Drosophila melanogaster and Homo sapiens and is associated with the centrosome.* Cell, 65 pp 817–823. 1991.

[58] Stearns, T., Evans, L. & Kirschner, M. *γ-tubulin is a highly conserved component of the centrosome.* Cell. 65 pp 825–836. 1991.

[59] Sobel, S. G. & Snyder, M. *A highly divergent γ-tubulin gene is essential for cell growth and proper microtubule organization in Saccharomyces cerevisiae.* J. Cell Biol. 131 pp 1775–1788. 1995.

[60] Horio, T. *et al. The fission yeast γ-tubulin is essential for mitosis and is localized at microtubule organizing centers*. J. Cell Sci., 99 pp 693–700. 1991.

[61] Spang, A., Geissler, S., Grein, K. & Schiebel, E. *γ-tubulin-like Tub4p of Saccharomyces cerevisiae is associated with the spindle pole body substructures that organize microtubules and is required for mitotic spindle formation.* J. Cell Biol. 134, 429–441. 1996.

[62] Raff, J. W., Kellogg, D. R. & Alberts, B. M. Drosophila γ-tubulin is part of a complex containing two previously identified centrosomal MAPs. J. Cell Biol. 121 pp 823–835. 1993.

[63] Stearns, T. & Kirschner, M. *In vitro reconstitution of centrosome assembly and function: the central role of γ-tubulin.* Cell 76 pp 623–637. 1994.

[64] Zheng, Y., Wong, M. L., Alberts, B. & Mitchison, T. *Nucleation of microtubule assembly by a γ-tubulin-containing ring complex.* Nature 378 pp 578–583. 1995.

[65] Knop, M., Pereira, G., Geissler, S., Grein, K. & Schiebel, E. *The spindle pole body component Spc97p interacts with the γ-tubulin of Saccharomyces cerevisiae and functions in microtubule organization and spindle pole body duplication*. EMBO J., 16 pp 1550–1564. 1997.

[66] Geissler, S. *et al. The spindle pole body component Spc98p interacts with the γ-tubulin-like Tub4p of Saccharomyces cerevisiae at the sites of microtubule attachment.* EMBO J. 15 pp 3899–3911. 1996.

[67] Mishra, R. K., Chakraborty, P., Arnaoutov, A., Fontoura, B. M. & Dasso, M. *The Nup107–160 complex and γ-TuRC regulate microtubule polymerization at kinetochore*s. Nature Cell Biol., 12 pp 164–169.

[68] Murata, T. *et al. Microtubule-dependent microtubule nucleation based on recruitment of γ-tubulin in higher plants*. Nature Cell Biol. 7 pp 961–968. 2005.

[69] Oegema, K. *et al. Characterization of two related Drosophila γ-tubulin complexes that differ in their ability to nucleate microtubules.* J. Cell Biol, 144 pp 721–733. 1999.

[70] Vinh, D. B., Kern, J. W., Hancock, W. O., Howard, J. & Davis, T. N. *Reconstitution and characterization of budding yeast γ-tubulin complex.* Mol. Biol. Cell 13 pp 1144–1157. 2002.

[71] Gunawardane, R. N. *et al. Characterization and reconstitution of Drosophila γ-tubulin ring complex subunits*. J. Cell Biol., 151 pp 1513–1524. 2000.

[72] Murphy, S. M. *et al. GCP5 and GCP6: two new members of the human γ-tubulin complex*. *Mol. Biol.* Cell, 12 pp 3340–3352. 2001.

[73] Murphy, S. M., Urbani, L. & Stearns, T. *The mammalian γ-tubulin complex contains homologues of the yeast spindle pole body components Spc97p and Spc98p*. J. Cell Biol., 141 pp 663–674 (1998).

[74] Moritz, M., Braunfeld, M. B., Guenebaut, V., Heuser, J. & Agard, D. A. *Structure of the γ-tubulin ring complex: a template for microtubule nucleation.* Nature Cell Biol., 2 pp 365–370. 2000.

[75] Wiese, C. & Zheng, Y. *A new function for the γ-tubulin ring complex as a microtubule minus-end cap.* Nature Cell Biol., 2 pp 358–364. 2000.

[76] Keating, T. J. & Borisy, G. G. *Immunostructural evidence for the template mechanism of microtubule nucleation.* Nature Cell Biol., 2 pp 352–357. 2000.

[77] Byers, B., Shriver, K. & Goetsch, L. *The role of spindle pole bodies and modified microtubule ends in the initiation of microtubule assembly in Saccharomyces cerevisiae.* J. Cell Sci., 30 pp 331–352. 1978.

[78] Erickson, H. P. & Stoffler, D. *Protofilaments and rings, two conformations of the tubulin family conserved from bacterial FtsZ to α/β and γtubulin*. J. Cell Biol. 135 pp 5–8. 1996.

[79] Erickson, H. P. *γ-tubulin nucleation: template or protofilament?* Nature Cell Biol., 2 pp E93–E96. 2000.

[80] Aldaz, H., Rice, L. M., Stearns, T. & Agard, D. A. *Insights into microtubule nucleation from the crystal structure of human γ-tubulin*. Nature, 435 pp 523–527. 2005.

[81] Kollman, J. M. *et al. The structure of the γ-tubulin small complex: implications of its architecture and flexibility for microtubule nucleation.* Mol. Biol. Cell, 19 pp 207–215. 2008.

[82] Choy, R. M., Kollman, J. M., Zelter, A., Davis, T. N. & Agard, D. A. *Localization and orientation of the γ-tubulin small complex components using protein tags as labels for single particle EM.* J. Struct. Biol. 168 pp 571–574. 2009.

[83] Kollman, J. M., Polka, J. K., Zelter, A., Davis, T. N. & Agard, D. A. *Microtubule nucleating γ-TuSC assembles structures with 13-fold microtubule-like symmetry*. Nature, 466 pp 879–882. 2010.

[84] Guillet, Valérie, et al. *Crystal structure of γ-tubulin complex protein GCP4 provides insight into microtubule nucleation*. Nature structural & molecular biology, 18.8 pp 915-919. 2011.

[85] Jordan MA, Wilson L (2004) Microtubules as a target for anticancer drugs. Nat Rev Cancer 4: 253–265.

[86] Bouissou A, Verollet C, Sousa A, Sampaio P, Wright M, et al. *{gamma}-Tubulin ring complexes regulate microtubule plus end dynamics.* J Cell Biol, 187 pp 327–334. 2009.

[87] Haren L, Remy MH, Bazin I, Callebaut I, Wright M, et al. *NEDD1-dependent recruitment of the gamma-tubulin ring complex to the centrosome is necessary for centriole duplication and spindle assembly.* J Cell Biol, 172 pp 505–515. 2006.

[88] Tillement V, Haren L, Roullet N, Etievant C, Merdes A. *The centrosome protein NEDD1 as a potential pharmacological target to induce cell cycle arrest*. Mol Cancer, 8 pp 10. 2009.

[89] Bottegoni G, Favia AD, Recanatini M, Cavalli A. *The role of fragment based and computational methods in polypharmacology*. Drug Discov Today, 17 pp 23–34. 2012.

[90] Whitehurst AW, Bodemann BO, Cardenas J, Ferguson D, Girard L, et al. *Synthetic lethal screen identification of chemosensitizer loci in cancer cells*. Nature 446 pp 815–819. 2007.

[91] Lo¨we, J., Li, H., Downing, K.H., and Nogales, E. *Refined structure of alpha beta-tubulin at 3.5 A resolution.* J. Mol. Biol., 313 pp 1045–1057. 2001.

[92] Aldaz, H., Rice, L.M., Stearns, T., and Agard, D.A. *Insights into microtubule nucleation from the crystal structure of human gamma-tubulin*. Nature, 435 pp 523–527. 2005.

[93] Alushin, Gregory M., Gabriel C. Lander, Elizabeth H. Kellogg, Rui Zhang, David Baker, and Eva Nogales. *High-Resolution Microtubule Structures Reveal the Structural Transitions in αβ-Tubulin upon GTP Hydrolysis*. Cell, 157 pp 1117-1129. 2014.

[94] Friesen DE, Barakat KH, Semenchenko V, Perez-Pineiro R, Fenske BW, et al. *Discovery of small molecule inhibitors that interact with gamma-tubulin.* Chem Biol Drug Des, 79 pp 639–652. 2012.

[95] Ye K, Ke Y, Keshava N, Shanks J, Kapp JA, Tekmal RR, Petros J, Joshi HC. *Opium alkaloid noscapine is an antitumor agent that arrests metaphase and induces apoptosis in dividing cells.* Proc Natl Acad Sci USA, 95 pp 1601-1606. 1998.

[96] Naik PK, Chatterji BP, Vangapandu SN, Aneja R, Chandra R, Kanteveri S, Joshi HC. *Rational design, synthesis and biological evaluations of amino-noscapine: a high affinity tubulin-binding noscapinoid.* J Comput Aided Mol Des, 25 pp 443–454. 2011.

[97] Zhou J, Panda D, Landen JW, Wilson L, Joshi HC. *Minor alteration of microtubule dynamics causes loss of tension across kinetochore pairs and activates the spindle checkpoint*. J Biol Chem, 277 pp 17200–17208. 2002.

[98] Zhou J, Gupta K, Yao J, Ye K, Panda D, Giannakakou P, Joshi HC. *Paclitaxel-resistant human ovarian cancer cells undergo c-Jun NH_2-terminal kinase-mediated apoptosis in response to noscapine*. J Biol Chem, 277 pp 39777-39785. 2002

[99] Aneja R, Asress S, Dhiman N, Awasthi A, Rida PCG, Arora AK, Zhou J, Glass JD, Joshi HC. *Non-toxic melanoma therapy by a novel tubulin-binding agen*t. Intl J Cancer, 126 pp 256-265. 2010.

CHAPTER 2

INSIGHT INTO γ-γ TUBULIN LATERAL INTERACTIONS OF THE γ-COMPLEX RING

Abstract

γ-tubulin is essential for the nucleation and organization of mitotic microtubules in dividing cells. It is localized at the microtubule organizing centers and mitotic spindle fibres and experimentally observed to interact with the minus end of microtubules. The most well accepted hypothesis for the initiation of microtubule polymerization is that αβ-tubulin dimers add onto a γ-tubulin ring complex (γTuRC), in which adjacent γ-tubulin subunits bind to the underlying non-tubulin components of the γTuRC. This template thus determines the resulting microtubule lattice. In this study we use molecular modelling and molecular dynamics simulations, combined with computational MM-PBSA/MM-GBSA methods, to determine the extent of the lateral atomic interaction between two adjacent γ-tubulins. To do this we simulated γ-γ homodimer complex for 10 ns and calculated the ensemble average of binding free energy of -107.76 kcal/mol by the MM-PBSA method and -87.12 kcal/mol by the MM-GBSA method. These highly favourable binding free energy values imply robust lateral interactions between γ-tubulin subunits in addition to their end-interactions longitudinally with other proteins of γTuRC and γ-tubulin of the tubulin dimer. Next we identified the hot spot amino acids that play key role in the γ-γ interactions by computational alanine scanning mutagenesis and free energy decomposition per residue. Experimental mutagenesis validated these hot spot amino acids. The results from the experimental findings were consistent with the theoretical calculations and offer important insights on the mechanism of interaction between the γ-tubulin homodimers.

2.1 INTRODUCTION

γ-tubulin is a small globular protein and is most noticeably localized at the microtubule organization centers (MTOC) in eukaryotes [1-6]. γ-tubulin was first discovered by Oakley and Oakley, in Aspergillus as the third member of the tubulin super-family [7]. Unlike α and β-tubulins, γ-tubulin does not polymerize into the microtubule lattice, but is instead recruited to the microtubule organizing centers [5, 6]. Microtubules, composed primarily of αβ-tubulin heterodimers, are key component of mitotic spindle apparatus that is necessary for the alignment and subsequent segregation of duplicated chromosomes into daughter cells during cell division. They play a vital role in many other cellular functions including cell polarity, cell motility, transport of intracellular organelles, and maintenance of the overall cellular morphology. Such a myriad of roles calls for a very rapid reorganization. Microtubule assemblies, obtained *in vitro* from purified tubulin, differ from microtubule assemblies formed *in vivo* both in structure as well the constrained manner in which new microtubules are initiated [8]. *In vitro*, disassembly is energetically favored over the assembly process until a critically large oligomer is formed [9]. Cells overcome this slow initial phase of the assembly process by providing specific nucleation sites called microtubule organization centers, which in most animal cells is a centrosome [10]. Experimental methods have shown that γ-tubulin interacts with the minus end of the microtubules to facilitate microtubule nucleation [11]. γ-tubulin is present at the MTOC in a complex called γ-tubulin small complex (γTuSC), which is composed of two copies of γ-tubulin and one copy each of gamma complex protein 2 (GCP2) and gamma complex protein 3 (GCP3) [12]. Multiple copies of γTuSC along with GCP4, GCP5 and GCP6 associate together to form γ-tubulin ring complex (γTuRC) in eukaryotes as a unit for microtubule assembly nucleation [13]. Among the multiple proposed hypothetical models, the 'template model' is widely accepted that presents a ring of γ-tubulin on top of the γTuRC as the template. In this model each γ-tubulin subunit interacts longitudinally with the α/β-tubulin subunits to form microtubules lattice and laterally with another γ-tubulin unit. Nevertheless the mode and mechanism of interaction of γ-tubulin with α/β-tubulin as well as γ-tubulin is not clearly described. Therefore, in the present study we have made an attempt to explore the molecular basis of γ-γ tubulin lateral interactions. Agard *et al.* (2008) deciphered the crystal form of γ-tubulin bound to GDP (PDB: 3CB2, Res: 2.3Å) that contained two subunits of γ-

tubulin, pointing towards the existence of γ-tubulin in the form of dimer *in vivo* [9]. Hence, the interaction between the two γ-tubulin units in the dimer were studied utilizing *in silico* molecular modelling and molecular dynamics (MD) methods followed by further validation using experimental methods. Molecular dynamics is one of the predominant approaches to theoretically study bio-molecules. It allows the study of time dependent behaviour of molecular systems computationally and furnishes a wealth of thermodynamic and energetics information. Therefore, in recent years, MD simulation has gained lot of popularity in elucidating protein–protein interactions [14-19]. The robustness of protein–protein interactions have been quantified in terms of binding free energy. Binding free energies in solution can be calculated using the molecular mechanics Poisson Boltzman solvation area (MM-PBSA) and molecular mechanics generalized Born solvation area (MM-GBSA) approaches [20-23]. Generalized Born (GB) model has been successfully used to determine the energy contributions of each residue in the complex to identify the binding hot spot amino acids [14-16, 24]. To verify binding hot spots virtual alanine scanning might be employed to obtain the difference in the free energy of binding between the alanine mutants and the wild types. Therefore in this endeavour we elucidated the protein-protein interactions between adjacent γ-tubulin using molecular dynamics simulations followed by MMPB/GBSA and *in silico* alanine scanning mutation analyses. Findings were further validated using computational and experimental alanine scanning mutation analyses.

2.2 MATERIAL AND METHODS

2.2.1 Computational Methods

2.2.1.1 Molecular system

The initial co-ordinates of γ-tubulin homodimer (PDB_ID:3CB2, Res: 2.3Å) [9] were obtained from Protein DataBank (PDB). The structure contained two chains of γ-tubulin (‘A’ and ‘B’) with 446 amino acids each. During the initial screening of the γ-tubulin dimer many errors such as missing residues and missing side chains were observed. Therefore, it was imperative to fix these structural anomalies before proceeding with further molecular modelling calculations. Forty three residues of chain A and 51 residues of chain B were found to be missing and this resulted in gaps in the crystal structure. To reconstitute the homodimer only the ‘A’ chain was used from the

crystal structure. In the 'A' chain 14 residues were missing from three different locations (278-283, 311-312 and 367-371) while remaining 15 residues were missing from the terminals (1 from N terminal and 14 from C terminal). The three non-terminal gaps were filled following homology modelling using multiple templates in Prime (version 3.0, Schrödinger).

The modelled structure was subjected to energy minimization in Macromodel (version 9.9, Schrödinger) using Polak-Ribiere Conjugate Gradient (PRCG) algorithm and OPLS 2005 force field with a gradient of 0.001 kcal/mol and 1000 steps of iterations. The resultant structure was then optimized using protein preparation wizard (PPrep, Schrödinger). Missing side chains were filled using Prime (version 3.0, Schrodinger). The structure obtained was energy minimized using OPLS 2005 force field with PRCG algorithm. The minimization was stopped either after 5,000 steps or after the energy gradient converged below 0.001 kcal/mol.

To further refine the structure, a small run of all atom Molecular Dynamics (MD) simulations was carried out for 1000 ps with a time step of 2 fs on the modelled structure using Gromacs package (Version 4.5.4) [25]. The simulations were set up with Gromos96 force field, in a dodecahedron solvation box at a distance of 12Å from the periphery of the protein with simple point charges (spc216 model) of water molecules, using periodic boundary conditions [26]. Particle-Mesh-Ewald algorithm was employed to calculate the electrostatic interactions between atoms [27, 28]. The Lenard-Jones and electrostatic interaction cut-off were set at 1.0 nm distance. LINCS algorithm was used to constraint the bond lengths [29]. Prior to the 1000 ps MD Simulation the molecular system was neutralized with 9 Na+ ions, energy relaxed using steepest descent algorithm for 1000 steps and then equilibrated for 100 ps of MD run. An average structure was generated using the last 200 frames from the total of 1000 frames generated during MD simulation. The γ-dimer was than reconstituted by substituting the coordinates from the refined structure of 'A' chain onto the original crystal structure, preserving the original geometry and orientation (Figure 2.1). Furthermore, the γ-γ dimer obtained was energy minimized. The overall quality of the reconstituted γ-γ homodimer was determined using PROCHECK [30, 31], ERRAT [32] and VERIFY3D [33].

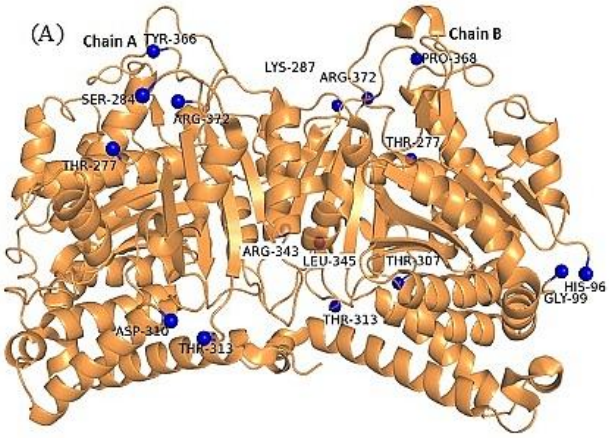

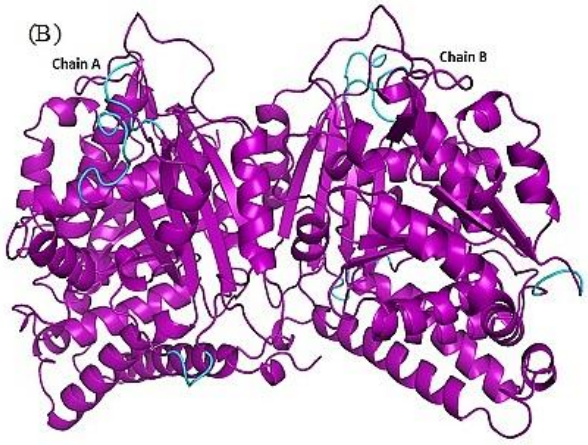

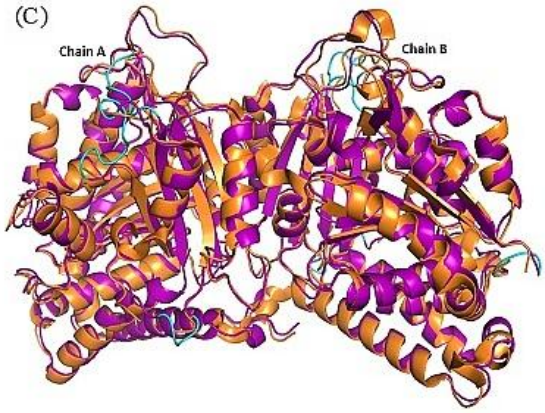

(D)

	Crystal structure of γ-γ dimer (3CB2)	Refined structure of γ-γ dimer
Verify3D	88.91%	91.93%
Errat	96	91.44
Ramachandran plot:		
Allowed region	99.7%	99.7%
Disallowed region	0.3%	0.3%

Figure 2.1: Crystal structure of γ-γ dimer and its refined structure. Panel 'A' shows the crystal structure of γ-γ dimer (PDB ID: 3CB2) with gaps. Gap flanking residues are shown as blue spheres. Panel 'B' shows the refined structure of γ-γ dimer. A total of 14 missing residues were added and these can be seen in cyan colour. Panel 'C' shows the refined structure of γ-γ dimer (purple) superimposed over the initial crystal structure of γ-γ dimer obtained from 3CB2 (orange); calculated RMSD was 0.73Å. Panel 'D' gives the structure quality parameters of both the wild type and refined structure of γ-γ dimer.

2.2.1.2 Molecular dynamics simulations of the γ-γ complexes

In order to study the molecular interactions in γ-γ complex, the dimer structure reconstituted above was simulated using Molecular Dynamics in Amber 11.0 and Ambertools 1.5 [34, 35]. The proteins were prepared for simulations using Leap program implemented in Ambertools. In leap, AMBER ff99SB [36, 37] force fields were assigned to proteins, hydrogens were added, counter ions were added to neutralize the system and protein system was solvated using TIP3P water model in an octahedral box with a span of 15.0 Å from the periphery of the protein [38]. The molecular system was made to go through three consecutive rounds of energy minimizations to relax the molecular system and to remove any disallowed "bad" contacts. In each 1000 step minimization, protein was first minimized for 500 steps using steepest descent method followed by 500 steps using conjugate gradient with a

time step of 2 fs. In the first and second rounds positions restraints of 10 $kcal^{-1}Å^{-2}$ and 2 $kcal^{-1}Å^{-2}$ respectively, were imposed on the protein system to allow relaxation of solvent molecules. Third minimization was carried out with no restraints. The system was gradually heated from 0 to 300 K after which was density equilibrated for 100 ps. The system was then equilibrated for 500 ps at 300 K and 1 atm pressure. After all the thermodynamic properties were stabilized, the molecular system was simulated for 10 ns with a time step of 2 fs. For MD simulations, isobaric (NPT) conditions were maintained with the target pressure of 1 bar utilizing the Berendsen barostat [39]. The temperature was regulated using Langevin thermostat. All electrostatic interactions were described using Particle Mesh Ewald (PME) [27, 28] method and all bonds were constrained using Shake algorithm [29]. The non-bonded cutoff distance was kept at 10Å. Co-ordinates were written to the trajectory file every 2 ps to obtain a total of 5000 frames. All trajectories were analysed using PTRAJ program implemented in ambertools [40].

2.2.1.2 Theoretical binding affinity calculation

The calculation of binding free energy in solvation, between the γ-tubulin units in the dimer was determined using the conventional MM-PBSA and MM-GBSA approaches described in Amber 11 [20, 41]. Out of the total 5000 frames obtained during MD simulation 250 frames were extracted every 20 ps from last 5 ns of the MD trajectory for calculation of the ensemble average of binding free energy. The binding free energy was calculated considering each molecular species (complex, receptor and ligand) and the binding free energy was calculated as follows.

$$\Delta G_{bind} = \Delta G_{complex} - [\Delta G_{protein} + \Delta G_{lig}]$$

The free energy, G, for each molecular species was calculated by the following MM-PBSA and MMGBSA methods described in Amber:

Gibbs's free energy (G) for each molecular species was calculated as follows:

$$G = E_{gas} + G_{sol} - TS$$

T and S are the temperature and the total solute entropy, respectively. E_{gas} describes the gas phase energy and represents the sum of internal energy, van der Waals interaction energy and electrostatic interaction energy. It is calculated using parameters described in the Amber FF99SB force fields [36, 37].

$$E_{gas} = E_{int} + E_{ele} + E_{vdw}$$

G_{sol} describes the free energy of solvation and was calculated as the sum of polar and nonpolar solvation contributions as described below:

$$G_{sol} = G_{PB(GB)} + G_{sol\text{-}np}$$

$G_{PB(GB)}$ describes the polar solvation contribution and are obtained solving the Poisson Boltzman(PB) and Generalized Borne(GB) equations [20, 41].

Total polar interaction contributions were obtained as the sum of the electrostatic energy components and polar solvation components as given below:

$$G_{ele,PB(GB)} = E_{ele} + G_{PB(GB)}$$

The non-polar solvation contribution ($G_{sol\text{-}np}$) was estimated using 0.0072 kcal mol^{-1} $Å^{-2}$ as the value for constant γ and by determining the solvent-accessible surface area (SAS) using a water probe radius of 1.4Å [42].

$$G_{sol\text{-}np} = \gamma_{SAS}$$

Dielectric constants for solute and solvent were set to 1 and 80, respectively.

2.2.1.3 Energy decomposition and computational alanine scanning

Binding free-energy contributions of each residue at the protein-protein interaction interface were calculated using the GB model, implemented in Amber11, on the basis of 250 snapshots extracted every 20 ps from the last 5 ns of MD simulation trajectory [43, 44]. On the basis of individual contributions to the binding free energy of the complex, those amino acids contributed more significantly to the binding free energy (contribution > 2.0 kcal/mol) were identified as the hot spot amino acids [45-47]. These hot spot amino acids were believed to contribute most to the stability of complex and are significant for the γ-γ tubulin interaction.

To further study the energy contribution of these amino acids in the interaction of γ-γ tubulin, computational alanine scanning was performed. In this method an amino acid of interest is replaced with alanine and absolute binding free energy is recalculated. In our study the hotspot amino acids were mutated to alanine and binding free energies were calculated for the resulting mutated system using the MM-GBSA approach on the 250 snapshots extracted every 20 ps from the last 5 ns of MD simulation. Finally, the difference in the binding free energies of the mutant and wild type, $\Delta\Delta G_{bind}$, was computed as follows:

$$\Delta\Delta G_{bind} = \Delta G_{bind}\,[\text{Mutant}] - \Delta G_{bind}\,[\text{Wild Type}]$$

Positive values of $\Delta\Delta G_{bind}$ indicate the favourable contribution while negative values indicate unfavorable contributions.

2.2.1.4 Preparation of mutant structure of γ-γ tubulin homodimer

To further investigate the molecular interactions between γ-γ tubulin homodimer a stretch of polar amino acids (Arg339, Glu342, Arg343 and Lys344) was identified at the interface in the close vicinity of Arg341. Due to their polar nature and their location at the interface of the γ-γ dimer, this stretch of polar amino acids would play an important role in binding of two γ tubulin subunits. To precisely investigate the role of this stretch of amino acids in the binding of the γ-tubulin units, computational site directed mutagenesis was performed. In the refined structure of gamma tubulin, all five mentioned amino acids were mutated to alanine using Maestro interface in Schrodinger. The mutant structure was then optimized and energy minimized for 5,000 steps with OPLS 2005 force field and PRCG algorithm using PPrep (Schrödinger). Furthermore, a 10 ns MD simulation was performed on the resultant structure in Amber keeping the method and parameters consistent with those used for the wild type. After 10 ns simulation, the ensemble average of the theoretical binding affinity was calculated for the last 5 ns mutant complex trajectories using the MM-PBSA and MM-GBSA methods.

2.2.2 Experimental methods

2.2.2.1 Experimental alanine scanning mutation and phenotypes

pALTER-EX1 vector (Promega, Madison, WI) was used to subclone *TUBG1* cDNA into the *NdeI* site downstream from the SP6 promoter to create pTWH101 as described by Hendrickson et al. [48]. Based on our findings from the molecular modelling methods, a stretch of five polar amino acids (Arg339, Arg341, Glu342, Arg343 and Lys344) that contributed significantly to the lateral γ-γ tubulin interactions was identified. These amino acids were mutated to alanine by oligonucleotide-directed mutagenesis using pTWH101 as the template. pALTER-EX1 contains a tetracycline resistance gene and an inactivated ampicillin resistance gene. The ampicillin-repair oligonucleotide restores the activity of the inactivated AmpR gene, and the tetracycline knockout oligonucleotide inactivates the TetR gene. This schema, i.e., inactivation of the TetR gene and the activation of the AmpR gene, provided a rapid method for

selecting potential alanine-scanning mutants. Because contiguous alanine codons can be used to create a *PstI* site, we used *PstI* digestion to further screen for potential alanine-scanning mutants. We then verified the mutated sequences that represented the only differences between the mutant (*tubg1*) and the wild type (*TUBG1*).

The yeast expression plasmids were constructed by subcloning each of the *tubg1* alleles into pREP1 at the *NdeI* site downstream of the *nmt1+* promoter [49, 50]. Wildtype cells [51] were transformed with either one of the *tubg1*-pREP1 plasmids or the control *TUBG1*-pREP1 and grown in minimal media supplemented with adenine, histidine, and uracil. Transformants were screened at 18 and 36 °C to identify conditional mutants in the presence of endogenous γ-tubulin. The strains were maintained at 30 and 26 °C, respectively. A diploid strain, NC377 [4, 52], bearing one endogenous wild-type copy of *S. pombe* γ-tubulin, *gtb1+* and one disrupted copy, *gtb1::ura4+*, was also transformed with the mutant plasmids. The resulting yeast transformants were randomly sporulated and selected for *ura+*, *leu+*, and the spores were tested for conditional growth.

2.3 RESULTS AND DISCUSSION

2.3.1 Refinement of γ-γ tubulin dimer structure

The original crystal structure of γ-γ tubulin dimer (PDB ID: 3CB2, 2.3 Å) has missing amino acids (we called as gaps) at certain places (Figure 2.1 A). These gaps were filled based on the homology model building and the γ-γ tubulin dimer was reconstituted and refined further by performing 10 ns MD simulation (Figure 2.1B and 2.1C). The overall quality of the model obtained, stereo-chemical values and non-bonded interactions were tested using PROCHECK, ERRAT and VERIFY3D. The PROCHECK results showed 99.2% of backbone angles are in allowed regions with G-factors of - 0.25. Ramachandran plot analysis revealed only 0.3% residues in the disallowed region (Figure 2.1D). ERRAT is an "overall quality factor" calculator program for non-bonded atomic interactions. The accepted range in ERRAT is 50 and higher scores indicate the precision of the model. In the case of γ-γ tubulin dimer, the ERRAT score was 91.43% that is within the range of high quality model. Similarly, the VERIFY 3D score of 91.93 indicates a good quality model.

2.3.2 Structural stabilities from MD simulations

To decipher the molecular insight of the interaction of γ-γ tubulin dimer we have performed MD simulation of 10 ns. The relative fluctuation in the root-mean-square deviations (RMSDs) of the Cα atoms of γ-γ tubulin dimer is very small after the initial equilibration (~4 ns), demonstrating the stability of the molecular system (Figure 2.2).

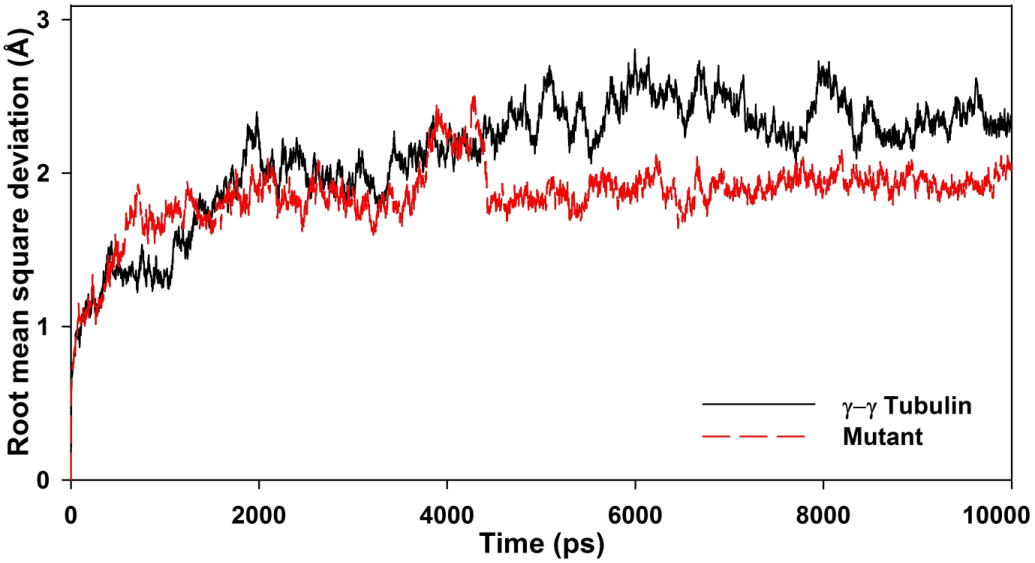

Figure 2.2: Root mean square deviation of γ-γ tubulin complex and mutant complex with respect to time over 10,000 picoseconds.

To further test the convergence of the system we have monitor the root mean square fluctuation (RMSF) of the amino acids. As can be seen from Figure 2.3, the fluctuations of individual amino acids are very small (< 3.0 Å) along the whole trajectory except 2 amino acids: Arg285 and Tyr365 (with RMSF > 3.0 Å) in chain 'A' and Val285, Arg311 and Gln312 (with RMSF > 3.0 Å) in chain 'B'. The small fluctuation in RMSF reveals that the system is stable during the monitored molecular dynamics simulation.

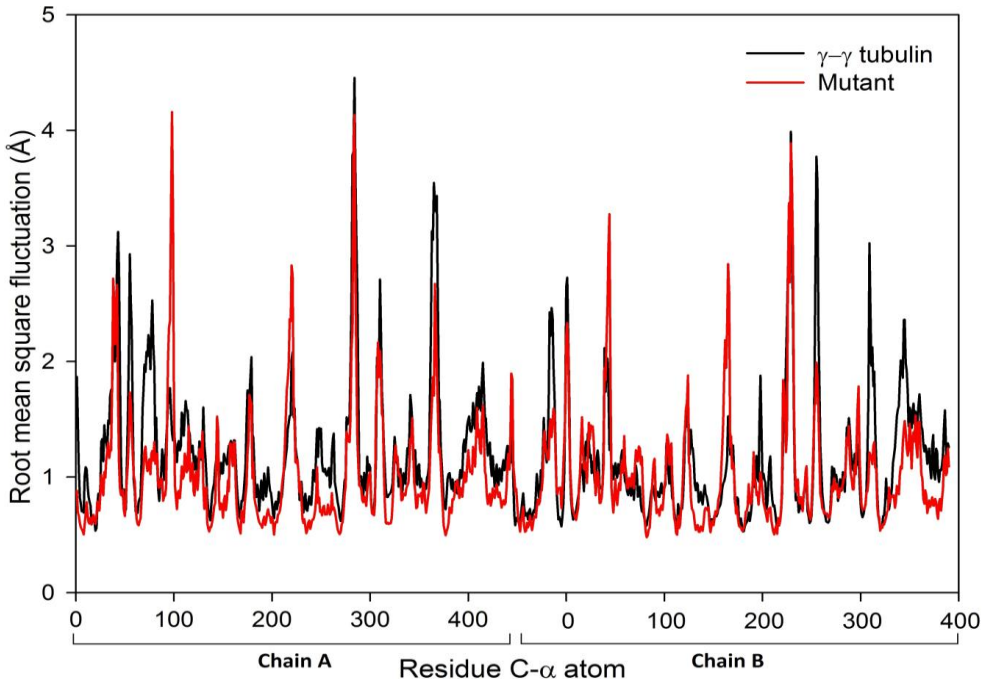

Figure 2.3: Root mean square fluctuations of residue Cα atom over 10,000 picosecond.

2.3.3 Analysis of calculated binding free energy

The molecular interaction and binding free energy between γ-γ tubulin dimer was calculated based on MM-PBSA and MM-GBSA of the MD trajectories. Both the methods indicated very robust interactions between the two γ-tubulin subunits (Table 2.1). The ensemble average of binding free energy using MM-PBSA and MM-GBSA was determined as -107.76 kcal/mol and -87.12 kcal/mol. The difference in the values obtained could be attributed to the calculated polar solvation energy which was 749.15 kcal/mol obtained by MM-GBSA, higher than 726.91 kcal/mol as obtained using MM-PBSA. Energy value was calculated as the average value of 250 snapshots, generated every 10 ps, from the last 5 ns of the MD trajectory. All molecular interactions in polar solvent are guided by polar (the polar interaction, $\Delta G_{(ele,PB/GB)} = \Delta E_{ele} + \Delta G_{(PB/GB)}$) and non-polar energy components. The non polar component generally yields a more favourable contribution as compared to the polar component to the molecular interactions as the non-polar residues have the tendency to bury themselves in the hydrophobic pockets allowing the water in the binding site to displace [53]. However, these non-polar forces are not strong enough to steer the association of two proteins.

Table 2.1: Ensemble average of binding free energy (kcal/mol) of γ-γ tubulin complex calculated using the MM-GBSA and MM-PBSA methods in Amber

Contribution	γ-γ Complex	Mutant γ-γ
ΔE_{int}	0.00	0.00
ΔE_{vdw}	-158.10	-155.06
ΔE_{ele}	-676.57	410.33
ΔE_{gas}	-834.67	255.27
ΔG_{sol-np}	-18.70	-17.68
ΔG_{PB}	745.61	-324.61
$\Delta G_{solv, PB}$	726.91	-342.28
$\Delta G_{ele, PB}$	69.04	85.72
$H_{tot, PB}$	-107.76	-87.02
ΔG_{GB}	770.11	-316.08
$\Delta G_{solv, GB}$	749.15	-335.44
$\Delta G_{ele, GB}$	93.55	94.25
$H_{tot, GB}$	-85.52	-80.17

Therefore charge residues are often found to be located at the protein-protein interaction interface as they play a key role in electrostatic steering which can be explained as a long range electrostatic mechanism that might lead to recognition of the binding interface [54]. As evident from Table 2.1, though the Coulombic contributions ΔE_{ele} of -676.57 kcal/mol are highly favourable to binding, they cannot compensate the large penalty imposed by the desolvation component ($\Delta G_{PB/GB}$) of 745.61 kcal/mol and 770.11 kcal/mol as calculated by MM-PBSA and MM-GBSA, respectively. The non-polar components comprising of van der Waals interaction contribution (ΔE_{vdw}) and the non-polar solvation contribution (ΔG_{sol-np}) were estimated to be highly favourable with the values of -158.10 kcal/mol and -18.70 kcal/mol respectively. This highly favourable non-polar component might explain the solute–water dispersion and the hydrophobic effects.

2.3.4 Decomposition of the binding free energy into the per residue contribution

To further understand the γ-γ interactions at the atomic level, binding free energy contributions were determined for each residue in the γ-γ complex using the MM-GBSA method and plotted in Figure 2.4. The residues having a contribution of more than 2 kcal/mol were designated as hot spot amino acids and they were positioned to contribute most to the stability of the γ-γ complex. As an example Asp252, Met249, His334 of chain ‘A’ and Arg341, Met249, Asp252 of chain ‘B’ make very high free energy contributions > 4 kcal/mol hence, making considerably large

contribution to the overall binding free energy of the complex. In addition to these residues, seven more residues of chain 'A' (Arg341, Arg265, Trp446, Ile 444, Tyr443, Pro353, Asn250) and nine amino acid residues of chain 'B' (Arg265, Hie334, Tyr443, Gln357, Lys164, Pro353, Val358, Ile444, Trp446) show high energy contribution > 2 kcal/mol. Significantly, all the hot spot amino acids were observed to lie at the γ-γ complex interface (Figure 2.5). Furthermore, to determine the detailed contribution of each important residue, the binding energy was decomposed into several other components like the electrostatic, van der Waals, solvation and total contribution (Table 2.2). Most hot spot amino acids like Met249, Asn250, Arg265, Trp446 of chain 'A' and Met249, His334, Trp446 of chain 'B' were observed to make significant non-polar contributions (> 4 kcal/mol). However, some residues like Asp252, Arg265 of chain 'A' and residues Lys164, Asp252, Arg265 and Arg341 of chain 'B' were observed to make considerable polar contributions (> 2 kcal/mol) (Figure 2.6).

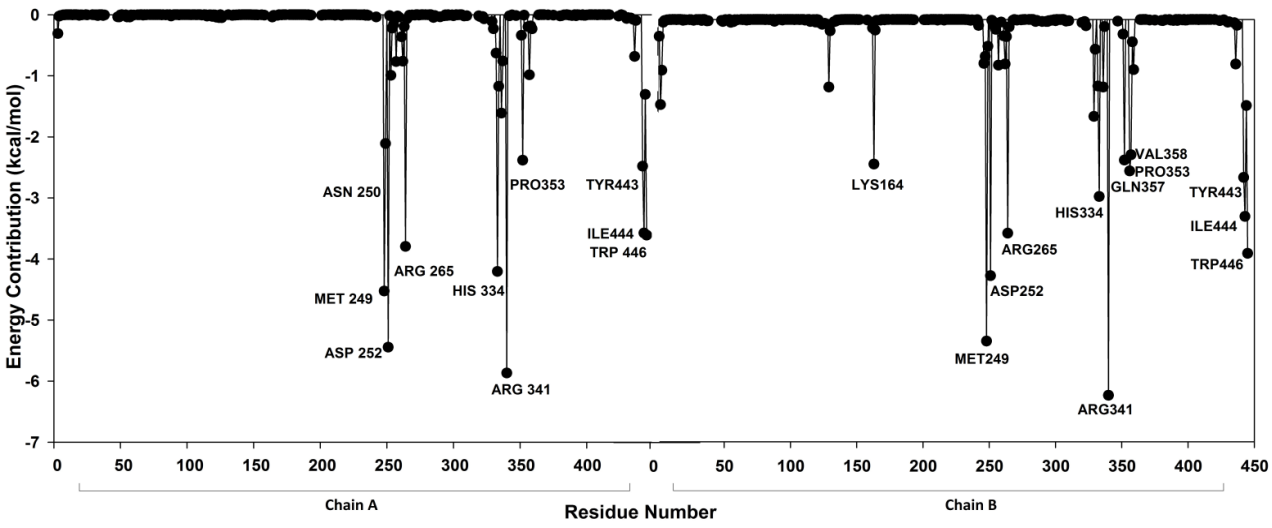

Figure 2.4: Per residue energy contribution of amino acids to the stability of γ-tubulin dimer, calculated using the MM-GBSA method.

Table 2.2 Decomposition of calculated $\Delta G_{bind,\,GB}$ (kcal/mol) on per residue basis into van der Waals, electrostatic, polar solvation and non-polar solvation energy components.

	Residue	$\Delta E_{i,vdw}$	$\Delta E_{i,ele}$	$\Delta G_{i,sol\,GB}$	$\Delta G_{i,sol\text{-}np}$	$\Delta H_{i,tot,GB}$
Chain A	MET249	-6.93	-4.61	8.20	-1.19	-4.53
	ASN250	-4.80	-12.12	15.63	-0.83	-2.11
	ASP252	-0.50	-40.48	35.85	-0.31	-5.45
	ARG265	-0.34	-66.03	62.85	-0.27	-3.80
	HIE334	-4.92	1.26	0.21	-0.75	-4.20
	ARG341	-2.91	-101.40	101.24	-0.80	-3.87
	PRO353	-2.39	-2.60	3.12	-0.50	-2.38
	TYR443	-3.44	-2.16	3.48	-0.36	-2.48
	ILE 444	-3.11	-2.51	2.51	-0.47	-3.58
	TRP 446	-6.72	49.44	-45.05	-1.28	-3.61
Chain B	LYS164	-0.07	5.71	-7.90	-0.14	-2.40
	MET249	-6.45	-3.78	6.07	-1.18	-5.33
	ASP252	-0.66	-24.97	21.49	-0.11	-4.25
	ARG265	-0.51	-67.09	64.34	-0.28	-3.54
	HIE334	-4.39	-3.34	5.51	-0.72	-2.93
	ARG341	-1.24	-102.51	98.15	-0.63	-6.23
	PRO353	-2.33	-2.75	3.23	-0.49	-2.33
	GLN357	-1.63	-6.28	5.65	-0.25	-2.51
	VAL358	-2.08	-2.73	2.78	-0.22	-2.24
	TYR443	-3.61	-2.14	3.53	-0.40	-2.62
	ILE 444	-2.89	-2.34	2.42	-0.45	-3.27
	TRP446	-6.94	49.51	-45.12	-1.34	-3.88

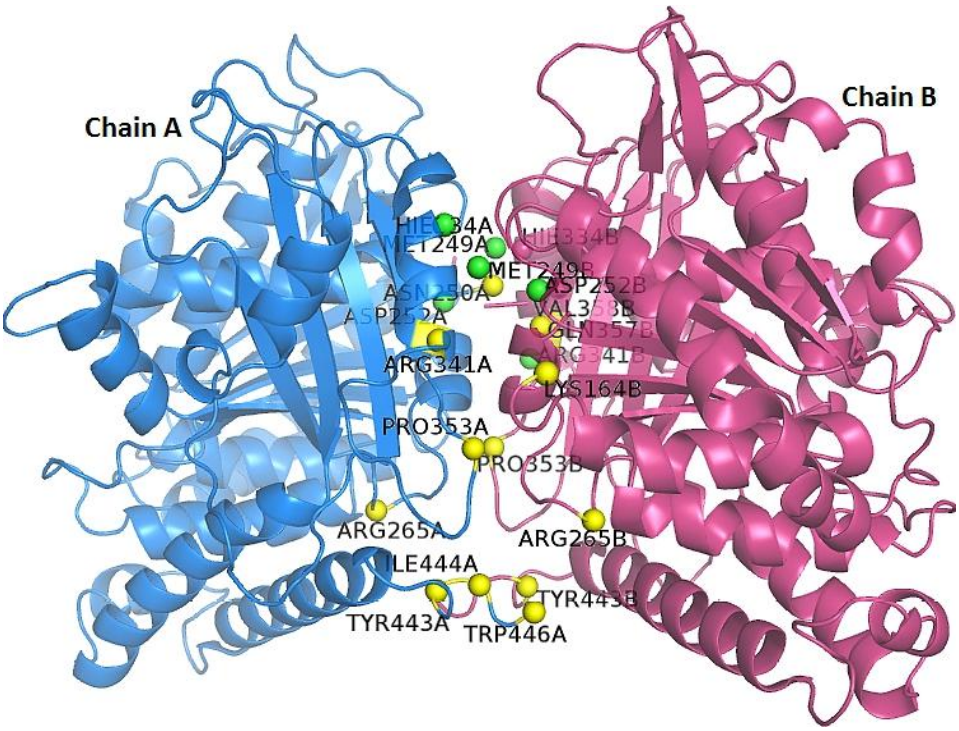

Figure 2.5: Hot spot amino acids to the stability of the γ-γ tubulin dimer calculated using the MM-GBSA method. C-α atoms of amino acid residues contributing > 4 kcal/mol are marked green spheres while those with a contribution of 2-4 kcal/mol are marked yellow.

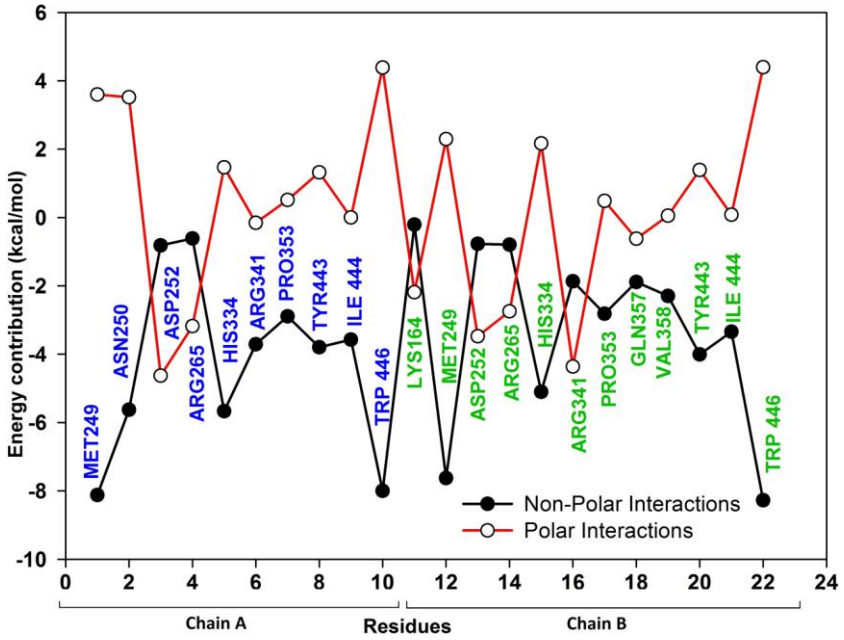

Figure 2.6: The polar and the non polar contributions of residues of chain A (labelled blue) and chain B (labelled green) in the γ-γ tubulin dimer calculated using MM-GBSA method.

Arginine is a versatile amino acid which is capable of forming different types of favourable interactions like hydrogen bond and salt bridge formation. Arg341 and Arg 265 of chain 'A' forms two hydrogen bonds with Asp252 and Trp446 of chain 'B', respectively, while Arg341 and Arg 265 of chain 'B' forms four hydrogen bonds each with Asp252 and Trp446 of chain 'A' (Figure 2.7). The occurrence of H-bond throughout the 10ns simulation is described in table 2.3.

Table 2.3: Occurrence (%) of H-bond between the two γ- tubulin units during the 10 ns MD simulation.

Chain	Donor Residue	Donor Atom	Chain	Acceptor residue	Acceptor atom	Occurrence (%)	Distance (Å)
A	Asp252	OD1	B	Arg341	NH1	81.1	2.9
		OD2			NH2	69.4	2.9
		OD1			NH2	71.5	3
		OD2			NH1	58.1	3.1
	Trp446	OXT		Arg265	NH2	56.6	2.9
		O			NH2	40	2.9
B	Gly247	O	A	His444	NE2	85.6	2.9
	Asp252	OD1		Arg3	NH1	93.6	2.8
		OD2		Arg341	NH1	92.3	2.9
		OD2			NH2	30.5	3
	Trp446	OXT		Arg265	NH2	48	2.9
		O			NH2	42	2.9

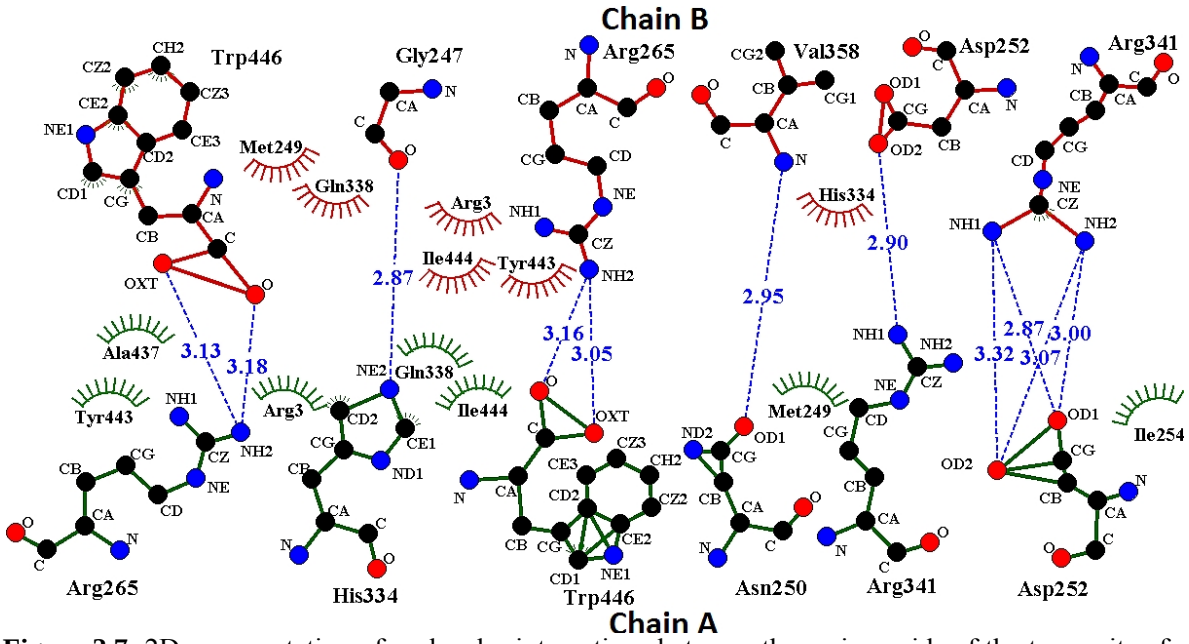

Figure 2.7: 2D representation of molecular interactions between the amino acids of the two units of γ-γ tubulin (chain 'A' and chain 'B'). Hydrogen bonding residues are shown in green and red for chain A and chain B, respectively. The Dashed lines denote hydrogen bonds, and numbers indicate hydrogen bond lengths in Å. Hydrophobic interactions are shown as arcs with radial spokes. The figures was made using Dimplot[55].

2.3.5 Computational alanine scanning

To further validate the contribution of hot spot amino acids identified above to binding free energy between γ-γ interactions we performed computational alanine scanning. Here we consider only those amino acids contributing binding free energy of > 4 kcal/mol. The method proposes that a minute local change in the protein does not affect the overall conformation of the protein-protein complex. The results obtained by the decomposition of the binding free energy and computational alanine scanning were found to be quite consistent and this indicates the reliability of our analysis. After performing computational alanine scanning in Amber for six hotspots which had contribution of > 4 kcal/mol to the overall binding free energy of the complex and recalculating the binding affinity, a substantial decrease in the binding affinity was observed. The mutation to alanine led to a decrease in the binding affinity, for each hot spots amino acid, at least by 4.8 kcal/mol, while for Asp252 of chain 'A' as well as Asp252 and Arg341 of chain 'B', the binding affinity was decreased by more than 10 kcal/mol using both MM-PBSA and MM-GBSA methods, thereby reducing the strength of γ-γ tubulin lateral association (Table 2.4). This reiterates that the hot spots amino acids identified in the interaction between γ-γ subunits are very crucial.

Table 2.4: Computational Alanine scanning results for hotspot residues, for which free energy contribution was high (> 4 kcal/mol), determined using MM-PBSA and MM-GBSA method, implemented in Amber.

S.No	Chain	Hot spot	$\Delta\Delta G_{GB}$	$\Delta\Delta G_{PB}$
1	A	Met249	6.43	6.15
2	A	His334	7.52	4.8
3	A	Asp252	17.49	25
4	B	Met249	6.75	5.74
5	B	Asp252	10.92	29.76
6	B	Arg341	13.37	16.59

2.3.6 Predicted binding free energy between mutant γ-γ subunits

To further validate the molecular interaction between γ-γ subunits we have modelled a mutant structure of γ-γ homodimer by mutating a stretch of 5 polar amino acids (Arg339, Glu342, Arg343 and Lys344) to Alanine neighbouring to Arg341 which contribute significantly in the binding free energy (Figure 2.8). Besides, Arg341 of chain 'B' has a tendency to form multiple H-bonds with Asp252 of chain 'A' at the binding interface. Hence calculated binding free energy of mutant γ-γ subunits as determined using both MM-PBSA and MM-GBSA methods led to substantial decrease in the total free energy of binding in comparison to wild type γ-γ homodimer. The Van der Waal's contribution was comparable for both wild type (-158.10 kcal/mol) and mutant (-155.06 kcal/mol) structures. However, the electrostatic contribution of the mutant structure was found to be less favourable (410.33 kcal/mol) compared to wild type (-676.57 kcal/mol). This was anticipated as the polar amino acids which contributed to the total electrostatic contribution were changed to Alanine. Since the electrostatic complementarity steers the complex formation and also determines the lifetime of association it was observed that the total binding affinity using the MM-GBSA (H_{tot}, GB) method was decreased from -85.52 kcal/mol, as calculated for the wild type γ-γ tubulin homodimer, to -80.17 kcal/mol for the mutant γ-γ tubulin homodimer, while the binding affinity using the MM-PBSA (H_{tot}, PB) method was decreased quite significantly from -107.76 kcal/mol, as calculated for the wild type, to -87.02 kcal/mol for the mutant γ-γ tubulin structure. There was noticeable rearrangement in the hydrogen bonding pattern between the mutant γ-tubulin units. In general, the number of hydrogen bonds decreased and this can be explained by the absence of Arg341 from both the γ-tubulin units (Figure 2.9).

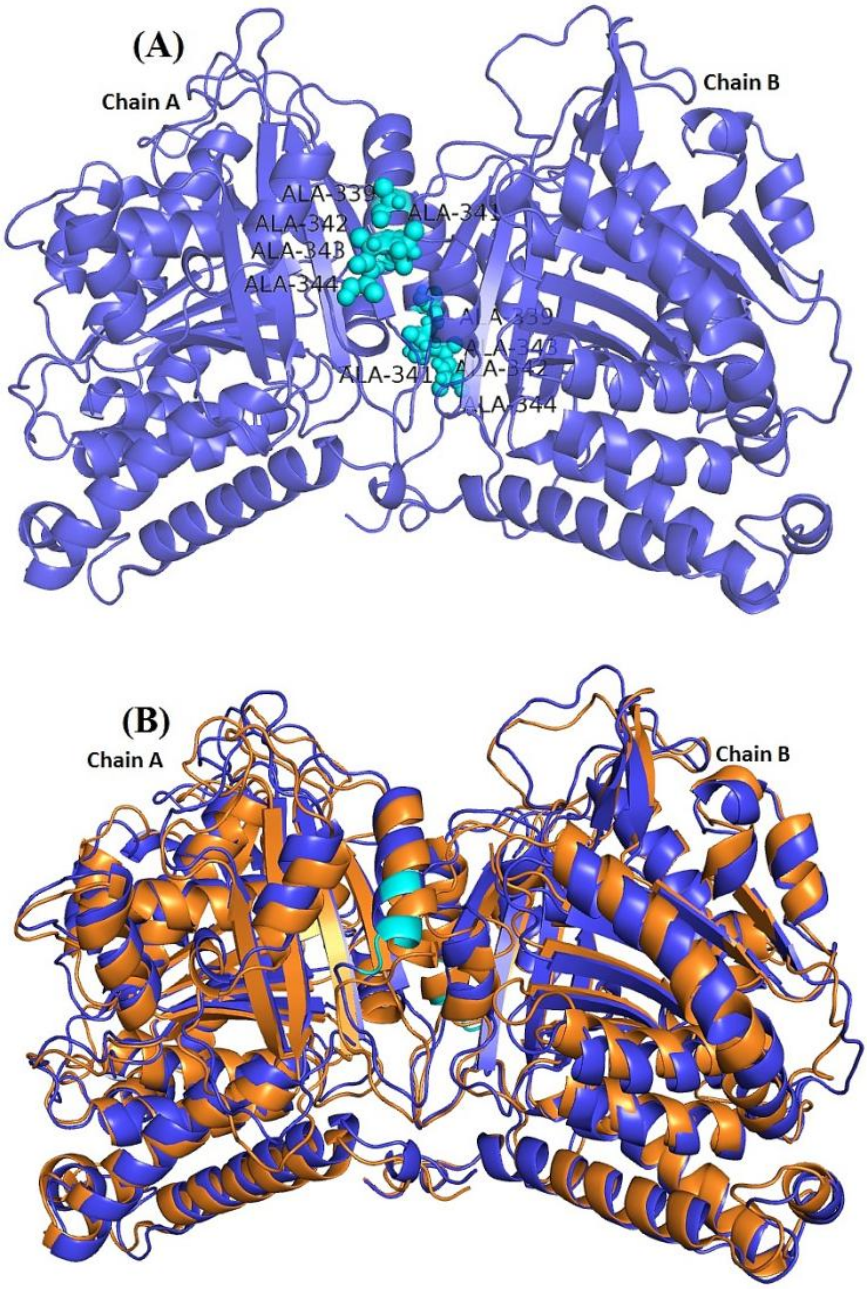

Figure 2.8. Mutant structure of γ-γ dimer. Panel 'A' shows the mutant structure of γ-γ dimer along with the residues mutated to alanine in cyan colour spheres. Panel 'B' shows the mutated structure of γ-tubulin dimer obtained after 10 ns MD simulation in Amber (blue) superimposed over the structure of wild type γ-tubulin dimer (Orange) obtained after 10 ns MD simulations in amber. Calculated RMSD was 1.75 Å.

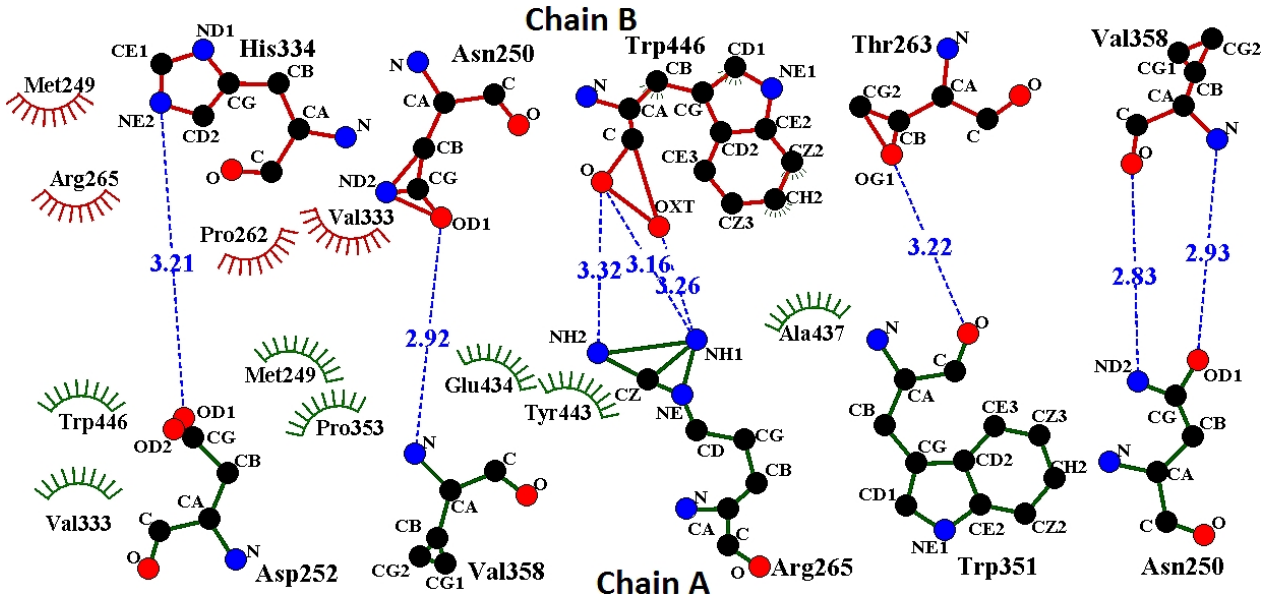

Figure 2.9: 2D representation of molecular interactions between the amino acids of the two mutated units of γ-γ tubulin (chain 'A' and chain 'B'). Hydrogen bonding residues are shown in green and red for chain A and chain B, respectively. The Dashed lines denote hydrogen bonds, and numbers indicate hydrogen bond lengths in Å. Hydrophobic interactions are shown as arcs with radial spokes. The figures was made using Dimplot [55].

2.3.7 Growth of Alanine scanning mutant in fission yeast and its phenotype

γ-tubulin, a highly evolutionarily conserved protein, is required for cell division and growth and its loss is lethal in yeast. However, some mutations that perturb γ-tubulin function produce conditional growth phenotypes [7, 48]. Since we were interested in identifying evolutionarily conserved features of γ-tubulin, we took advantage of the fact that the human γ-tubulin gene (*TUBG1*) can replace the fission yeast γ-tubulin (*gtb1*). Using alanine-scanning mutagenesis a series of γ-tubulin mutants, which targeted key residues predicted to be involved in protein-protein interactions, were generated. To test the effect of the alanine substitution on protein function haploid yeast cells, wild-type and *gtb1*-, were transformed with the alanine mutants. Wild-type *TUBG1* transformants served as controls. It was observed that the γ-γ tubulin mutant (*gtb1-/alanine-TUBG1*) was unable to support growth in the absence of endogenous *gtb1+* (referred to as recessive lethal). This might be attributed to the mutation of key polar residues to alanine that intercepted the molecular recognition between adjacent γ-tubulins which led to malformation of the γTuSC, γTuRC and hence the mitotic spindle.

2.4 CONCLUSION

In this study, the molecular basis of interaction between two lateral γ-tubulin units were elucidated by making extensive use of molecular mechanics and molecular dynamics techniques. A refined structure of γ-γ tubulin homodimer was obtained based on the initial co-ordinates from the PDB (PDB_ID:3CB2, Res: 2.3Å). The refined structure was MD simulated to obtain a 10 ns trajectory that was utilized to perform MM-PBSA/GBSA calculations and binding free-energy decomposition analyses in order to characterize interactions between two γ-tubulin units. MM-PBSA and MM-GBSA calculations revealed highly favourable non-polar component. Although some columbic contribution were found to be favourable and probably played a crucial role in the binding site recognition, the overall polar contribution was less significant to the overall binding free energy- due to penalty imposed by very large desolvation energy component. Therefore, the non-polar component was considered as the driver of the molecular interactions between γ-γ tubulin. Also, on the basis of per residue free energy decomposition a total of twenty two hot spot amino- acids were identified which were found to contribute highly (> 2 kcal/mol) to the binding affinity between the two γ-tubulins. Computational alanine scanning was carried out for six hot spot amino acids with high energy contribution (> 4 kcal/mol) resulted in a drop of at least 4.8 kcal/mol for each hotspot amino acid. On the basis of these findings, a mutant structure of γ-γ tubulin homodimer was obtained after mutating a stretch of five polar amino acids (Arg339, Arg341, Glu342, Arg343 and Lys344) to alanine. The results from MM-PBSA and MM-GBSA showed a significant drop in the binding affinity between γ-γ tubulin interactions. To test whether these mutant proteins can support life, experimental alanine scanning mutagenesis was performed and the cDNA encoding the mutant and the endogenous fission yeast γ-tubulin (*gtb1*) gene was replaced with the mutant γ-tubulin gene (*TUBG1*) in haploid cells. We found that the γ-γ tubulin mutant (*gtb1*-/alanine-TUBG1) that was predicted to disrupt interactions was unable to support growth in the absence of endogenous $gtb1^{+}$ (referred to as recessive lethal). These findings further reiterated that the hotspot amino acids identified using computational methods indeed play crucial essential role in γ-γ tubulin interactions, and when the key residues were mutated they could not support yeast cell division and growth. The observed phenotypes thus correlate well with our computer predictions of important residues for γ -tubulin interactions.

REFERENCES

[1] B.R. Oakley, C.E. Oakley, Y. Yoon, and M.K. Jung, "γ-Tubulin is a component of the spindle pole body that is essential for microtubule function in Aspergillus nidulans," *Cell*, vol. 61, (no. 7), pp. 1289-1301, 1990.

[2] Y. Zheng, M.K. Jung, and B.R. Oakley, "γ-Tubulin is present in Drosophila melanogaster and Homo sapiens and is associated with the centrosome," *Cell*, vol. 65, (no. 5), pp. 817-823, 1991.

[3] T. Stearns, L. Evans, and M. Kirschner, "γ-Tubulin is a highly conserved component of the centrosome," *Cell*, vol. 65, (no. 5), pp. 825-836, 1991.

[4] T. Horio, S. Uzawa, M.K. Jung, B.R. Oakley, K. Tanaka, and M. Yanagida, "The fission yeast gamma-tubulin is essential for mitosis and is localized at microtubule organizing centers," *Journal of cell science*, vol. 99, (no. 4), pp. 693-700, 1991.

[5] H.C. Joshi, M.J. Palacios, L. McNamara, and D.W. Cleveland, "γ-Tubulin is a centrosomal protein required for cell cycle-dependent microtubule nucleation," *Nature*, vol. 365, pp. 80-83, 1992.

[6] H.C. Joshi, "γ-Tubulin: The hub of cellular microtubule assemblies," *Bioessays*, vol. 15, (no. 10), pp. 637-643, 1993.

[7] C.E. Oakley and B.R. Oakley, "Identification of γ-tubulin, a new member of the tubulin superfamily encoded by mipA gene of Aspergillus nidulans," *Nature*, vol. 338, pp. 662-664, 1989.

[8] H. Sui and K.H. Downing, "Structural basis of interprotofilament interaction and lateral deformation of microtubules," *Structure*, vol. 18, (no. 8), pp. 1022-1031, 2010.

[9] L.M. Rice, E.A. Montabana, and D.A. Agard, "The lattice as allosteric effector: Structural studies of αβ-and γ-tubulin clarify the role of GTP in microtubule assembly," *Proceedings of the National Academy of Sciences*, vol. 105, (no. 14), pp. 5378-5383, 2008.

[10] E.B. Wilson, "The cell in development and heredity," 1928.

[11] Q. Li and H.C. Joshi, "gamma-tubulin is a minus end-specific microtubule binding protein," *The Journal of cell biology*, vol. 131, (no. 1), pp. 207-214, 1995.

[12] K. Oegema, C. Wiese, O.C. Martin, R.A. Milligan, A. Iwamatsu, T.J. Mitchison, and Y. Zheng, "Characterization of two related Drosophila γ-tubulin complexes that differ in their ability to nucleate microtubules," *The Journal of cell biology*, vol. 144, (no. 4), pp. 721-733, 1999.

[13] Y. Zheng, M.L. Wong, B. Alberts, and T. Mitchison, "Nucleation of microtubule assembly by a gamma-tubulin-containing ring complex," *Nature*, vol. 378, (no. 6557), pp. 578-583, 1995.

[14] H. Gohlke and D.A. Case, "Converging free energy estimates: MM-PB (GB) SA studies on the protein–protein complex Ras–Raf," *Journal of computational chemistry*, vol. 25, (no. 2), pp. 238-250, 2004.

[15] H. Gohlke, C. Kiel, and D.A. Case, "Insights into protein–protein binding by binding free energy calculation and free energy decomposition for the Ras–Raf and Ras–RalGDS complexes," *Journal of molecular biology*, vol. 330, (no. 4), pp. 891-913, 2003.

[16] V. Zoete, M. Meuwly, and M. Karplus, "Study of the insulin dimerization: Binding free energy calculations and per-residue free energy decomposition," *Proteins: Structure, Function, and Bioinformatics*, vol. 61, (no. 1), pp. 79-93, 2005.

[17] L. Michalik, V. Zoete, G. Krey, A. Grosdidier, L. Gelman, P. Chodanowski, J.N. Feige, B. Desvergne, W. Wahli, and O. Michielin, "Combined Simulation and Mutagenesis Analyses Reveal the Involvement of Key Residues for Peroxisome Proliferator-activated Receptorα Helix 12 Dynamic Behavior," *Journal of biological chemistry*, vol. 282, (no. 13), pp. 9666-9677, 2007.

[18] W.E. Stites, "Protein-protein interactions: interface structure, binding thermodynamics, and mutational analysis," *Chemical reviews*, vol. 97, (no. 5), pp. 1233-1250, 1997.

[19] V. Zoete and O. Michielin, "Comparison between computational alanine scanning and per-residue binding free energy decomposition for protein–protein association using MM-GBSA: Application to the TCR-p-MHC complex," *Proteins: Structure, Function, and Bioinformatics*, vol. 67, (no. 4), pp. 1026-1047, 2007.

[20] P.A. Kollman, I. Massova, C. Reyes, B. Kuhn, S. Huo, L. Chong, M. Lee, T. Lee, Y. Duan, and W. Wang, "Calculating structures and free energies of complex molecules: combining molecular mechanics and continuum models," *Accounts of chemical research*, vol. 33, (no. 12), pp. 889-897, 2000.

[21] A. Onufriev, D. Bashford, and D.A. Case, "Modification of the generalized Born model suitable for macromolecules," *The Journal of Physical Chemistry B*, vol. 104, (no. 15), pp. 3712-3720, 2000.

[22] J. Srinivasan, T.E. Cheatham, P. Cieplak, P.A. Kollman, and D.A. Case, "Continuum solvent studies of the stability of DNA, RNA, and phosphoramidate-DNA helices," *Journal of the American Chemical Society*, vol. 120, (no. 37), pp. 9401-9409, 1998.

[23] V. Tsui and D.A. Case, "Theory and applications of the generalized Born solvation model in macromolecular simulations," *Biopolymers*, vol. 56, (no. 4), pp. 275-291, 2000.

[24] V. Lafont, M. Schaefer, R.H. Stote, D. Altschuh, and A. Dejaegere, "Protein–protein recognition and interaction hot spots in an antigen–antibody complex: free energy decomposition identifies "efficient amino acids"," *Proteins: Structure, Function, and Bioinformatics*, vol. 67, (no. 2), pp. 418-434, 2007.

[25] B. Hess, C. Kutzner, D. Van Der Spoel, and E. Lindahl, "GROMACS 4: Algorithms for highly efficient, load-balanced, and scalable molecular simulation," *Journal of chemical theory and computation*, vol. 4, (no. 3), pp. 435-447, 2008.

[26] H. Berendsen, J. Postma, W. Van Gunsteren, and J. Hermans, "Intermolecular Forces, ed," *B. Pullman, Reidel, Dordrecht*, vol. 331, 1981.

[27] T. Darden, D. York, and L. Pedersen, "Particle mesh Ewald: An N· log (N) method for Ewald sums in large systems," *The Journal of chemical physics*, vol. 98, (no. 12), pp. 10089-10092, 1993.

[28] U. Essmann, L. Perera, M.L. Berkowitz, T. Darden, H. Lee, and L.G. Pedersen, "A smooth particle mesh Ewald method," *The Journal of Chemical Physics*, vol. 103, (no. 19), pp. 8577-8593, 1995.

[29] J.-P. Ryckaert, G. Ciccotti, and H.J. Berendsen, "Numerical integration of the cartesian equations of motion of a system with constraints: molecular dynamics of< i> n</i>-alkanes," *Journal of Computational Physics*, vol. 23, (no. 3), pp. 327-341, 1977.

[30] R.A. Laskowski, M.W. MacArthur, D.S. Moss, and J.M. Thornton, "PROCHECK: a program to check the stereochemical quality of protein structures," *Journal of applied crystallography*, vol. 26, (no. 2), pp. 283-291, 1993.

[31] G. Ramachandran, C.t. Ramakrishnan, and V. Sasisekharan, "Stereochemistry of polypeptide chain configurations," *Journal of molecular biology*, vol. 7, (no. 1), pp. 95-99, 1963.

[32] C. Colovos and T.O. Yeates, "Verification of protein structures: patterns of nonbonded atomic interactions," *Protein Science*, vol. 2, (no. 9), pp. 1511-1519, 1993.

[33] D. Eisenberg, R. Lüthy, and J.U. Bowie, "VERIFY3D: assessment of protein models with three-dimensional profiles," *Methods in enzymology*, vol. 277, pp. 396, 1997.

[34] D.A. Case, T.E. Cheatham, T. Darden, H. Gohlke, R. Luo, K.M. Merz, A. Onufriev, C. Simmerling, B. Wang, and R.J. Woods, "The Amber biomolecular simulation programs," *Journal of computational chemistry*, vol. 26, (no. 16), pp. 1668-1688, 2005.

[35] D.A. Pearlman, D.A. Case, J.W. Caldwell, W.S. Ross, T.E. Cheatham III, S. DeBolt, D. Ferguson, G. Seibel, and P. Kollman, "AMBER, a package of computer programs for applying molecular mechanics, normal mode analysis, molecular dynamics and free energy calculations to simulate the structural and energetic properties of molecules," *Computer Physics Communications*, vol. 91, (no. 1), pp. 1-41, 1995.

[36] W.D. Cornell, P. Cieplak, C.I. Bayly, I.R. Gould, K.M. Merz, D.M. Ferguson, D.C. Spellmeyer, T. Fox, J.W. Caldwell, and P.A. Kollman, "A second generation force field for the simulation of proteins, nucleic acids, and organic molecules," *Journal of the American Chemical Society*, vol. 117, (no. 19), pp. 5179-5197, 1995.

[37] V. Hornak, R. Abel, A. Okur, B. Strockbine, A. Roitberg, and C. Simmerling, "Comparison of multiple Amber force fields and development of improved protein backbone parameters," *Proteins: Structure, Function, and Bioinformatics*, vol. 65, (no. 3), pp. 712-725, 2006.

[38] W.L. Jorgensen, J. Chandrasekhar, J.D. Madura, R.W. Impey, and M.L. Klein, "Comparison of simple potential functions for simulating liquid water," *The Journal of chemical physics*, vol. 79, (no. 2), pp. 926-935, 1983.

[39] H.J. Berendsen, J.P.M. Postma, W.F. van Gunsteren, A. DiNola, and J. Haak, "Molecular dynamics with coupling to an external bath," *The Journal of chemical physics*, vol. 81, (no. 8), pp. 3684-3690, 1984.

[40] B. Honig and A. Nicholls, "Classical electrostatics in biology and chemistry," *SCIENCE-NEW YORK THEN WASHINGTON-*, pp. 1144-1144, 1995.

[41] I. Massova and P.A. Kollman, "Combined molecular mechanical and continuum solvent approach (MM-PBSA/GBSA) to predict ligand binding," *Perspectives in Drug Discovery and Design*, vol. 18, (no. 1), pp. 113-135, 2000.

[42] D. Sitkoff, K.A. Sharp, and B. Honig, "Accurate calculation of hydration free energies using macroscopic solvent models," *The Journal of Physical Chemistry*, vol. 98, (no. 7), pp. 1978-1988, 1994.

[43] J. Guo, X. Wang, H. Sun, H. Liu, and X. Yao, "The molecular basis of IGF-II/IGF2R recognition: a combined molecular dynamics simulation, free-energy calculation and computational alanine scanning study," *Journal of molecular modeling*, vol. 18, (no. 4), pp. 1421-1430, 2012.

[44] V. Zoete, M. Irving, and O. Michielin, "MM–GBSA binding free energy decomposition and T cell receptor engineering," *Journal of Molecular Recognition*, vol. 23, (no. 2), pp. 142-152, 2010.

[45] T. Kortemme and D. Baker, "A simple physical model for binding energy hot spots in protein–protein complexes," *Proceedings of the National Academy of Sciences*, vol. 99, (no. 22), pp. 14116-14121, 2002.

[46] T. Kortemme, D.E. Kim, and D. Baker, "Computational alanine scanning of protein-protein interfaces," *Science Signaling*, vol. 2004, (no. 219), pp. pl2, 2004.

[47] H. Liu and X. Yao, "Molecular basis of the interaction for an essential subunit PA− PB1 in influenza virus RNA polymerase: insights from molecular dynamics simulation and free energy calculation," *Molecular pharmaceutics*, vol. 7, (no. 1), pp. 75-85, 2009.

[48] T.W. Hendrickson, J. Yao, S. Bhadury, A.H. Corbett, and H.C. Joshi, "Conditional mutations in γ-tubulin reveal its involvement in chromosome segregation and cytokinesis," *Molecular biology of the cell*, vol. 12, (no. 8), pp. 2469-2481, 2001.

[49] K. Maundrell, "nmt1 of fission yeast. A highly transcribed gene completely repressed by thiamine," *Journal of Biological Chemistry*, vol. 265, (no. 19), pp. 10857-10864, 1990.

[50] K. Maundrell, "Thiamine-repressible expression vectors pREP and pRIP for fission yeast," *Gene*, vol. 123, (no. 1), pp. 127-130, 1993.

[51] J. Paluh and D. Clayton, "A functional dominant mutation in Schizosaccharomyces pombe RNase MRP RNA affects nuclear RNA processing and requires the mitochondrial-associated nuclear mutation ptp1-1 for viability," *The EMBO journal*, vol. 15, (no. 17), pp. 4723, 1996.

[52] T. Horio and B.R. Oakley, "Human gamma-tubulin functions in fission yeast," *The Journal of cell biology*, vol. 126, (no. 6), pp. 1465-1473, 1994.

[53] C.J. Tsai and R. Nussinov, "Hydrophobic folding units at protein-protein interfaces: Implications to protein folding and to protein-protein association," *Protein Science*, vol. 6, (no. 7), pp. 1426-1437, 1997.

[54] S.J. Davis, E.A. Davies, M.G. Tucknott, E.Y. Jones, and P.A. Van Der Merwe, "The role of charged residues mediating low affinity protein–protein recognition at the cell surface by CD2," *Proceedings of the National Academy of Sciences*, vol. 95, (no. 10), pp. 5490-5494, 1998.

[55] A.C. Wallace, R.A. Laskowski, and J.M. Thornton, "LIGPLOT: a program to generate schematic diagrams of protein-ligand interactions," *Protein engineering*, vol. 8, (no. 2), pp. 127-134, 1995.

CHAPTER 3

MOLECULAR INTERACTION OF NOSCAPINOIDS AT THE INTERFACE OF γ-TUBULIN DIMER

Abstract

γ-tubulin plays crucial role in the nucleation and organization of microtubules during cell division. Recent studies have also indicated their role in the regulation of microtubule dynamics at the plus end of the microtubules. Moreover, γ-tubulin has been found to be over-expressed in many cancer types like carcinomas of the breast and glioblastoma multiforme etc. These studies have led to immense interest in the identification of chemical leads that might interact with γ-tubulin and disrupt its function in order to explore γ-tubulin as potential chemotherapeutic target. Recently a colchicine-interacting cavity was identified on γ-tubulin that might also interact with other similar compounds. In the same direction we found a class of compounds, noscapinoids (noscapine and its derivatives) that fits well in a cavity close to the interface of γ-tubulin dimer. Molecular interaction of Noscapine and two of its derivatives- amino-noscapine and bromo-noscapine was investigated by molecular docking, molecular dynamics simulation and binding free energy calculation. All noscapinoids displayed stable interaction throughout simulation of 10 ns. The predictive binding free energy (ΔG_{bind}) indicates that noscapinoids bind strongly with γ-tubulin dimmer. However, bromo-noscapine showed the best binding affinity (ΔG_{bind} -37.6 kcal/mol) followed by noscapine (ΔG_{bind} -29.85 kcal/mol) and amino noscapine (ΔG_{bind} -23.99 kcal/mol) using the MM-PBSA method. Similarly using the MM-GBSA method also, bromo-noscapine showed highest binding affinity with ΔG_{bind} value of -43.64 kcal/mol followed by amino-noscapine with ΔG_{bind} value of -37.56 kcal/mol and noscapine with ΔG_{bind} value of -34.57 kcal/mol. The results thus generate compelling evidence that these noscapinoids indicate a great potential for preclinical and clinical evaluation.

3.1 Introduction

γ-tubulin is an essential component of the microtubule organization center (MTOC). It is known to interact with the minus end of microtubules and found to be localised at the centrosome. It plays an extremely crucial role in the nucleation and organization of microtubules [1, 2]. At the MTOC, γ -tubulin forms complexes with other proteins to form γ-tubulin small complex (γTuSC, around 280 kDa) comprises two molecules of γ–tubulin and one molecule each of GCP (γ-tubulin complex protein) 2 and 3. These proteins structurally associate to form Y-shaped flexible structure with γ-tubulins located on the two arms. Furthermore, 5-7 γTuSCs associate together to form the larger cone shaped complex known as γ-tubulin-ring complex (γTuRC), in association with GCP4, GCP5 and GCP6 [3-9]. γ-tubulin form the rim of this cone shaped complex. γ-tubulin interacts directly via one of its longitudinal interface with the minus end of microtubules and via the other longitudinal interface with the GCPs (GCP2, GCP3, GCP4). γ–tubulin interacts laterally with another γ-tubulin.

Many drugs that are currently administered as chemotherapeutic regime like paclitaxel derivatives and vinca-alkaloids, bind to αβ-tubulin and target the mitotic spindle dynamics [10]. However, these drugs are plagued with many drawbacks like development of multi-drug resistance over time which often leaves patients with more aggressive tumors and side effects. Indiscriminate and prolonged use of microtubule targeting drugs affects the normal rapidly dividing cells like those of the hair follicles and intestinal lining causing hair loss and nausea. These drawbacks call for continuous progressive research to come up with newer drugs with no or negligible side effects.

In recent studies γ-tubulin has been found to be over-expressed in pre-invasive lesions, carcinomas of the breast and glioblastoma multiforme (GBM) [11-13]. Since γ-tubulin over-expression is associated with tumor progression, a potent inhibitor of γ-tubulin would possibly halt mitosis in cancer cells. In the endeavour to explore if small ligands could bind at the interface and disrupt the γ-γ tubulin lateral interactions, we studied probable binding interaction of noscapinoids (noscapine, amino-noscapine and bromo-noscapine) with γ-tubulin homodimer. In this direction, we first prepared the structure of the γ-tubulin homodimer and ligands. We then performed molecular docking to obtain the protein –ligand complexes, which were then simulated in Amber 11 for 10 ns and then predicted the binding affinity using the MM-PBSA and MM-GBSA methods.

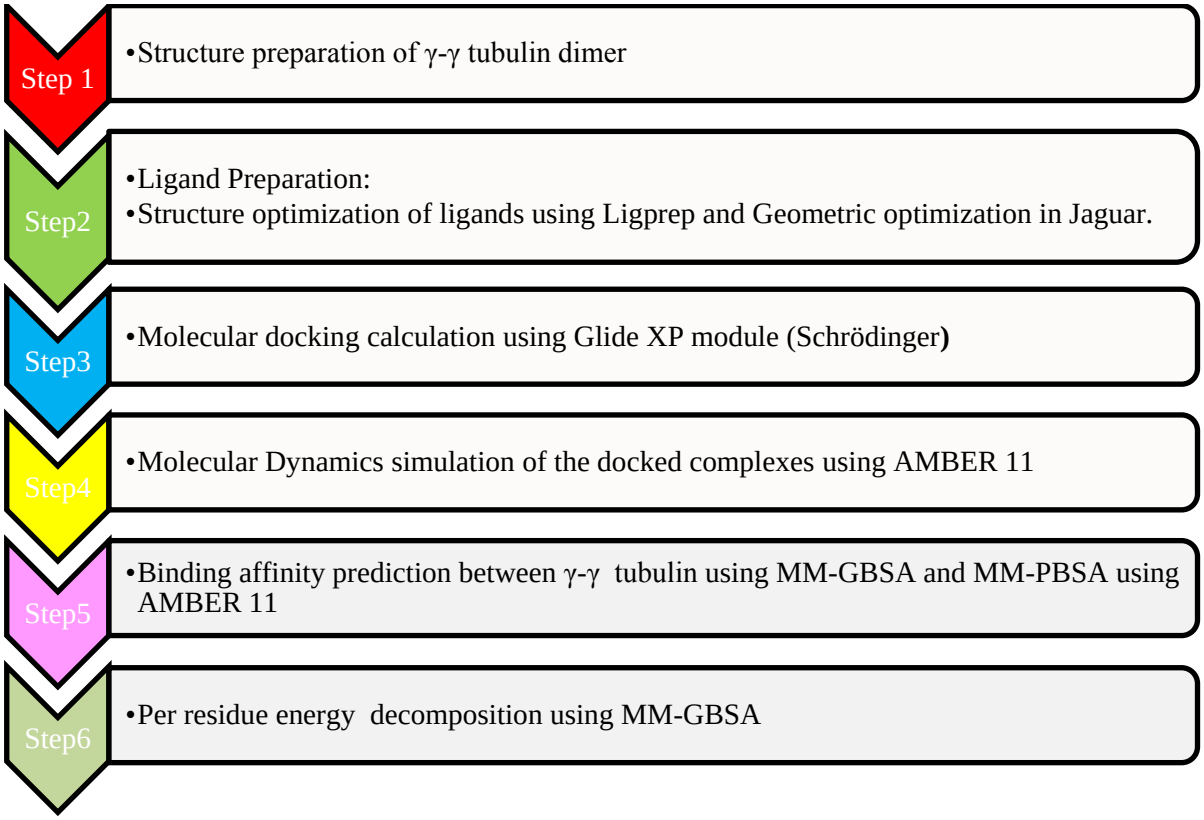

Figure 3.1: Schematic representaion of overall methodology followed to study the molecular interaction of noscapinoids with of γ-γ tubulin dimer.

3.2 Materials and Methods

3.2.1 Protein structure preparation

In order to study the molecular interaction of noscapinoids at the binding interface of γ-γ tubulin dimer, the structure of γ-tubulin dimer was first prepared as described in chapter 1.

3.2.2 Ligand preparation

The molecular structure of the lead molecule, noscapine and two of its derivatives such as amino-noscapine and bromo-noscapine **1-3** (Figure 3.2) were built using molecular builder of Maestro (version 8.5, Schrodinger LLC). All these structures were energy minimized *in-vacuo* using Impact (version 5.6, Schrodinger, LLC). Appropriate bond orders were assigned to each structure using Ligprep (version 2.4, Schrodinger LLC) and initial optimization was performed on each structure by employing OPLS 2005 force field using default setting. Furthermore, geometrical optimization of these ligands was performed in Jaguar (version 7.7, Schrodinger, LLC) using hybrid density functional theory with Becke's

three-parameter exchange potential and the Lee–Yang–Parr correlation functional (B3LYP) [14, 15] using basis set 3-21G* level [16-18].

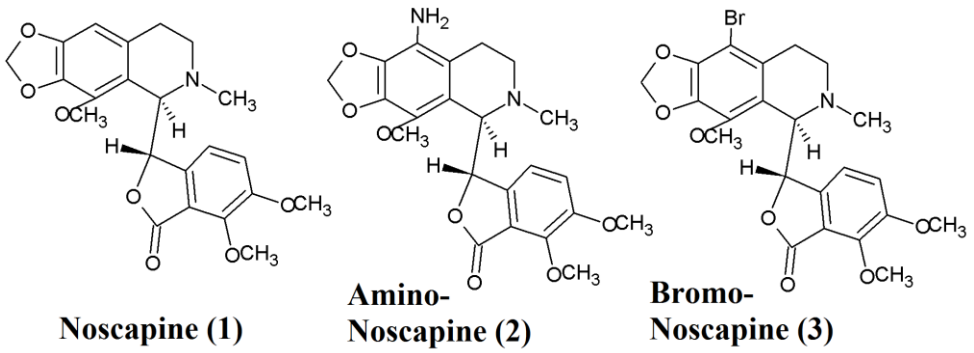

Figure 3.2: Molecular structure of Noscapine (1), Amino-noscapine (2), Bromo-noscapine (3)

3.2.3 Molecular docking

After ensuring that protein and ligands are in correct form, molecular docking of the optimized ligands onto the γ-tubulin dimer was performed using Glide (version 4.5, Schrodinger, LLC). The receptor-grid file was generated using grid receptor generation program with van der Waals scaling of 0.4 Å. A grid box size of 10 Å each for the bounding and enclosing boxes were generated at the centroid of the predicted binding sites (using SiteMap, version 2.4, Schrodinger, LLC) [19, 22]. The ligands were first docked using the "standard precision" method and further refined using "extra precision" Glide algorithm [22-24] (Table 3.1). Single best conformation for each ligand–protein complex was selected for further molecular modeling calculations.

Table 3.1 : Molecular docking evaluation of binding sites. All the three ligands were docked onto the 10 predicted binding sites of γ-tubulin dimer complex. The binding site that showed better docking score with all the ligands was selected as the probable binding site of interaction of these ligands on γ-γ tubulin dimer. On the basis of docking score, site 6 was selected.

Ligand	Site1	Site2	Site3	Site4	Site5	Site6	Site7	Site8	Site9	Site10
Amino	-2.81	-2.9	-3.48	-3.36	-3.1	**-3.55**	-1.88	-2.54	-3.08	-3.61
Bromo	-2.54	-2.94	-3.09	-2.7	-2.42	**-4.23**	-1.66	-2.48	-2.36	-3.82
Noscapine	-1.63	-4.26	-3.91	-3.97	-1.84	**-2.67**	-2.74	-2.14	-1.93	-3.88

3.2.4 Molecular dynamics simulation and binding affinity calculation

The protein ligand complexes obtained after molecular docking were then simulated for 10 ns in Amber11 using the parameters as described in chapter 2. Before simulation, the

missing parameters for all three ligands were estimated with the antechamber program [22, 25] implemented in Amber 11. AM1-BCC charge model was used to calculate the atomic point charges [23]. Missing hydrogens were added and FF99SB forcefield was employed to assigned parameters to the complex of GCP4 and γ-tubulin, while GAFF forcefield was used to assigned the parameters to each ligand using tleap module available in Amber 11. Each system was neutralized using sodium ions and solvated using TIP3 water model in a truncated octahedron with distance of at least 15 Å between the wall of the box and the closest atom of the complex [24]. All systems were simulated for 10 ns keeping the parameters consistent with those employed for γ-tubulin dimer in chapter 2. A total of 10,000 frames were obtained after 10 ns simulation. Binding affinity of noscapinoids at the γ-γ tubulin binding interface was then calculated using MM-PBSA and MM-GBSA methods [25, 26]. Free energy of binding was calculated as the ensemble average of the binding free energy of a total of 500 snapshots, extracted every 10 ps from the last 5 ns of the MD simulation trajectory.

$$\mathbf{\Delta G_{bind} = \Delta G_{complex} - [\Delta G_{Rec} + \Delta G_{lig}]}$$

$$\mathbf{G = E_{gas} + G_{sol} - TS}.$$

$$\mathbf{E_{gas} = E_{int} + E_{ele} + E_{vdw}}$$

$$\mathbf{G_{sol} = G_{PB(GB)} + G_{sol\text{-}np}}$$

$$\mathbf{G_{sol\text{-}np} = \gamma SAS}$$

Where, **G** is Gibbs free energy, $\mathbf{E_{gas}}$ is the gas phase energy calculated as the sum of internal energy ($\mathbf{E_{int}}$), energy generated as a result of the electrostatic interaction ($\mathbf{E_{ele}}$) and the van der Waals interaction($\mathbf{E_{vdw}}$). G_{sol} is the solvation free energy calculated as the sum of polar($\mathbf{G_{PB(GB)}}$) and nonpolar contributions ($\mathbf{G_{sol\text{-}np}}$). Polar interaction contribution ($\mathbf{G_{PB(GB)}}$) was calculated as the summation of electrostatic contribution ($\mathbf{E_{ele}}$) and polar solvation contribution ($\mathbf{G_{PB(GB)}}$). The nonpolar solvation contribution ($G_{sol\text{-}np}$) is approximated as linearly dependent on the solvent accessible surface area (SAS) and γ is the surface tension constant that was set to 0.0072 kcal mol^{-1} $Å^{-2}$ [26][30].

3.2.5 Per residue energy decomposition

The contribution of each amino acid residue of the γ-tubulin dimer was calculated to identify those residues which show strong interaction with noscapinoids. These calculations

were performed using MM-GBSA method implemented in Amber 11 over 500 frames obtained every 10 ps from last 5 ns trajectory.

3.3 Results and discussions

3.3.1 Molecular dynamics simulation

The γ-tubulin dimer complex bound to drugs (**1-3**) were simulated for 10 ns to obtain a trajectory of 10,000 frames, each frame recorded every 1 ps. Root mean square deviations (RMSD) of Cα-atoms during the entire duration of simulation were calculated for all the frames to monitored the stability of the system. The molecular systems were observed to get stabilized after 4 ns of simulation (Figure 3.3), since the relative fluctuation in the RMSD of Cα carbon atoms (Cα-rmsd) is very small after equilibration. The overall RMSD ranges from 0 to 2.2 Å. Furthermore, root mean square fluctuations (RMSF) of Cα-atoms were also calculated for all four molecular systems to find any changes in the residue flexibilities. The RMSF values were plotted against residue numbers as shown in Figure 3.4. The residues with higher RMSF tend to show more flexibility (Figure 3.4).

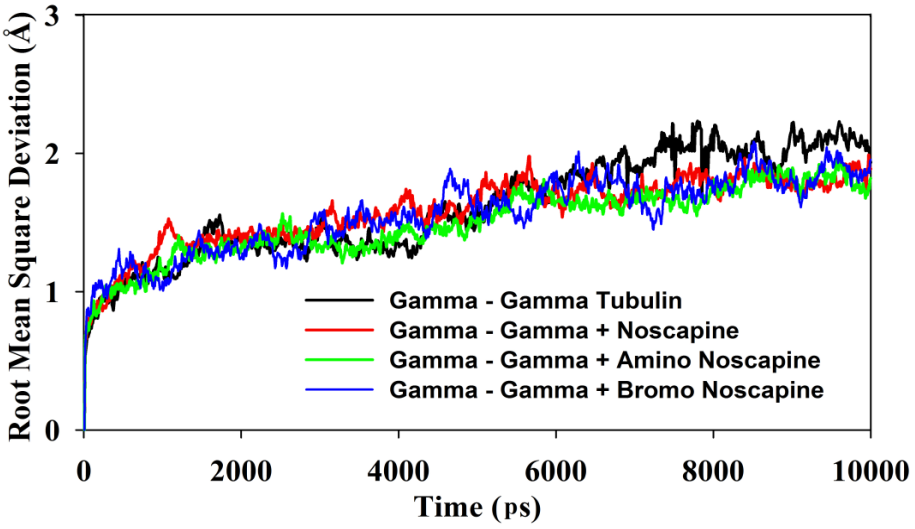

Figure 3.3: Root mean square deviation. The root mean square deviation (RMSD) of Cα atoms of the γ-tubulin dimer in the free form and bound form with different ligands (noscapine, amino-noscapine and bromo-noscapine) during the entire duration of MD simulation.

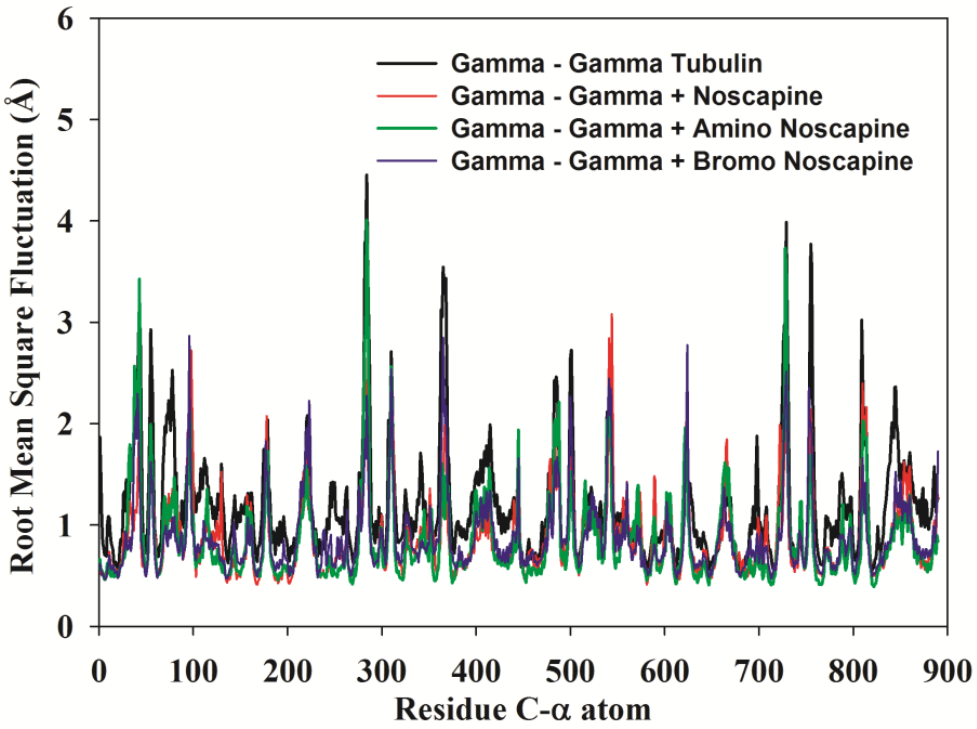

Figure 3.4: Root mean square fluctuation (RMSF) of Cα atoms. RMSF of residues in γ-tubulin dimer in the free form and in the bound form with different ligands (noscapine, amino-noscapine, bromo-noscapine) during the entire duration of MD simulation. The residues with higher RMSF tend to show more flexibility. The residues in the bound form show a small degree of flexibility when compared with free γ-tubulin dimer.

3.2 Theoretical binding affinity calculation

The binding affinity of all the three noscapinoids (1-3) was calculated using MM-PBSA and MM-GBSA methods as described in chapter 1. All three noscapinoids displayed stable interaction throughout simulations (Figure 3.3 and 3.4). Among all the three noscapinoids, bromo-noscapine showed the best binding affinity with the value of -37.6 kcal/mol followed by noscapine with -29.85 kcal/mol and amino noscapine with the -23.99 kcal/mol using the MM-PBSA method (Table 3.2). Using the MM-GBSA method also, bromo-noscapine showed highest binding affinity with the value of -43.64 kcal/mol followed by amino-noscapine with -37.56 kcal/mol and noscapine with the value of -34.57 kcal/mol. This could be attributed to the formation of hydrogen bonds between bromo-noscapine and surrounding amino acid residues like Met249, Asn250 and Gly247 in chain A (Figure 3.5). Noscapine also forms hydrogen bonds with Met249 and Ans250 of chain B. No significant hydrogen bonding was observed for amino-noscapine.

Table 3.2: Calculated binding free energy between GCP4 and γ-tubulin. Binding free energy calculated using MM-GBSA and MM-PBSA to ascertain the strength of interaction between GCP4 and γ-tubulin for both dimer 1 and dimer 2. The major energy components like van der Waals, electrostatic, polar solvation and non-polar solvation, contributing to the binding free energy were also estimated.

Contribution	Noscapine (kcal/mol)	Amino-noscapine (kcal/mol)	Bromo-noscapine (kcal/mol)
ΔE_{INT}	0.00	0.00	0.00
ΔE_{VDW}	-47.74	-54.15	-55.17
ΔE_{ELE}	-121.68	-108.00	-139.56
$\Delta E_{GAS/\ \Delta E\ MM}$	-169.41	-162.14	-194.72
ΔG_{PB}	142.84	141.70	160.60
ΔG_{SOL-NP}	-3.28	-3.55	-3.48
$\Delta G_{SOLV,PB}$	139.56	138.15	157.12
$\Delta G_{ELE,PB}$	17.89	30.15	17.56
$H_{TOT,PB}$	**-29.85**	**-23.99**	**-37.60**
G_{GB}	139.59	129.89	156.21
$G_{SOLV,GB}$	134.84	124.58	151.08
$G_{ELE\ GB}$	17.91	21.89	16.65
$H_{TOT,\ GB}$	**-34.57**	**-37.56**	**-43.64**

(A)

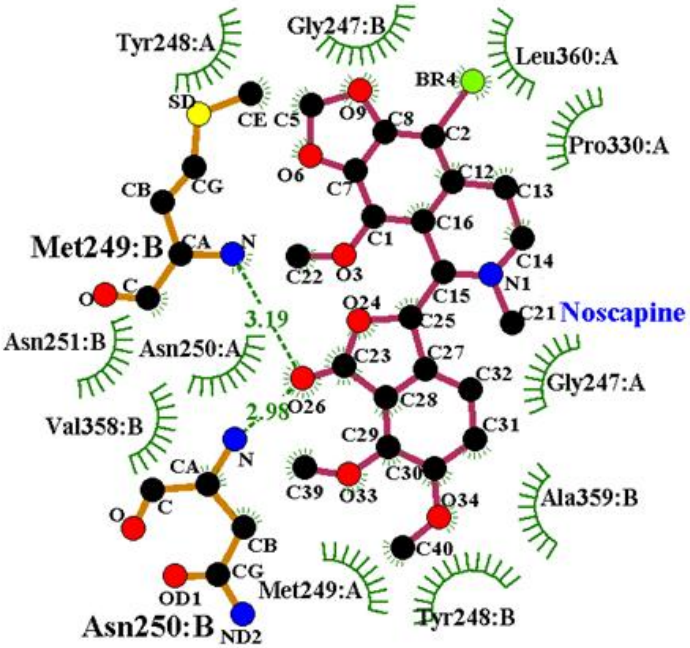

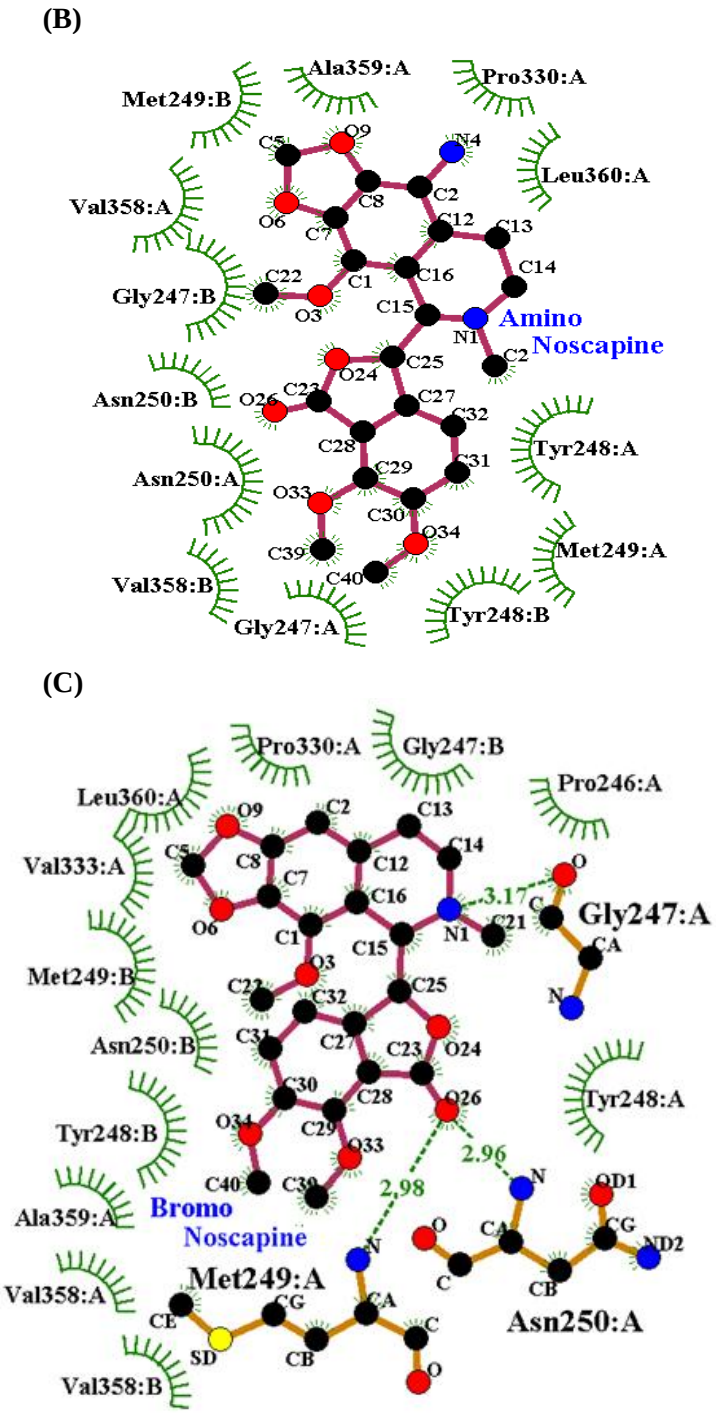

Figure 3.5: 2-D ligplot of noscapinoids: A 2-D representation of the binding mode of noscapinoids (A: Noscapine, B: Amino-Noscapine and C: Bromo-Noscapine) with the γ-tubulin dimer. 'A' and 'B' denote the chains in γ-tubulin dimer. Hydrogen bonding residues are shown in green and red for chain A and chain B, respectively. The Dashed lines denote hydrogen bonds, and numbers indicate hydrogen bond lengths in Å. Hydrophobic interactions are shown as arcs with radial spokes. The figures were made using Dimplot [27].

All identified hot spot amino acids were observed to lie at the interaction interface of γ-tubulin dimer (Figure 3.6). For all complexes, the binding energy was decomposed into its

various energy components (the electrostatic, van der Waals and solvation). Both van der Waals ($\mathbf{\Delta E}_{VDW}$) and the electrostatic component ($\mathbf{\Delta E}_{ELE}$) were observed to make very significant contributions to the free energy of binding. However, the net polar contribution ($\Delta G_{(ele,PB/GB)} = \Delta E_{ele} + \Delta G_{(PB/GB)}$) was rendered unfavourable due to very large penalty imposed by the desolvation component ($\Delta G_{PB/GB}$) while the net nonpolar component ΔE_{vdw} and ΔG_{sol-np} were observed to make highly favourable contribution to the binding free energy (Figure 3.7).

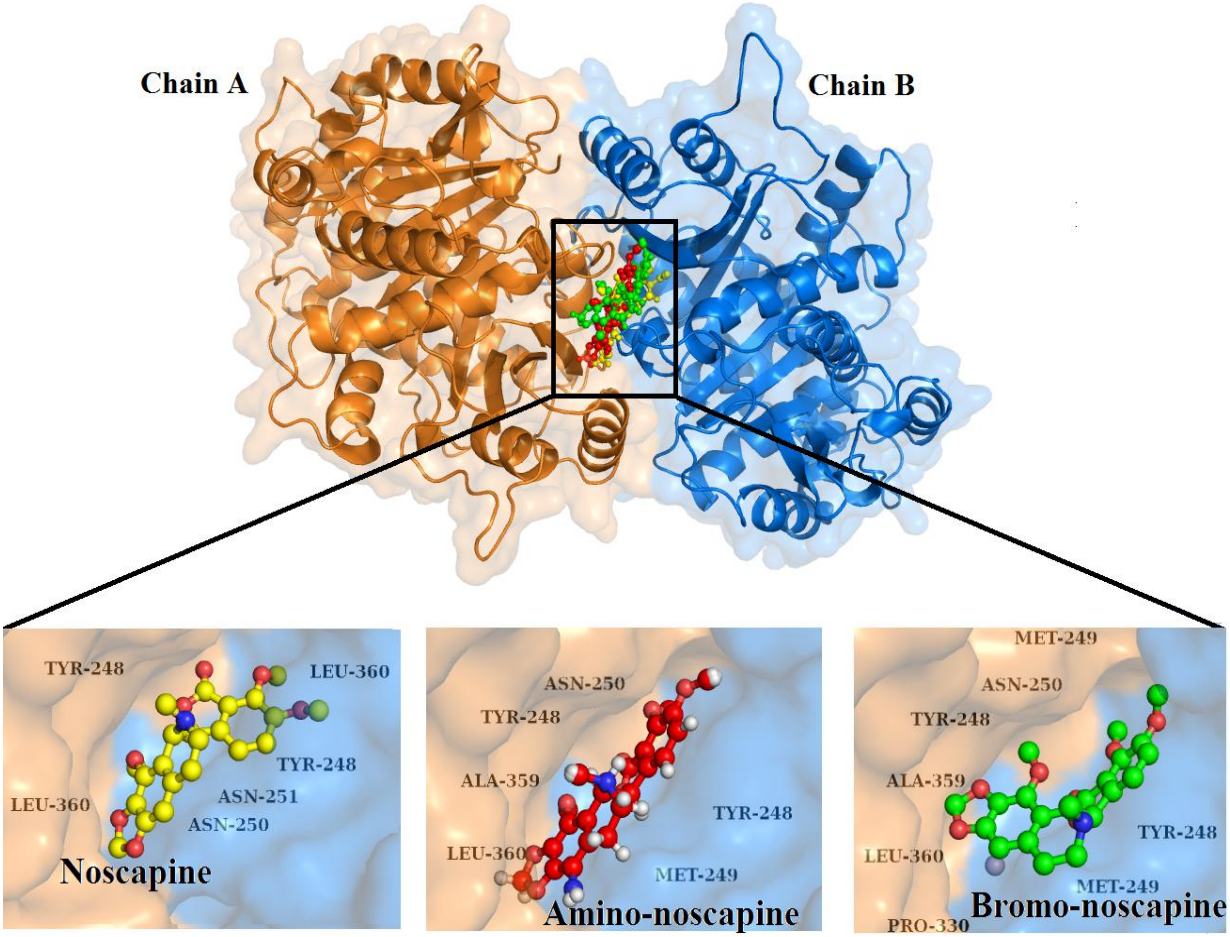

Figure 3.6 A: Binding mode of noscapinoids. Noscapinoids (Noscapine, Amino-noscapine and Bromo-noscapine) docked into γ-tubulin dimer. The zoomed views show the binding mode of the noscapinoids alone. The residues which show contribution of less than -1 kcal/mol to the binding free energy (ΔG_{bind}) are only labeled.

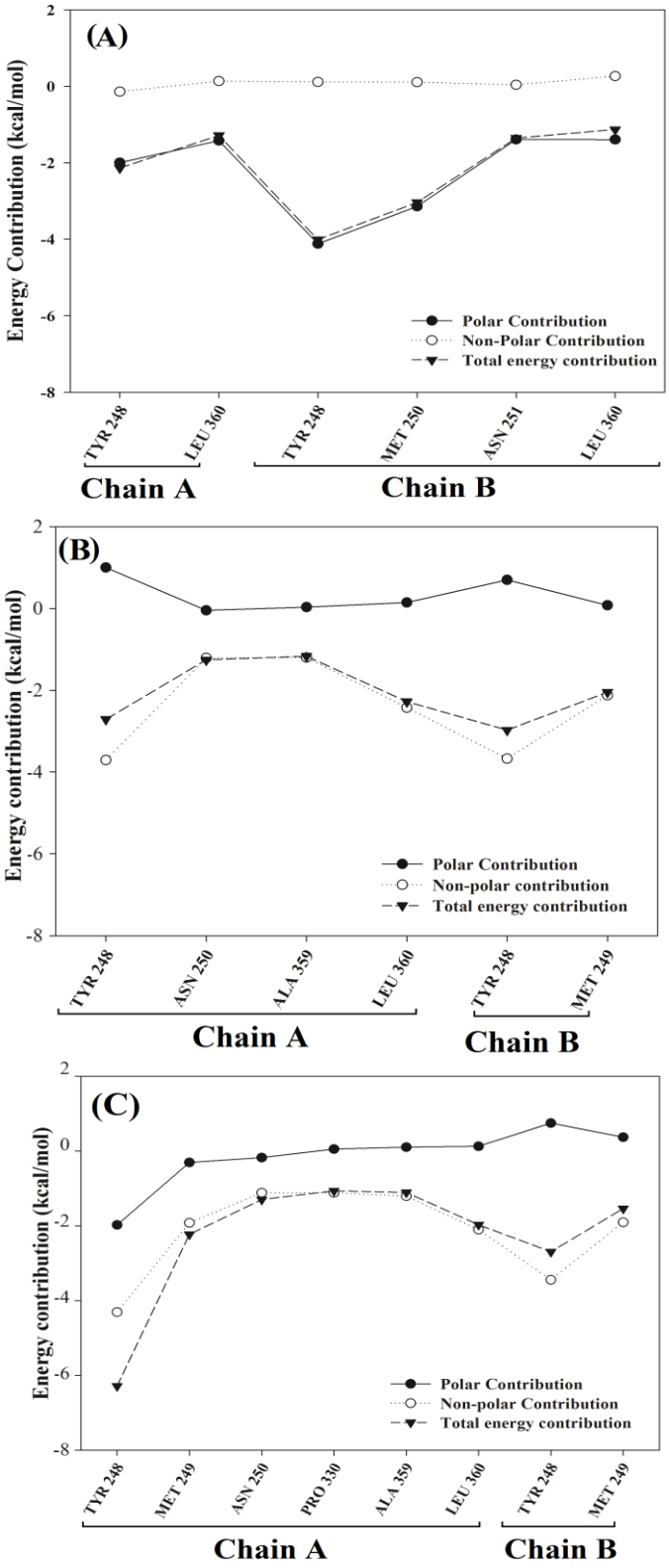

Figure 3.7: Energy contribution of hot spot amino acids. Non-polar, polar as well as total energy contributions of the amino acid residues that contribute most to the stability of the protein ligand (A: Noscapine, B:Amino-noscapine and C: Bromo-noscapine) complex. Polar interactions were calculated as sum of electrostatic ($\Delta E_{i,ele}$) and polar solvation ($\Delta G_{i,sol,GB}$) energy components while the non-polar interactions were calculated as sum of van der Waals ($\Delta E_{i,vdw}$) and non-polar solvation component ($\Delta G_{i,sol-np}$).

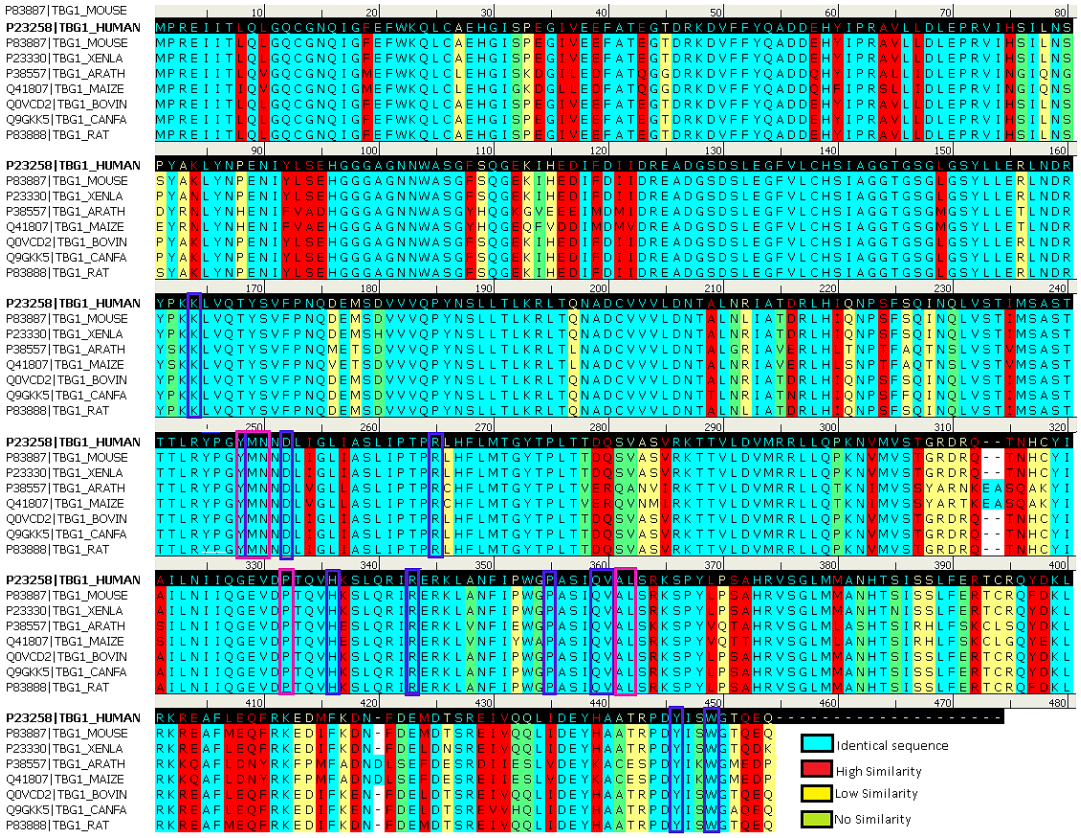

Figure 3.8: Multiple sequence alignment of γ-tubulin. γ-tubulin sequence show high level of homology across different species. The residues in the cyan region are identical. The residues enclosed with blue rectangle were identified as hot spot amino acids at the γ-γ tubulin dimer while those enclosed in magenta rectangle were observed to make strong contribution while binding with noscapinoids.

Conclusion

In this study, the binding modes of the three noscapinoids with the γ-γ tubulin dimer were illustrated using MD simulation and binding free energy calculations. All the three ligands lodged themselves in the pockets located very close to the binding interface of the γ-tubulin dimer. All three ligands showed stable interaction throughout the simulations however, the best binding affinity was calculated for bromo-noscapine. The binding modes of noscapine and bromo-noscapine are quite similar with both the drugs showing strong interaction with Tyr248, Met249, Asn250 of γ-tubulin. Multiple sequence alignment analysis showed the amino acid residues which interact with noscapinoids were observed to lie in the highly conserved regions (Figure 3.8). Therefore, if these drugs can interfere with a subset of the hot spot amino acids they might be able to perturb some of the interactions between γ-tubulin units in the γTuRC and further destabilize the γTuRC. Nevertheless, our results offer noscapinoids an important possible chemical framework for the further design of more potent compounds.

REFERENCES

[1] H.C. Joshi, M.J. Palacios, L. McNamara, and D.W. Cleveland, "γ-Tubulin is a centrosomal protein required for cell cycle-dependent microtubule nucleation," *Nature*, vol. 365, pp. 80-83, 1992.

[2] B.R. Oakley, C.E. Oakley, Y. Yoon, and M.K. Jung, "γ-Tubulin is a component of the spindle pole body that is essential for microtubule function in Aspergillus nidulans," *Cell*, vol. 61, (no. 7), pp. 1289-1301, 1990.

[3] V.r. Guillet, M. Knibiehler, L. Gregory-Pauron, M.-H.l.n. Remy, C.c. Chemin, B. Raynaud-Messina, C.c. Bon, J.M. Kollman, D.A. Agard, and A. Merdes, "Crystal structure of Î³-tubulin complex protein GCP4 provides insight into microtubule nucleation," *Nature structural & molecular biology*, vol. 18, (no. 8), pp. 915-919, 2011.

[4] T. Horio, S. Uzawa, M.K. Jung, B.R. Oakley, K. Tanaka, and M. Yanagida, "The fission yeast gamma-tubulin is essential for mitosis and is localized at microtubule organizing centers," *Journal of cell science*, vol. 99, (no. 4), pp. 693-700, 1991.

[5] H.C. Joshi, "γ-Tubulin: The hub of cellular microtubule assemblies," *Bioessays*, vol. 15, (no. 10), pp. 637-643, 1993.

[6] J.M. Kollman, A. Zelter, E.G.D. Muller, B. Fox, L.M. Rice, T.N. Davis, and D.A. Agard, "The structure of the Î³-tubulin small complex: implications of its architecture and flexibility for microtubule nucleation," *Molecular biology of the cell*, vol. 19, (no. 1), pp. 207-215, 2008.

[7] K. Oegema, C. Wiese, O.C. Martin, R.A. Milligan, A. Iwamatsu, T.J. Mitchison, and Y. Zheng, "Characterization of two related Drosophila γ-tubulin complexes that differ in their ability to nucleate microtubules," *The Journal of cell biology*, vol. 144, (no. 4), pp. 721-733, 1999.

[8] Y. Zheng, M.K. Jung, and B.R. Oakley, "γ-Tubulin is present in Drosophila melanogaster and Homo sapiens and is associated with the centrosome," *Cell*, vol. 65, (no. 5), pp. 817-823, 1991.

[9] J. Zhou and P. Giannakakou, "Targeting microtubules for cancer chemotherapy," *Current Medicinal Chemistry-Anti-Cancer Agents*, vol. 5, (no. 1), pp. 65-71, 2005.

[10] C. Dumontet and M.A. Jordan, "Microtubule-binding agents: a dynamic field of cancer therapeutics," *Nature reviews Drug discovery*, vol. 9, (no. 10), pp. 790-803, 2010.

[11] C.D. Katsetos, E. DrÃ¡berovÃ¡, B. Å mejkalovÃ¡, G. Reddy, L. Bertrand, J.-P. de ChadarÃ©vian, A. Legido, J. Nissanov, P.W. Baas, and P. DrÃ¡ber, "Class III Î²-tubulin and Î³-tubulin are co-expressed and form complexes in human glioblastoma cells," *Neurochemical research*, vol. 32, (no. 8), pp. 1387-1398, 2007.

[12] C.D. Katsetos, E. DrÃ¡berovÃ¡, A. Legido, and P. DrÃ¡ber, "Tubulin targets in the pathobiology and therapy of glioblastoma multiforme. II. Î³â€tubulin," *Journal of cellular physiology*, vol. 221, (no. 3), pp. 514-520, 2009.

[13] C.D. Katsetos, G. Reddy, E. DrÃ¡berovÃ¡, B. Å mejkalovÃ¡, L. Del Valle, Q. Ashraf, A. Tadevosyan, K. Yelin, T. Maraziotis, and O.P. Mishra, "Altered cellular distribution and subcellular sorting of Î³-tubulin in diffuse astrocytic gliomas and human glioblastoma cell lines," *Journal of Neuropathology & Experimental Neurology*, vol. 65, (no. 5), pp. 465-477, 2006.

[14] A.D. Becke, "A new mixing of Hartreeâ€"Fock and local densityâ€functional theories," *The Journal of Chemical Physics*, vol. 98, (no. 2), pp. 1372-1377, 1993.

[15] C. Lee, W. Yang, and R.G. Parr, "Development of the Colle-Salvetti correlation-energy formula into a functional of the electron density," *Physical Review B*, vol. 37, (no. 2), pp. 785, 1988.

[16] J.S. Binkley, J.A. Pople, and W.J. Hehre, "Self-consistent molecular orbital methods. 21. Small split-valence basis sets for first-row elements," *Journal of the American Chemical Society*, vol. 102, (no. 3), pp. 939-947, 1980.

[17] M.S. Gordon, J.S. Binkley, J.A. Pople, W.J. Pietro, and W.J. Hehre, "Self-consistent molecular-orbital methods. 22. Small split-valence basis sets for second-row elements," *Journal of the American Chemical Society*, vol. 104, (no. 10), pp. 2797-2803, 1982.

[18] W.J. Pietro, M.M. Francl, W.J. Hehre, D.J. DeFrees, J.A. Pople, and J.S. Binkley, "Self-consistent molecular orbital methods. 24. Supplemented small split-valence basis sets for second-row elements," *Journal of the American Chemical Society*, vol. 104, (no. 19), pp. 5039-5048, 1982.

[19] P.K. Naik, S. Santoshi, A. Rai, and H.C. Joshi, "Molecular modelling and competition binding study of Br-noscapine and colchicine provide insight into noscapinoidâ€"tubulin binding site," *Journal of Molecular Graphics and Modelling*, vol. 29, (no. 7), pp. 947-955, 2011.

[20] R.A. Friesner, J.L. Banks, R.B. Murphy, T.A. Halgren, J.J. Klicic, D.T. Mainz, M.P. Repasky, E.H. Knoll, M. Shelley, and J.K. Perry, "Glide: a new approach for rapid, accurate docking and scoring. 1. Method and assessment of docking accuracy," *Journal of medicinal chemistry*, vol. 47, (no. 7), pp. 1739-1749, 2004.

[21] T.A. Halgren, R.B. Murphy, R.A. Friesner, H.S. Beard, L.L. Frye, W.T. Pollard, and J.L. Banks, "Glide: a new approach for rapid, accurate docking and scoring. 2. Enrichment factors in database screening," *Journal of medicinal chemistry*, vol. 47, (no. 7), pp. 1750-1759, 2004.

[22] J. Wang, W. Wang, P.A. Kollman, and D.A. Case, "Automatic atom type and bond type perception in molecular mechanical calculations," *Journal of molecular graphics and modelling*, vol. 25, (no. 2), pp. 247-260, 2006.

[23] A. Jakalian, D.B. Jack, and C.I. Bayly, "Fast, efficient generation of high-quality atomic charges. AM1-BCC model: II. Parameterization and validation," *Journal of computational chemistry*, vol. 23, (no. 16), pp. 1623-1641, 2002.

[24] W.L. Jorgensen, J. Chandrasekhar, J.D. Madura, R.W. Impey, and M.L. Klein, "Comparison of simple potential functions for simulating liquid water," *The Journal of chemical physics*, vol. 79, (no. 2), pp. 926-935, 1983.

[25] P.A. Kollman, I. Massova, C. Reyes, B. Kuhn, S. Huo, L. Chong, M. Lee, T. Lee, Y. Duan, and W. Wang, "Calculating structures and free energies of complex molecules: combining molecular mechanics and continuum models," *Accounts of chemical research*, vol. 33, (no. 12), pp. 889-897, 2000.

[26] I. Massova and P.A. Kollman, "Combined molecular mechanical and continuum solvent approach (MM-PBSA/GBSA) to predict ligand binding," *Perspectives in Drug Discovery and Design*, vol. 18, (no. 1), pp. 113-135, 2000.

[27] A.C. Wallace, R.A. Laskowski, and J.M. Thornton, "LIGPLOT: a program to generate schematic diagrams of protein-ligand interactions," *Protein engineering*, vol. 8, (no. 2), pp. 127-134, 1995.

CHAPTER 4

MOLECULAR MODELLING REVEALS BINDING INTERFACE OF γ-TUBULIN WITH GCP4 PERTAINING TO MICROTUBULE NUCLEATION

Abstract

The initiation of microtubule assembly within cells is guided by a cone shaped multi-protein complex containing γ-tubulin and atleast five other γ-tubulin-complex proteins (GCPs) i.e., GCP2, GCP3, GCP4, GCP5, and GCP6. The rim of complex is a ring of γ-tubulin molecules that interacts, via one of its longitudinal interfaces, with GCP2, GCP3 or GCP4 of γ-tubulin ring complex (γTuRC) and, via other interface, with α-β tubulin dimers recruited for the microtubule lattice formation. These interactions however, are not well understood. Therefore, in this study we used molecular modelling and MD simulations, combined with MM-PBSA and MM-GBSA computational methods to understand atomic interactions between γ-tubulin and GCP4. We simulated two conformations of γ-tubulin-GCP4 complex for 10 ns and calculated the binding free energy of -172.7 kcal/mol and -188.5 kcal/mol using MM-PBSA and MM-GBSA method respectively, for dimer1 and -124.6 kcal/mol and -93.58 kcal/mol by MM-PBSA and MM-GBSA methods for dimer 2. These values points to very robust interactions between GCP4 and γ-tubulin. We also identified amino acids crucial for the interaction of γ-tubulin with GCP4, called hot spots, by computational alanine-scanning mutagenesis.

4.1 Introduction

Microtubules are hollow tube-like assemblies composed primarily of hetero-dimers of two globular protein subunits, α- and β- tubulin. These tubulin dimers associate in a head to tail fashion into linear protofilaments, thirteen to fourteen of which associated laterally constitute the tubular lattice of the microtubule. The linear arrangement of αβ-tubulin also gives a polarity to resulting microtubules that display dynamic instability in that they continually undergo lengthening and shortening at both ends—more rapidly at one end, named the plus end, than the other slower minus end.

Within cells, microtubule assembly is mostly initiated at a specialized structure called microtubule organizing center (MTOC) which lies at the minus ends of radially arranged microtubules. The microtubule nucleating large multiprotein complex located at the MTOCs and within mitotic spindles [1] contains a cone like γ-tubulin ring complex (γTuRC). γTuRC itself contains 6-7 copies of smaller tetrameric γ-tubulin small complexes (γTuSCs) composed of two copies of γ-tubulin and two other γ-tubulin-complex proteins (GCPs) [2-10]. A recent 8 A^0 resolution electron density map of a tetramer sub-complex containing two hetero-dimers of γ-tubulin and GCP4 [11] is a very welcome and timely beginning in the precise understanding of the binding interfaces of γ-tubulin, on its interface with components of the γTuRC. Therefore, in this study we first strive to extensively utilize molecular modelling and molecular dynamics (MD) simulation techniques to further investigate the precise mode and mechanism of interaction between GCP4 and γ-tubulin by theoretically estimating the free energy of binding between the protein units and identifying the key residues participating in the protein–protein interaction.

4.2 Materials and Method

4.2.1 Molecular System

A pseudo atomic model of the GCP4 and γ-tubulin tetramer was obtained from Georges Czaplicki, from the Universite´ de Toulouse, UPS, Toulouse, France. The coordinates of the atoms were obtained by fitting the crystal structures of GCP4 and γ-tubulin (PDB_ID 3RIP and 3CB2 respectively) onto the 8 Å cryo-electron microscopy (EM) reconstruction of the *Saccharomyces cerevisiae* γ–tubulin small complex (γ-TuSC) [11]. The GCP4 and γ-tubulin tetramer structure was then prepared using protein preparation wizard (PPrep) workflow in Schrodinger package. During protein preparation all the water molecules

were removed from the complex, missing hydrogen atoms were added to the structure using Maestro interface (version 9.2, Schrödinger) and hydrogen bonds were optimized. Missing side chains were filled using Prime (version 3.0, Schrodinger, LLC). Finally the structure was energy minimized using Macromodel (Schrodinger Inc). The minimization was done with Polak-Ribiere Conjugate Gradient (PRCG) algorithm. The minimization was stopped either after 5,000 steps or after the energy gradient converged below 0.001 kcal/mol.

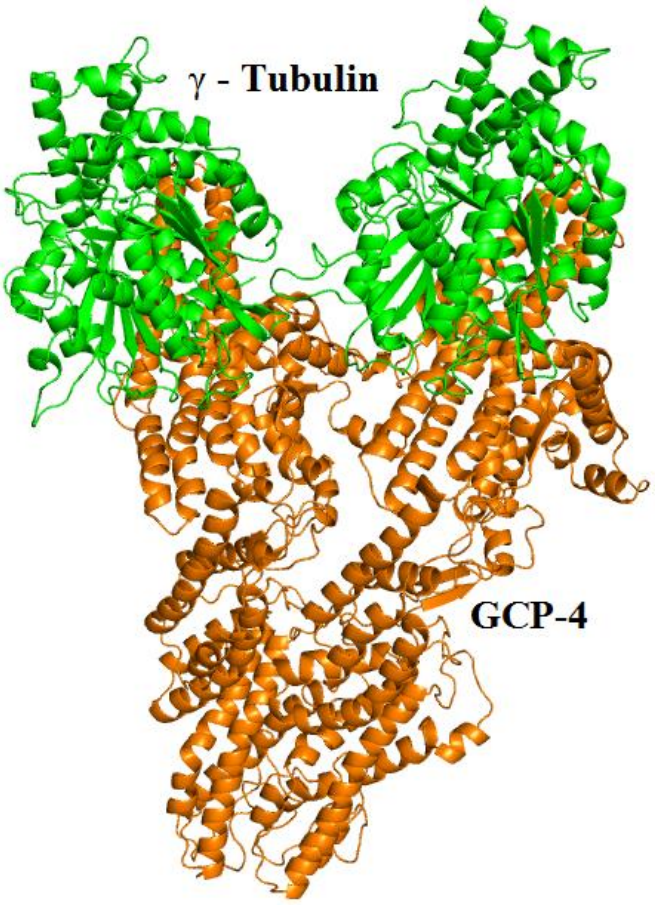

Figure 4.1 : Tetramer comprising of two molecules of GCP4 (orange) and two molecules of γ-tubulin (green).

4.2.2 Molecular dynamics simulation of GCP4 and γ-tubulin complex

Since we intended to understand the molecular interaction between GCP4 and γ-tubulin, we split the tetramer into two dimers (dimer 1 and dimer 2), each having a unit of GCP4 and γ-tubulin. Both dimers were then MD simulated using Amber 11.0 and Ambertools 1.5 [12, 13]. Tleap program implemented in Amber 11 was used to assign parameters from FF99SB force field, neutralize the system, solvate the system using TIP3P model and finaly generated the toplogy and co-ordinate files [14-16]. Prior to molecular dynamics simulation,

both the dimeric complexes were relaxed to remove bad contacts. Each complex was subjected to three consecutive rounds of 1000 step minimization employing 500 steps of steepest descent followed by 500 steps of conjugate gradient methods. For the first and second rounds only water molecules were relaxed while the protein was held fixed using force constants of 10 and 2 kcal mol^{-1} $Å^{-2}$ respectively. In the third round the entire system was allowed to relax without any restraint. The fully relaxed structure was then heated to 300 K in 100 ps. The system was subjected to density equilibration over 100 ps followed by 500 ps of constant pressure equilibration at 300 K and 1 atm pressure with a force constant of 2 kcal mol^{-1} $Å^{-2}$. A 10 ns MD simulation was carried out on the equilibrated system using Particle Mesh Ewald Molecular Dynamics method using the time step of 2 fs [17, 18]. Through out the simulation the Langevin thermostat was used to regulate the temperature and the bond lengths involving hydrogen bonds were constrained using SHAKE algorithm [19]. MD was carried out in an NPT ensemble using a Berendsen barostat [20] with a target pressure of 1 atm. The structures were recoreded every 1 ps resulting in a trajectory with 10,000 frames.

4.2.3 Calculation of binding free energy between GCP4 and γ-tubulin

Binding free energy calculations were carried out using the conventional MM-PBSA and MM-GBSA approaches using Amber 11 [21, 22]. A total of 500 snapshots were extracted, every 10 ps from the last 5 ns of the MD trajectory. For each snapshot, the free energy was calculated for each molecular species (complex, protein and ligand). Conceptually the binding free energy can be calculated as :

$$\mathbf{\Delta G_{bind} = \Delta G_{complex} - [\Delta G_{Rec} + \Delta G_{lig}]}$$

The free energy, G, for each species can be calculated by the following scheme using the MM-PBSA and MM-GBSA methods as implemeted in Amber 11:

For each molecular species, Gibbs's free energy G was calculated as follows.

$$\mathbf{G = E_{gas} + G_{sol} - TS}$$

Where E_{gas} is the gas phase energy calculated as the sum of internal energy, energy generated as a result of the electrostatic interaction and the van der Waals interaction. The E_{gas} was calculated using parameters from FF99SB force field [14, 15].

$$\mathbf{E_{gas} = E_{int} + E_{ele} + E_{vdw}}$$

G_{sol} is the solvation free energy which was calculated as the sum of polar and nonpolar cntributions as

$$\mathbf{G_{sol} = G_{PB(GB)} + G_{sol\text{-}np}}$$

where $G_{PB(GB)}$ is the polar solvation contribution calculated by solving the PB and GB equations.

Polar interaction contribution was calculated as the summation of electrostatic contribution and polar solvation contribution.

$$\mathbf{G_{ele,PB(GB)} = E_{ele} + G_{PB(GB)}}$$

The nonpolar solvation contribution ($G_{sol\text{-}np}$) is approximated as linearly dependent on the solvent accessible surface area (SAS), which was determined using a water probe radius of 1.4Å, surface tension constant γ was set to 0.0072 kcal mol^{-1} $Å^{-2}$ [23].

$$\mathbf{G_{sol\text{-}np} = \gamma SAS}$$

Dielectric constant for solute and solvent were set to 1 and 80, respectively. T and S are the temperature and the total solute entropy.

4.2.4 Per residue energy contribution

In order to identify those residues wich play a more substantial role in the binding of GCP4 with γ-tubulin, energy contribution of each amino acid in the complex was determined. Energy decompostion method, implemented in Amber 11, was employed on the 500 frames extracted every 10 ps from last 5 ns of simulation using the MM-GBSA method. The residues contributing more than 3 kcal/mol were considered very significant for the binding of GCP4 with γ-tubulin and these residues were designated as hotspot amino acids.

4.2.5 Alanine scanning mutagenesis

The hot spot residues identified in both the dimer (18 in each dimer) were mutated to Alanine, one by one to recalculated the binding free energy using the MM-GBSA and MM-PBSA methods. A total of 18 alanine scanning runs were carried out for each dimer to calculate $\Delta\Delta G_{bind}$ given by:

$$\Delta\Delta G_{bind} = \Delta_{Gmutant} - \Delta G_{wild\ type.}$$

4.3 Results and Discussions

The dimers of GCP4 and γ-tubulin were simulated for 10 ns and the resultant trajectories were utilized for the calculation of binding free energies using the MM-GBSA and MM-PBSA methods. Furthermore, energy decomposition analysis was performed for both the dimers to estimate the energy contribution of each residue take part in the interaction between GCP4 and γ-tubulin in order to identify the hot spot amino acids. The energy contributions of these amino acids were further decomposed into various energy components like the van der Waals, electrostatic and solvation energy components to understand the nature of contribution.

4.3.1 Molecular dynamics simulation

The complexes (dimer1 and dimer2) of GCP4 and γ-tubulin were simulated for 10 ns to obtain a trajectory of 10,000 frames, each frame recorded every 1 ps.

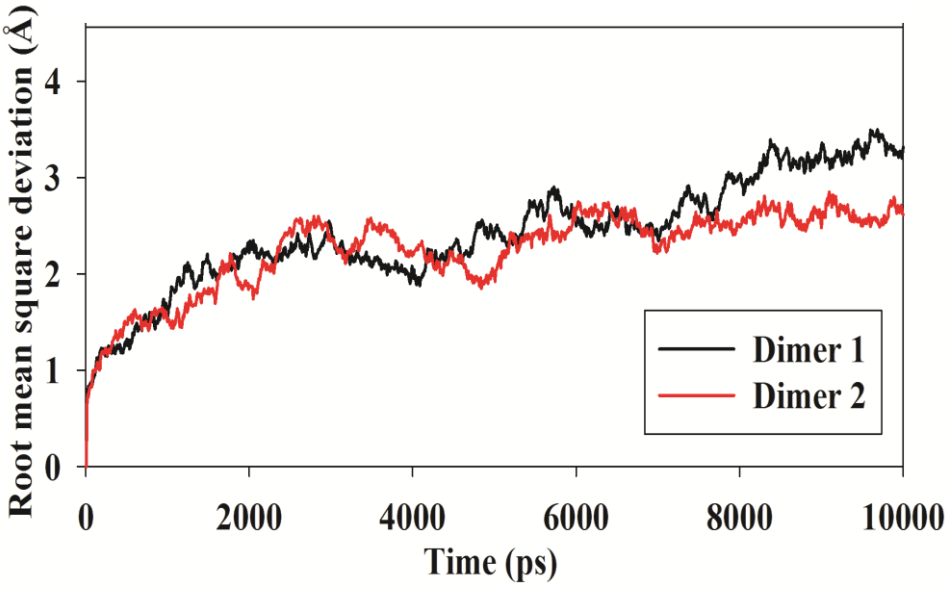

Figure 4.2: Root mean square deviation. The root mean square deviations (RMSD) of Cα atoms in the GCP4 and γ-tubulin complex in dimer 1 and dimer 2 during the entire duration of MD simulation. The relative fluctuation in the RMSD of the Cα atoms is very small after 4000 ps, revealed that each system reaches equilibrium at 4000 ps.

Root mean square deviations (RMSD) of Cα-atoms during the entire duration of simulation were calculated for all the frames to monitor the stability of the system. Both the systems observed to get stabilized after 4 ns of simulation (Figure 4.2), since the relative fluctuation in the RMSD of Cα carbon atoms (Cα-rmsd) is very small after equilibration. The overall RMSD ranges from 0 to 3.5 Å. Furthermore, root mean square fluctuations (RMSF) of

Cα-atoms were also calculated for both dimer1 and dimer2 to find any changes in the residue flexibilities. The RMSF values were plotted against residue numbers as shown in Figure 3. The residues with higher RMSF tend to show more flexibility (Figure 4.3).

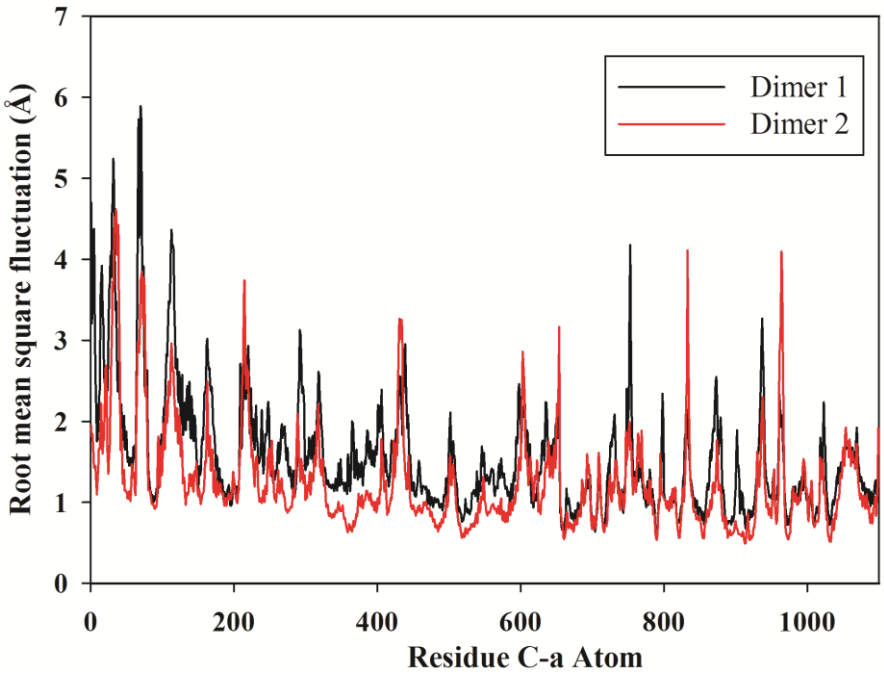

Figure 4.3: Root mean square fluctuation (RMSF) of Cα atoms. RMSF of residues in the complex of GCP4 and γ-tubulin in dimmer 1 and dimmer 2 during the entire duration of MD simulation. The residues with higher RMSF tend to show more flexibility.

4.3.2 Calculated binding affinities between GCP4 and γ-tubulin

The binding free energies and their components between GCP4 and γ-tubulin were calculated independently for both dimer 1 and dimer 2 and presented in Table 1. We have considered last 500 frames from the last 5 ns of trajectory to calculate the ensemble average of the free energy of binding using both MM-GBSA and MM-PBSA methods. The results obtained from both the methods suggested very robust interactions between the GCP4 and γ-tubulin, essentially driven by the non-polar forces. The predicted binding free energies (ΔG_{bind}) based on MM-GBSA method for both dimmer 1 and dimer 2 are -188.5 kcal/mol and -93.58 kcal/mol respectively. In contrary the ΔG_{bind} based on MM-PBSA are estimated to be -172.7 kcal/mol for dimer 1 and -124.6 kcal/mol for dimer 2. Hence, there is a difference of 15.8 kcal/mol and 31.03 kcal/mol between the two methods. This derives from the difference in calculation of the contribution to the polar solvation energy, which is slightly higher in the MM-PBSA calculation (47.57 and -37.57 kcal/mol) compared to MM-GBSA (31.77 and -6.53 kcal/mol) among both the dimers. Very robust van der Waals (ΔE_{VDW}) interactions, to

the magnitude of -220.3 kcal/mol and -87.04 kcal/mol were observed for dimer 1 and dimer 2 respectively. The net polar component ($\Delta G_{(ele,\ PB/GB)} = \Delta E_{ele} + \Delta G_{(PB/GB)}$) was observed to be unfavourable in the interaction between GCP4 and γ-tubulin among both the dimers (Table 4.1).

Table 4.1: Calculated binding free energy between GCP4 and γ-tubulin. Binding free energy calculated using MM-GBSA and MM-PBSA to ascertain the strength of interaction between GCP4 and γ-tubulin for both dimer1 and dimer2. The major energy components like van der Waals, electrostatic, polar solvation and non-polar solvation, contributing to the binding free energy were also estimated.

Contribution	Dimer1	Dimer 2
ΔE_{INT}	0.00	0.00
ΔE_{VDW}	-274.8	-193.9
ΔE_{ELE}	54.52	106.9
ΔE_{GAS}	-220.3	-87.04
ΔG_{PB}	76.53	-17.17
ΔG_{SOL-NP}	-28.95	-20.40
$\Delta G_{SOLV,PB}$	47.57	-37.57
$\Delta G_{ELE,PB}$	131.1	89.69
$\Delta G_{bind,PB}$	-172.7	-124.6
G_{GB}	67.49	17.78
$G_{SOLV,GB}$	31.77	-6.530
$G_{ELE\ GB}$	122.0	124.6
$\Delta G_{bind,\ GB}$	-188.5	-93.58

The unfavourable polar contributions were observed to overcome with highly favourable non-polar components ($\Delta E_{vdw} + \Delta G_{sol\text{-}np}$) among both the dimers. Interactions between GCP4 and γ-tubulin seem to be steered by nonpolar component. This can be explained by the tendency of the nonpolar residues to readily bury themselves in the hydrophobic pockets and displace water.

4.3.3 Per-residue energy decomposition

Energy contribution of each residue in the interface between GCP4 and γ-tubulin among both dimer 1 and dimer 2 was calculated using the MM-GBSA method to investigate the details of protein-protein interactions at the atomic level. Similar studies have been reported earlier in the insulin dimer [24], TCR-p-MHC [25], Ras-Raf and Ras-RalGDS [26, 27] complexes. The results from these studies demonstrated good correlations between the calculated per residue binding free energy and the experimental binding free energies differences for the alanine mutants. The predictive binding energy ($\Delta G_{bind,GB}$) between GCP4

and γ-tubulin was decomposed into contributions from the residues of the two partners and included in Table 4.2. We identified 18 hotspot amino acids that have the highest impact (per residue contribution > 3 kcal/mol) on the GCP4 and γ-tubulin interaction (Figure 4.4). The detailed energy components are included in Table 2 and the spatial distributions of these hotspots at the binding interface between GCP4 and γ-tubulin are shown in Figure 5 for both the dimers. As shown in Figure 4, for dimer 1, six amino acids (Asp359, Glu367, Arg515, Tyr529, Val533, Glu537) on the surface of GCP4 and five amino acids (Arg2, Arg46, Pro329, Arg361, Trp445) on the surface of γ-tubulin make greater contributions to the binding of GCP4 and γ-tubulin, each yielding >5 kcal/mol of binding free energy. In addition, three amino acids (Leu404, Trp514, Gln532) from GCP4 and four amino acids (Pro261, Glu326, Asp328, Val357) from γ-tubulin have considerable energy contributions to the binding process of GCP4 and γ-tubulin, each yielding between 3 to 5 kcal/mol of free energy. Contrastingly for dimer 2 albite different amino acids shown to contribute in the interaction betwenn GCP4 and γ-tubulin. As shown in Figure 4, four residues (Glu367, Trp514 , Phe522, Tyr529) on the surface of GCP4 and two amino acids (His333, Arg361) on the surface of γ-tubulin make larger contribution of > 5 kcal/mol each in the binding process. In addition, five amino acids (Arg515, Asn518, Asn526, Tyr530, Ser538) of GCP4 and seven amino acids (Arg46, Met248, Asn249, Ile253, Pro263, Pro329, Arg442) of γ-tubulin contributed binding free energy of 3 to 5 kcal/mol in the binding process. All hot spots were observed to lie at the interface of γ-tubulin-GCP4 complex (Figure 4.5). Furthermore, to determine the detailed contribution of each hotspot amino acids, the total binding free energy was further decomposed into various energy components like van der Waals, electrostatic, polar solvation and non-polar solvation (Table 4.2).

The results reveals that most of the important amino acids for both GCP4 and γ-tubulin make considerable van der Waals and nonpolar solvation contributions compared to the polar contributions (Figure 4.6). The hotspot amino acids were then mutated to alanine, one by one, to re-calculate the binding free energies using MM-PBSA and MM-GBSA methods (Table 4.3). It was observed that the binding free energy was reduced at least by 0.04 kcal/mol in dimer1 and 2.22 kcal/mol in dimer 2 using the MM-GBSA method while by using the MM-PBSA method the minimum drop in binding free energy was 0.65 kcal/mol in dimer1and 0.40 kcal/mol in dimer 2. Mutation of Glu367 resulted in maximum drop in the

overall binding affinity in both the dimers which correlates to the per residue energy contribution results.

Table 4.2: Energy decomposition. Decomposition of calculated $\Delta G_{bind,GB}$ (kcal/mol) on per residue basis into van der Waals, electrostatic, polar solvation and non-polar solvation energy components for the hotspot amino acids. Those amino acids which contributed more than 3 kcal/mol to the binding affinity of GCP4 and γ-tubulin complex were considered as hotspot amino acids.

Chain	Residue	$\Delta E_{i,vdw}$	$\Delta E_{i,ele}$	$\Delta G_{i,sol\ GB}$	$\Delta G_{i,sol-np}$	$\Delta G_{i,bind,GB}$
(a) Dimer1						
GCP4	ASP359	-0.631	17.37	-23.70	-0.112	-7.067
(Chain A)	GLU367	-2.371	-0.364	-9.287	-0.867	-12.89
	LEU404	-4.668	1.608	-0.628	-0.807	-4.494
	TRP514	-4.242	-1.422	2.171	-0.512	-4.005
	ARG515	-3.683	-91.82	86.54	-1.052	-10.02
	TYR529	-5.310	-13.17	9.977	-0.674	-9.178
	GLN532	-7.644	-8.654	13.10	-0.918	-4.113
	VAL533	-7.307	-4.964	5.069	-1.066	-8.268
	GLU537	-2.808	-1.211	-4.155	-0.459	-8.634
	ARG2	-0.109	-85.92	78.97	-0.015	-7.074
γ-tubulin	ARG46	-1.858	-97.65	93.88	-0.333	-5.961
(Chain B)	PRO261	-3.317	-6.037	6.473	-0.463	-3.343
	GLU326	-2.955	39.44	-39.92	-0.669	-4.112
	ASP328	-5.678	54.37	-52.29	-0.648	-4.245
	PRO329	-4.535	-4.084	4.201	-0.693	-5.111
	VAL357	-2.325	-3.763	2.728	-0.220	-3.580
	ARG361	-0.912	-88.03	82.05	-0.586	-7.472
	TRP445	-5.106	-40.32	41.29	-1.429	-5.566
(b) Dimer 2						
GCP4	GLU367	-1.559	29.45	-32.59	-0.379	-5.077
(Chain A)	TRP514	-5.879	-5.064	5.921	-0.772	-5.794
	ARG515	-4.269	-89.53	91.01	-0.946	-3.733
	ASN518	-3.379	-8.308	8.679	-0.478	-3.486
	PHE522	-6.696	-2.215	4.432	-1.109	-5.587
	ASN526	-3.109	-9.237	8.191	-0.470	-4.626
	TYR529	-6.190	-6.725	7.210	-0.948	-6.653
	TYR530	-4.573	-4.544	5.883	-0.694	-3.928
	SER538	-1.546	-4.497	3.018	-0.341	-3.367
	ARG46	-1.773	-73.68	71.89	-0.501	-4.065
γ-tubulin	MET248	-4.035	-2.106	3.273	-0.451	-3.319
(Chain B)	ASN249	-6.549	-7.999	11.72	-1.091	-3.920
	ILE 253	-3.722	-1.292	2.096	-0.783	-3.701
	PRO263	-2.992	0.623	-0.331	-0.586	-3.286
	PRO329	-3.847	-3.891	4.235	-0.469	-3.972
	HIS333	-4.105	-13.94	13.03	-0.722	-5.734
	ARG361	-0.159	-78.57	72.75	-0.335	-6.312
	TYR442	-0.759	-10.51	8.001	-0.171	-3.442

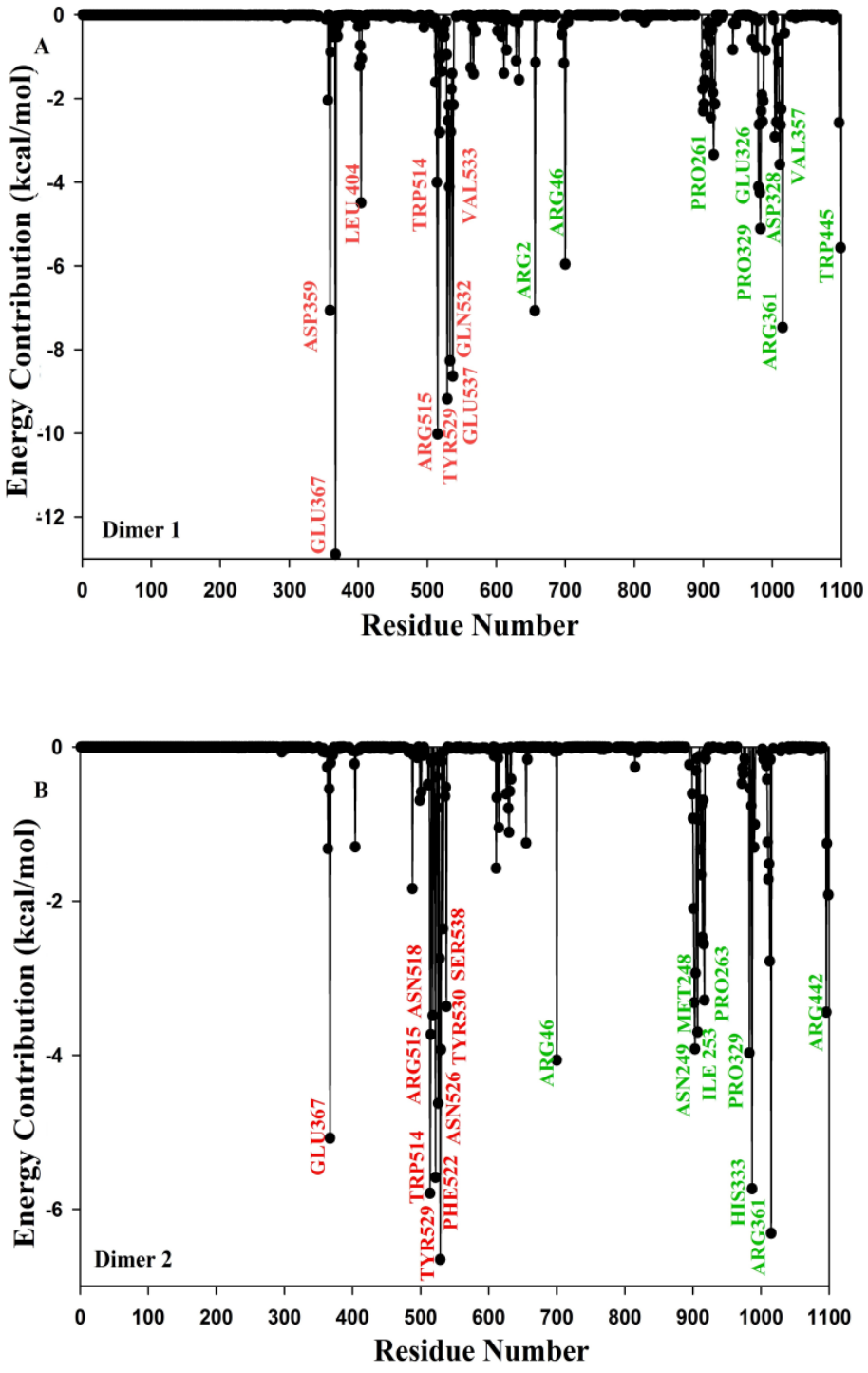

Figure 4.4: **Per residue free energy contribution of residues in the binding process of GCP4 and γ-tubulin.** Free energy contribution of each residue on the surface between GCP4 and γ-tubulin involve in the interaction in dimer1 (A) and dimer2 (B) calculated based on MM-GBSA. Only the residues contributing free energy of >3 kcal/mol (designated as hotspot amino acids) are labelled in the figure. The hotspot residues belonging to GCP4 are labelled red while those of γ-tubulin are labelled green.

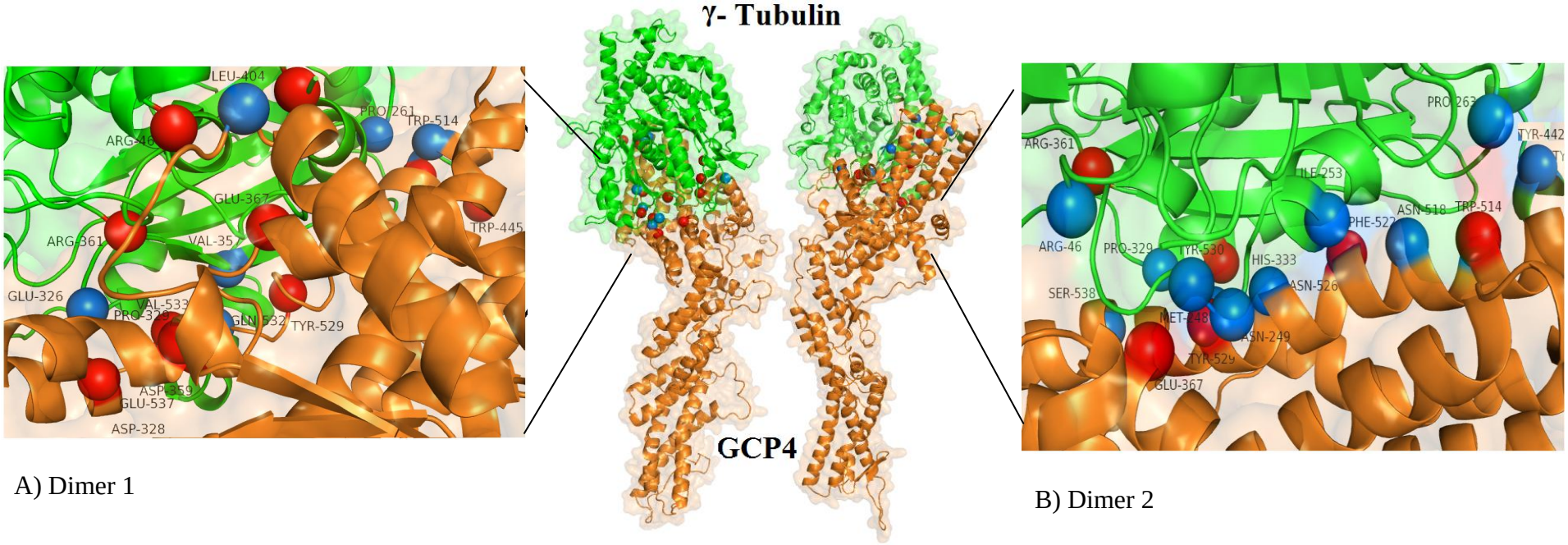

A) Dimer 1

B) Dimer 2

Figure 4.5: Spatial distribution of hotspot residues at the binding interface. Hot spot residues involve in the binding process of GCP4 and γ- tubulin at the interface in the dimmer1 (A) and dimer2 (B) are represented in the three dimensional space model of the complex. The hotspot residues contributing free energy of > 5 kcal/mol are marked red, while the residues contributing free energy in between 3 kcal/mol and 5 kcal/mol are marked blue. In total nine residues each on the surface of GCP4 and γ-tubulin involve in the binding process in both dimmer1 and dimmer2. However, the residues are albeit different between both the dimers. This is the reason that the predictive binding free energies between both the dimmers are different. The binding free energy between GCP4 and γ-tubulin calculated in dimer1 is much higher (-188.51 kcal/mol and -172.71 kcal/mol) compared to dimer2 (-93.58 kcal/mol and -172.71 kcal/mol) based on both MM-PBSA and MM-GBSA methods, respectively.

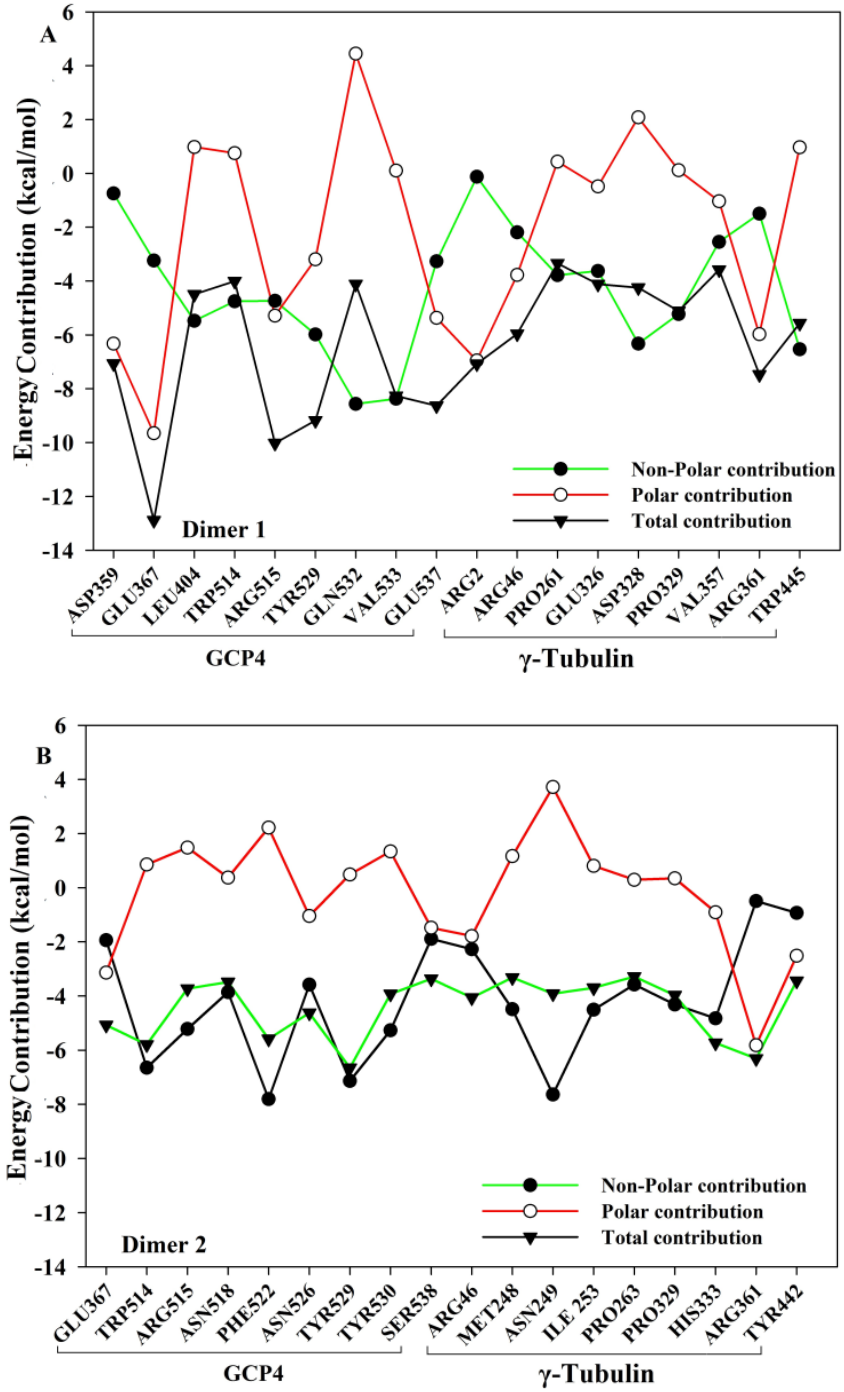

Figure 4.6: Polar and nonpolar energy contribution of hot spot residues. The decomposition of total energy contributions into polar and non-polar energy components of hotspot amino acids in the binding process of GCP4 and γ-tubulin in dimer1 (A) and dimer2 (B). For both GCP4 and γ- tubulin the hotspot amino acids make considerable nonpolar solvation contributions compared to the polar contributions. Polar interactions were calculated as sum of electrostatic ($\Delta E_{i,ele}$) and polar solvation ($\Delta G_{i,sol,GB}$) energy components while the non-polar interactions were calculated as sum of van der waals ($\Delta E_{i,vdw}$) and non-polar solvation component ($\Delta G_{i,sol-np}$).

Table 3: $\Delta\Delta G_{bind}$ for hot spot amino acids. Computational alanine scanning mutagenesis was carried for all the 36 hotspot amino acids between GCP4 and γ-tubulin for both dimer1 and dimer2. Those amino acid residues which contributed more than 3 kcal/mol to the binding affinity of GCP4 and γ-tubulin complex were mutated to alanine, one by one, to determine $\Delta\Delta G_{bind}$. $\Delta\Delta G_{bind}$ was calculated as $\Delta_{Gmutant} - \Delta G_{wild\ type}$.

Chain	Residue	$\Delta\Delta G_{bind}$ (MM-GBSA)	$\Delta\Delta G_{bind}$ (MM-PBSA)
(a) Dimer1			
GCP4	ASP359	13.66	27.89
(Chain A)	GLU367	34.22	43.37
	LEU404	4.20	2.20
	TRP514	5.28	4.32
	ARG515	15.02	13.94
	TYR529	7.28	3.89
	GLN532	5.04	7.83
	VAL533	3.60	5.06
	GLU537	20.73	22.17
	ARG2	17.52	32.50
γ-tubulin	ARG46	16.33	26.46
(Chain B)	PRO261	1.14	1.09
	GLU326	3.07	4.29
	ASP328	19.11	21.64
	PRO329	3.00	0.92
	VAL357	0.04	0.65
	ARG361	15.41	14.71
	TRP445	2.42	1.54
(b) Dimer 2			
GCP4	GLU367	16.49	25.21
(Chain A)	TRP514	10.42	9.74
	ARG515	8.11	10.04
	ASN518	4.99	4.75
	PHE522	8.17	4.41
	ASN526	6.13	6.46
	TYR529	12.13	7.89
	TYR530	9.73	2.73
	SER538	4.16	5.43
	ARG46	9.80	12.66
γ-tubulin	MET248	5.28	6.19
(Chain B)	ASN249	4.73	8.95
	ILE 253	2.22	0.40
	PRO263	2.52	2.98
	PRO329	3.14	5.09
	HIS333	10.60	8.30
	ARG361	8.54	9.65
	TYR442	3.40	1.43

4.4 Conclusion

The current computational study provides insights into the interactions between GCP4 and γ-tubulin in two different conformations (dimer 1 and dimer 2) using molecular dynamics to calculate the binding free energy of binding in solvation. We found very robust interactions

between GCP4 and γ-tubulin in both dimer1 and dimer2 using both MM-PBSA and MM_GBSA methods. For both the dimers, the unfavourable polar contributions were observed to overcome with highly favourable non-polar components ($\Delta E_{vdw} + \Delta G_{sol\text{-}np}$). This highly favourable non –polar energy component might explain hydrophobic effect and hence the robust binding. We also identified 36 hot spot amino acids which and identifying key residues participating in the interactions. These hotspot amino acids were then verified using alanine scanning mutagenesis. Mutation of any of the hotspot to alanine resulted in a fall of net binding affinity between GCP4 and γ-tubulin by a minimum of 0.40 kcal/mol for Ile 253 in dimer to maximum of 43.37 kcal/mol in dimer 1.

REFERENCES

[1] N. Lecland and J. LÃ¼ders, "The dynamics of microtubule minus ends in the human mitotic spindle," *Nature cell biology*, 2014.

[2] V.r. Guillet, M. Knibiehler, L. Gregory-Pauron, M.-H.l.n. Remy, C.c. Chemin, B. Raynaud-Messina, C.c. Bon, J.M. Kollman, D.A. Agard, and A. Merdes, "Crystal structure of Î³-tubulin complex protein GCP4 provides insight into microtubule nucleation," *Nature structural & molecular biology*, vol. 18, (no. 8), pp. 915-919, 2011.

[3] T. Horio, S. Uzawa, M.K. Jung, B.R. Oakley, K. Tanaka, and M. Yanagida, "The fission yeast gamma-tubulin is essential for mitosis and is localized at microtubule organizing centers," *Journal of cell science*, vol. 99, (no. 4), pp. 693-700, 1991.

[4] H.C. Joshi, "γ-Tubulin: The hub of cellular microtubule assemblies," *Bioessays*, vol. 15, (no. 10), pp. 637-643, 1993.

[5] H.C. Joshi, M.J. Palacios, L. McNamara, and D.W. Cleveland, "γ-Tubulin is a centrosomal protein required for cell cycle-dependent microtubule nucleation," *Nature*, vol. 365, pp. 80-83, 1992.

[6] J.M. Kollman, A. Zelter, E.G.D. Muller, B. Fox, L.M. Rice, T.N. Davis, and D.A. Agard, "The structure of the Î³-tubulin small complex: implications of its architecture and flexibility for microtubule nucleation," *Molecular biology of the cell*, vol. 19, (no. 1), pp. 207-215, 2008.

[7] B.R. Oakley, C.E. Oakley, Y. Yoon, and M.K. Jung, "γ-Tubulin is a component of the spindle pole body that is essential for microtubule function in Aspergillus nidulans," *Cell*, vol. 61, (no. 7), pp. 1289-1301, 1990.

[8] K. Oegema, C. Wiese, O.C. Martin, R.A. Milligan, A. Iwamatsu, T.J. Mitchison, and Y. Zheng, "Characterization of two related Drosophila γ-tubulin complexes that differ in their ability to nucleate microtubules," *The Journal of cell biology*, vol. 144, (no. 4), pp. 721-733, 1999.

[9] T. Stearns, L. Evans, and M. Kirschner, "γ-Tubulin is a highly conserved component of the centrosome," *Cell*, vol. 65, (no. 5), pp. 825-836, 1991.

[10] Y. Zheng, M.K. Jung, and B.R. Oakley, "γ-Tubulin is present in Drosophila melanogaster and Homo sapiens and is associated with the centrosome," *Cell*, vol. 65, (no. 5), pp. 817-823, 1991.

[11] O. Cala, M.-H.l.n. Remy, V.r. Guillet, A. Merdes, L. Mourey, A. Milon, and G. Czaplicki, "Virtual and Biophysical Screening Targeting the Î³-Tubulin Complexâ€"A New Target for the Inhibition of Microtubule Nucleation," *PloS one*, vol. 8, (no. 5), pp. e63908.

[12] D.A. Case, T.E. Cheatham, T. Darden, H. Gohlke, R. Luo, K.M. Merz, A. Onufriev, C. Simmerling, B. Wang, and R.J. Woods, "The Amber biomolecular simulation programs," *Journal of computational chemistry*, vol. 26, (no. 16), pp. 1668-1688, 2005.

[13] D.A. Pearlman, D.A. Case, J.W. Caldwell, W.S. Ross, T.E. Cheatham III, S. DeBolt, D. Ferguson, G. Seibel, and P. Kollman, "AMBER, a package of computer programs for applying molecular mechanics, normal mode analysis, molecular dynamics and free energy calculations to simulate the structural and energetic properties of molecules," *Computer Physics Communications*, vol. 91, (no. 1), pp. 1-41, 1995.

[14] W.D. Cornell, P. Cieplak, C.I. Bayly, I.R. Gould, K.M. Merz, D.M. Ferguson, D.C. Spellmeyer, T. Fox, J.W. Caldwell, and P.A. Kollman, "A second generation force field for the simulation of proteins, nucleic acids, and organic molecules," *Journal of the American Chemical Society*, vol. 117, (no. 19), pp. 5179-5197, 1995.

[15] V. Hornak, R. Abel, A. Okur, B. Strockbine, A. Roitberg, and C. Simmerling, "Comparison of multiple Amber force fields and development of improved protein backbone parameters," *Proteins: Structure, Function, and Bioinformatics*, vol. 65, (no. 3), pp. 712-725, 2006.

[16] W.L. Jorgensen, J. Chandrasekhar, J.D. Madura, R.W. Impey, and M.L. Klein, "Comparison of simple potential functions for simulating liquid water," *The Journal of chemical physics*, vol. 79, (no. 2), pp. 926-935, 1983.

[17] T. Darden, D. York, and L. Pedersen, "Particle mesh Ewald: An N· log (N) method for Ewald sums in large systems," *The Journal of chemical physics*, vol. 98, (no. 12), pp. 10089-10092, 1993.

[18] U. Essmann, L. Perera, M.L. Berkowitz, T. Darden, H. Lee, and L.G. Pedersen, "A smooth particle mesh Ewald method," *The Journal of Chemical Physics*, vol. 103, (no. 19), pp. 8577-8593, 1995.

[19] J.-P. Ryckaert, G. Ciccotti, and H.J. Berendsen, "Numerical integration of the cartesian equations of motion of a system with constraints: molecular dynamics of< i> n</i>-alkanes," *Journal of Computational Physics*, vol. 23, (no. 3), pp. 327-341, 1977.

[20] H.J. Berendsen, J.P.M. Postma, W.F. van Gunsteren, A. DiNola, and J. Haak, "Molecular dynamics with coupling to an external bath," *The Journal of chemical physics*, vol. 81, (no. 8), pp. 3684-3690, 1984.

[21] P.A. Kollman, I. Massova, C. Reyes, B. Kuhn, S. Huo, L. Chong, M. Lee, T. Lee, Y. Duan, and W. Wang, "Calculating structures and free energies of complex molecules: combining molecular mechanics and continuum models," *Accounts of chemical research*, vol. 33, (no. 12), pp. 889-897, 2000.

[22] I. Massova and P.A. Kollman, "Combined molecular mechanical and continuum solvent approach (MM-PBSA/GBSA) to predict ligand binding," *Perspectives in Drug Discovery and Design*, vol. 18, (no. 1), pp. 113-135, 2000.

[23] D. Sitkoff, K.A. Sharp, and B. Honig, "Accurate calculation of hydration free energies using macroscopic solvent models," *The Journal of Physical Chemistry*, vol. 98, (no. 7), pp. 1978-1988, 1994.

[24] V. Zoete, M. Meuwly, and M. Karplus, "Study of the insulin dimerization: Binding free energy calculations and per-residue free energy decomposition," *Proteins: Structure, Function, and Bioinformatics*, vol. 61, (no. 1), pp. 79-93, 2005.

[25] V. Zoete and O. Michielin, "Comparison between computational alanine scanning and per-residue binding free energy decomposition for protein–protein association using MM-GBSA: Application to the TCR-p-MHC complex," *Proteins: Structure, Function, and Bioinformatics*, vol. 67, (no. 4), pp. 1026-1047, 2007.

[26] H. Gohlke and D.A. Case, "Converging free energy estimates: MM-PB (GB) SA studies on the protein–protein complex Ras–Raf," *Journal of computational chemistry*, vol. 25, (no. 2), pp. 238-250, 2004.

[27] H. Gohlke, C. Kiel, and D.A. Case, "Insights into protein–protein binding by binding free energy calculation and free energy decomposition for the Ras–Raf and Ras–RalGDS complexes," *Journal of molecular biology*, vol. 330, (no. 4), pp. 891-913, 2003.

CHAPTER 5

IDENTIFICATION OF CHEMICAL LEADS THAT INTERACT AT THE INTERFACE BETWEEN γ-TUBULIN AND GCP4

Abstract

In recent years, there has been immense interest in the identification of chemical leads that might interact with γ-tubulin and disrupt its function. Towards this end, recently a colchicine-interacting cavity was identified on γ-tubulin that might also interact with other similar compounds. Therefore, in the endeavour to identify chemical leads that might interact with γ-tubulin and disrupt its function; we found a class of compounds, noscapinoids that fits well in a cavity close to γ-tubulin-GCP4 interface. All noscapinoids displayed stable interaction throughout simulation, however, most robust interaction was observed for bromo-noscapine followed by noscapine and amino-noscapine with binding free energy of -46.73 kcal/mol, -41.69 kcal/mol and -35.40 kcal/mol respectively, using the MM-GBSA method and -31.86 kcal/mol, -23.60 kcal/mol and -20.50 kcal/mol respectively, using the MM-PBSA method in one two different conformations of γ-tubulin-GCP4 complex. Similarly for the other conformation also the most robust interaction with the γ-tubulin-GCP4 dimer was observed for bromo-noscapine with the binding affinity of -40 kcal/mol followed by noscapine with -32.82 kcal/mol and -21.84 kcal/mol for amino-noscapine, using MM-GBSA method. This offers a novel chemical scaffold for γ-tubulin binding drugs near γ-tubulin-GCP4 interface.

5.1 Introduction

γ-tubulin is indispensible for the microtubule spindle function in mitosis and its absence causes cell death [1, 2]. Recent studies have also indicated that γ-tubulin might also have a role in the regulation of microtubule dynamics at the plus ends [3]. Additionally, although tubulins (α/β) are abundant proteins constituting roughly 2.5% of the total protein in a cell, γ-tubulin makes up for less than 1% of the total tubulin content of the cell [4]. Higher expression of γ-tubulin has been associated with pre-invasive lesions and carcinomas of the breast and prostate cancer, thyroid carcinomas and glioblastoma multiforme [5-10]. Therefore, γ-tubulin has a clearly high potential of proving to be an excellent drug target for cancer therapy. Therefore, there is intense interest in gaining insights into how to go about developing promising leads that will be useful to design γ-tubulin interacting agents that will interfere with its function. There are multiple approaches to this end. For example, using a fragment based approach combined with biophysical screening of several small molecules; Cala et al. (2013) identified potential γ-tubulin interacting agents preferably at the γ-tubulin-GCP4 binding interface [11]. This approach has lead to some promising leads, like NM87 and NM372, which we have also utilized as references in our study (Figure 5.1).

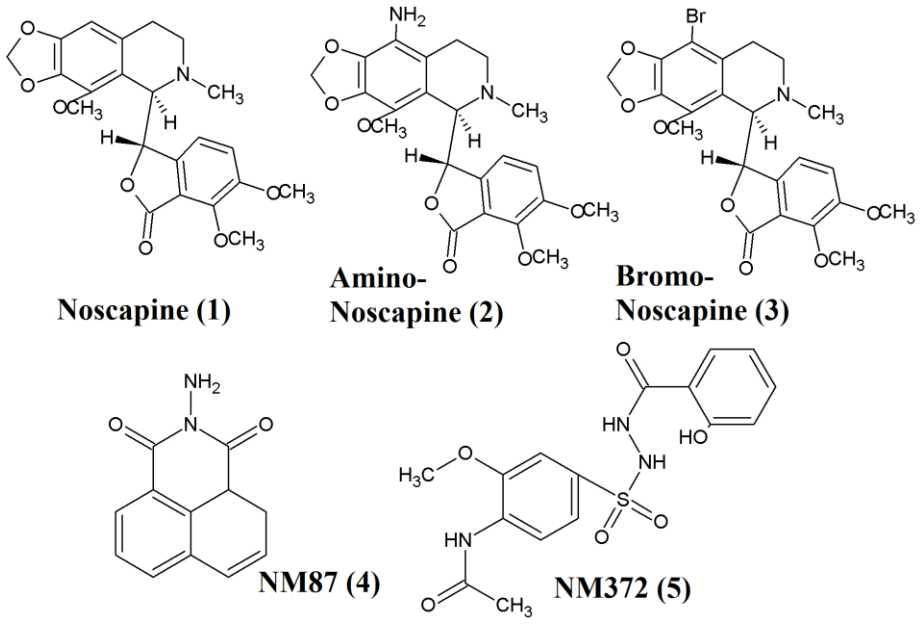

Figure 5.1: Molecular structure of the compounds: Noscapine (1), Amino-noscapine (2), Bromo-noscapine (3) and two reference compounds NM87 (4) and NM372 (5) used in the study. Both the reference compounds are previously reported to bind specifically onto the GCP4 and γ- tubulin interface

Advances in the crystal structures of alpha- beta- and gamma-tubulins yielded a realization that the overall structure of γ-tubulin was more similar to β-tubulin subunit than it is to the α-tubulin subunit [12-15]. Because β-tubulin has a very well characterized drug binding cavities, one straight approach is to explore how well these cavities are conserved in γ-tubulin structure and whether they can be used to identify additional potential lead compounds that can bind these cavities. To this end, Friesen et al. (2012) performed a rigorous search for colchicine binding site within the structure of γ-tubulin [16]. The colchicine site also accommodates many structurally related compounds such as podophyllotoxin and combrestatin. Not only did they find that the colchicine site is conserved between β-tubulin and γ-tubulin, but they showed that bacterially expressed γ-tubulin binds colchicine with a dissociation constant of 13.9 μM compared to a dissociation constant of 1.1 μM with β-tubulin suggesting that this is a good lead [16]. Colchicine and podophyllotoxin however, have been of limited use for cancer therapy because they are too toxic to animals at cancer therapeutic doses.

Based on the structures of colchicine, podophyllotoxin, combrestatin like compounds, Ye et al. (1998) identified a natural plant alkaloid, noscapine [17]. Several higher affinity analogues (noscapinoids) were then developed and shown to compete with the colchicine [18]. These compounds modulate microtubule dynamics upon binding and induce apoptosis both during mitosis and during interphase of the cell cycle [19, 20]. More importantly, perhaps due to milder effect on the normal cells, they do not display major side effects due to the disruption of haematopoiesis, hair follicles, gastrointestinal lining and the axonal transport and integrity. For example, Phase I/II studies showed low toxicity even at high dose of 300 mg/kg body weight [21]. Therefore it is necessary to investigate whether this class of compounds can also form suitable lead-compounds for the development of γ-tubulin interacting agents. Another attraction of investigating this class of compounds as structural leads comes from the fact that the binding pocket within the γ-tubulin lies in a close vicinity to its interaction site with a component of the TuSC, GCP4.

Therefore, in this study we first strive to extensively utilize molecular modelling and molecular dynamics (MD) simulation techniques to further investigate the precise mode and mechanism of interaction between GCP4 and γ-tubulin by theoretically estimating the free energy of binding between the protein units and identifying the key residues participating in the protein–protein interaction. Also, inspired by colchicine binding with γ-tubulin, we

investigated whether noscapinoids bind at the colchicine binding site of gamma-tubulin and how it might juxtapose with its interaction with GCP4.

We considered noscapine and its two derivatives, amino-noscapine and bromo-noscapine to investigate the mode and mechanism of interactions with respect to γ-tubulin-GCP4 complex using molecular docking, MD simulation and followed by molecular mechanics Poisson Boltzmann surface area (MM-PBSA) and Generalized Borne surface area (MM-GBSA). In order to compare and contrast our methods with those of the Cala et al. study, we also docked two fragments (NM372 and NM87 which binds at the interface) from the 20 top scoring fragments reported in this study with the γ-tubulin-GCP4 complex. Binding free energies were estimated as ensemble average of binding free energy, calculated using MM-PBSA/MM-GBSA methods.

5.2 Materials and Method

5.2.1 Ligand preparation

The molecular structure of the lead molecule, noscapine and two of its derivatives such as amino-noscapine and bromo-noscapine **1-3** (Figure 5.1) were built using molecular builder of Maestro (version 8.5, Schrodinger LLC). We also selected and built two compounds, NM87 and NM372 **4,5** (Figiure 5.1) as reference compounds, which have previously reported to bind specifically to the GCP4 and γ-tubulin interface [11]. All these five structures **1-5** were energy minimized *in vacuo* using Impact (version 5.6, Schrodinger, LLC). Appropriate bond orders were assigned to each structure using Ligprep (version 2.4, Schrodinger LLC) and initial optimization was performed on each structure by employing OPLS 2005 force field using default setting. Furthermore, geometrical optimization of these ligands was performed in Jaguar (version 7.7, Schrodinger, LLC) using hybrid density functional theory with Becke's three-parameter exchange potential and the Lee–Yang–Parr correlation functional (B3LYP) [22, 23] using basis set 3-21G* level [24-26].

5.2.2 Molecular docking

After ensuring that protein and ligands are in correct form, molecular docking of the optimized ligands onto the complex of GCP4 and γ-tubulin was performed using Glide (version 4.5, Schrodinger, LLC). The receptor-grid file was generated using grid receptor generation program with van der Waals scaling of 0.4 Å. A grid box size of 10 Å each for the

bounding and enclosing boxes were generated at the centroid of the predicted binding sites (using SiteMap, version 2.4, Schrodinger, LLC) [27]. The ligands were first docked using the "standard precision" method and further refined using "extra precision" Glide algorithm [27-29]. Van der Waals scaling of the ligand was set at 0.4 Å for all docking experiments. Out of the 50,000 poses that were sampled, 4,000 were subjected to energy minimization using conjugate gradients method over 1,000 steps. A total of thirty structures with lowest energy conformations were then screened for favourable Glide docking score. Single best conformation for each ligand–protein complex was selected for further molecular modeling calculations.

5.2.3 Structure preparation of docked complexes

The complexes obtained after molecular docking required some structure preparation to make them suitable for molecular dynamics simulations in Amber 11. The missing parameters for all four ligands were estimated with the antechamber programs [30] implemented in Amber 11. AM1-BCC charge model was used to calculate the atomic point charges [31]. Missing hydrogens were added and FF99SB forcefield was employed to assigned parameters to the complex of GCP4 and γ-tubulin, while GAFF forcefield was used to assigned the parameters to each ligand using tleap module available in Amber 11. Each system was neutralized using sodium ions and solvated using TIP3 water model in a truncated octahedron with distance of at least 15 Å between the wall of the box and the closest atom of the complex [32].

5.2.4 Molecular dynamics simulation of docked complexes

The parameter for the compounds **1-5** were estimated using antechamber program in Amber 11 simulation package. All the docked complexes were subjected to three rounds of minimization followed by heating, density equilibration and pressure equilibration. The equilibrated structure was then MD simulated for 10 ns. Similar methods, parameters and the constraints were used as described in chapter 4 for the MD simulation of GCP4 and γ-tubulin complex. The structures were recoreded every 1 ps resulting in a trajectory with 10,000 frames.

5.2.6 Calculation of binding free energy of docked complexes

The calculation of binding free energy between the ligand and the complex of GCP4 and γ-tubulin was carried out using the MM-GBSA and MM-PBSA method [33, 34]. The scoring scheme for the calculation of binding free energy is given below and the scheme is described in detail in Chapter 4, between GCP4 and γ-tubulin. Free energy of binding was calculated as the ensemble average of the binding free energy of a total of 500 snapshots, extracted every 10 ps from the last 5 ns of the MD simulation trajectory.

$$\mathbf{\Delta G_{bind} = \Delta G_{complex} - [\Delta G_{Rec} + \Delta G_{lig}]}$$

$$\mathbf{G = E_{gas} + G_{sol} - TS}.$$

$$\mathbf{E_{gas} = E_{int} + E_{ele} + E_{vdw}}$$

$$\mathbf{G_{sol} = G_{PB(GB)} + G_{sol\text{-}np}}$$

$$\mathbf{G_{sol\text{-}np} = \gamma SAS}$$

Where, **G** is Gibbs free energy, $\mathbf{E_{gas}}$ is the gas phase energy calculated as the sum of internal energy ($\mathbf{E_{int}}$), energy generated as a result of the electrostatic interaction ($\mathbf{E_{ele}}$) and the van der Waals interaction ($\mathbf{E_{vdw}}$). G_{sol} is the solvation free energy calculated as the sum of polar ($\mathbf{G_{PB(GB)}}$) and nonpolar contributions ($\mathbf{G_{sol\text{-}np}}$). Polar interaction contribution ($\mathbf{G_{PB(GB)}}$) was calculated as the summation of electrostatic contribution ($\mathbf{E_{ele}}$) and polar solvation contribution ($\mathbf{G_{PB(GB)}}$). The nonpolar solvation contribution ($G_{sol\text{-}np}$) is approximated as linearly dependent on the solvent accessible surface area (SAS) and γ is the surface tension constant that was set to 0.0072 kcal mol^{-1} $Å^{-2}$ [35].

5.2.7 Decomposition of ligand-residue interaction of docked complexes

The energy contribution of each residue in docked complexes was estimated using the MM-GBSA decomposition process in Amber 11.0 over the 500 frames obtained every 10 ps from the last 5 ns of simulation. The binding energy of each ligand-residue pair includes three energy terms: the van der Waals contribution (ΔE_{vdw}), the electrostatic contribution (ΔE_{ele}) and the solvation contribution (ΔE_{sol}). All the energy components are calculated using the same frames obtained from MD trajectories that were used for calculation of binding affinity.

5.3 Results and Discussions

After establishing the molecular interaction between GCP4 and γ-tubulin, molecular docking studies of noscapinoids (noscapine, amino-noscapine and bromo-noscapine) as well as two of the reference molecules (NM87 and NM372) were performed onto both the dimers. The docked complexes were then MD simulated for 10 ns to calculate the binding free energy of each ligand onto the complex of GCP4 and γ-tubulin dimers. The amino acid residues which showed significant interaction with the ligand molecules were identified using the energy decomposition analysis based on MM-GBSA method.

5.3.1 Molecular docking

We have adapted blind docking approach to predict the probable site of interaction of noscapinoids (noscapine, amino-noscapine and bromo-noscapine that were reported to have anticancer activities) with the GCP4 and γ-tubulin complex in the absence of co-crystal structure. In this approach we initially predicted all the binding sites of GCP4 and γ-tubulin tetramer complex which consists of at least 5 site points per reported site using sitemap program of Schrodinger package for molecular docking evaluation of binding sites. All these sites along with their various physico-chemical properties are included in Table 5.1. The probable site of interaction of noscapinoids onto GCP4 and γ-tubulin complex was screened out based on docking score. As mentioned in Table 5.2, all the molecules **1-5** shown better docking score with site 1 (belongs to dimer 1) and site 2 (belongs to dimer 2) were selected. The spatial localization of both site 1 and site 2 in the GCP4 and γ-tubulin tetramer complex is represented in Figure 5.2. As shown in figure, both the sites are located at the γ-tubulin surface that is juxtaposed wth its binding interface with GCP4. Eventually both the binding sites turned out to be consistent with the experimentally determined binding site reported previously by Cala et al. (2013) [11]. Cala et al. also screened 20 molecules and experimentally tested their binding affinity. We have used two molecules from this study, NM87 and NM372 as reference, along with three noscapinoids and docked into both the binding sites in a single experiment for comparison and to see any robust binding of noscapinoids with both the sites.

Table 5.1: Prediction of binding site. A total of 20 sites were predicted on γ-tubulin-GCP4 tetramer by sitemap prediction program available in Schrodinger package. The physico-chemical properties of these sites are included in the table.

Binding Site	Site Score	Size	Volume	Exposure	Enclosure	Contact	Phobic	Philic	Balance	Don/ Acc
1	1.03	782	1733.9	0.55	0.73	0.93	0.71	0.97	0.73	0.86
2	1.03	536	1385.4	0.54	0.74	0.92	0.42	1.07	0.39	1.01
3	1.01	661	1856.7	0.61	0.71	0.85	0.4	1.03	0.39	0.93
4	1.03	539	1507.5	0.52	0.74	0.93	0.38	1.13	0.33	0.91
5	1.01	343	1071.5	0.59	0.72	0.85	0.47	1.02	0.46	1
6	1.02	276	585.50	0.56	0.73	0.9	0.38	1.22	0.31	0.82
7	1.01	247	986.13	0.64	0.71	0.85	0.38	0.97	0.39	1.21
8	1	228	563.89	0.57	0.69	0.83	0.44	1.02	0.43	1.04
9	1.03	224	659.25	0.56	0.77	0.92	0.47	1.14	0.41	0.89
10	1.02	187	364.61	0.57	0.74	0.97	1.02	0.79	1.29	1.54
11	1.02	190	318.65	0.4	0.81	1.02	1.88	0.7	2.71	1.57
12	0.98	203	447.96	0.6	0.67	0.84	0.16	1.25	0.13	0.6
13	0.97	216	441.78	0.61	0.65	0.82	0.18	1.23	0.14	0.53
14	1.01	158	397.54	0.58	0.71	0.9	0.51	1.01	0.5	1.21
15	1.03	181	494.95	0.71	0.67	0.79	0.57	0.78	0.73	0.66
16	1.01	170	470.94	0.68	0.68	0.86	0.67	0.89	0.75	0.71
17	1.03	141	375.24	0.48	0.74	0.94	0.28	1.21	0.23	1.05
18	1.03	170	477.46	0.55	0.78	0.99	0.9	1.15	0.78	0.95
19	1.03	129	335.11	0.41	0.8	0.99	0.55	1.24	0.45	0.78
20	0.97	135	394.45	0.73	0.62	0.77	0.31	0.88	0.35	0.88

Surprisingly all the noscapinoids showed better docking scores compared to the reference molecules (Table 5.3), demonstrating the possibility of interactions of noscapinoids at the interface of GCP4 and γ-tubulin complex. Molecular docking methods are widely used by pharmaceutical industries to study drug-target interactions in order to understand the basic electronic/steric features required for therapeutic action and to design new drug candidates with improved activities. These docking calculations provide insight into interactions of noscaponoids with the GCP4 and γ-tubulin complex.

Table 5.2. Molecular docking evaluation of binding sites. All the ligands **1-5** were docked onto the predicted 20 binding sites of γ-tubulin-GCP4 tetramer complex. The binding sites that showed better docking score with all the ligands were selected as the probable sites of interaction of these ligands on γ-tubulin-GCP4 tetramer complex. On the basis of the site score and docking score with the predicted binding sites against which the ligands showed better binding score, both site1 (belongs to dimer1) and site2 (belongs to dimer2) were selected.

Site	Noscapine	Amino-Noscapine	Bromo-Noscapine	NM87	NM372
Site1	-7.59	-7.56	-9.08	-6.74	-7.28
Site2	-6.83	-6.73	-9.19	-6.66	-7.70
Site3	-5.56	-5.41	-5.95	-5.01	-6.32
Site4	-4.83	-5.13	-3.65	-5.90	-6.25
Site5	-3.38	-4.90	-5.23	-4.85	-6.57
Site6	-2.67	-3.28	-16.52	-5.73	-5.52
Site7	-4.98	-7.04	-6.23	-5.37	-5.85
Site8	-5.12	-6.75	-6.93	-5.56	-6.54
Site9	-5.46	-4.75	-5.68	-5.07	-5.99
Site10	-3.71	-1.70	-3.51	-5.29	-5.35
Site11	-6.25	-6.34	-6.40	-5.50	-5.88
Site12	-6.84	-7.25	-6.52	-4.19	-5.36
Site13	-6.92	-7.59	-7.01	-4.86	-4.95
Site14	-4.87	-6.68	-4.61	-3.51	-4.10
Site15	-5.96	-6.10	-5.28	-4.69	-4.88
Site16	-7.05	-7.81	-8.96	-5.26	-5.67
Site17	-5.67	-5.76	-4.09	-5.28	-5.67
Site18	-5.48	-6.80	-6.77	-4.18	-5.03
Site19	-7.47	-7.27	-7.93	-5.96	-5.15
Site20	-4.37	-6.38	-6.69	-3.26	-4.28

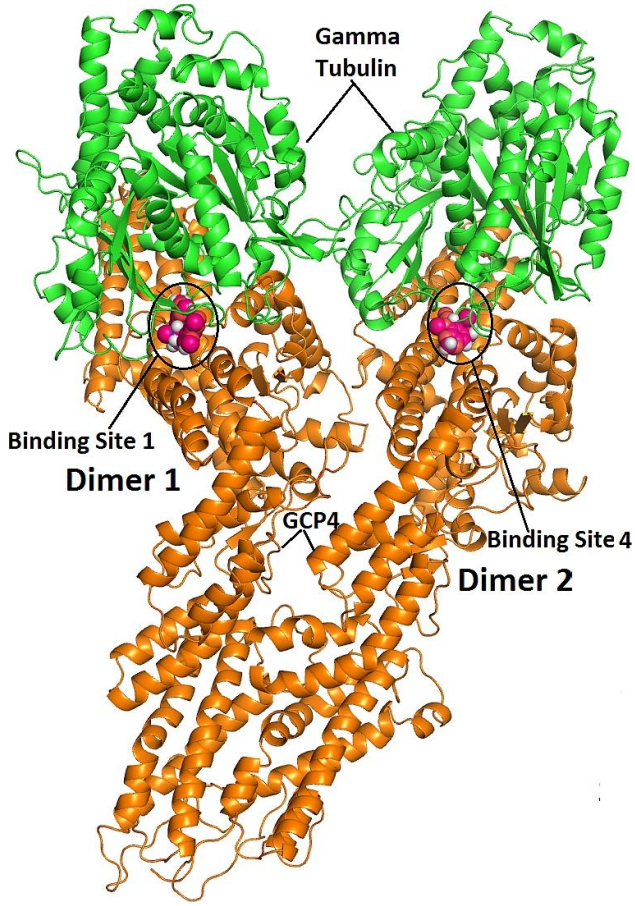

Figure 5.2: **Predicted binding sites.** γ-tubulin-GCP4 tetramer showing noscapinoid binding site 1 and binding site 2. Both the binding sites, marked as spheres, lie at the interface of γ-tubulin-GCP4 complex.

Table 5.3: Glide docking scores. After predicting the binding sites, extra-precision docking was performed using Glide XP dock protocol implemented in Schrodinger package. XP_{score} (kcal/mol) of noscapinoids (noscapine, amino-noscapine, bromo-noscapine) and the reference compounds (NM87 and NM372) with GCP4 and γ-tubulin hetero-dimer are presented in the table. Noscapinoids showed better docking score compared to the reference molecules, NM87 and NM372.

(A). Site 1					
Ligand	Glide e_{vdw}	Glide e_{coul}	Glide Emodel	Glide energy	XP GScore
Noscapine	-22.72	-4.34	-31.95	-27.06	-7.59
Amino	-9.18	-4.95	40.25	-14.13	-7.56
Bromo	-26.88	-5.67	-44.30	-32.55	-9.08
NM87	-23.46	-2.68	-31.04	-26.13	-6.74
NM372	-37.18	-10.93	-69.51	-48.11	-7.28
(B). Site 2					
Ligand	Glide e_{vdw}	Glide e_{coul}	Glide Emodel	Glide energy	XP GScore
Noscapine	-38.25	-8.17	-53.86	-46.41	-6.83
Amino	-27.64	-11.70	-51.58	-39.34	-6.73
Bromo	-38.84	-10.11	-47.14	-48.95	-9.19
NM87	-24.69	-4.28	-36.71	-28.97	-6.66
NM372	-36.61	-7.20	-63.52	-43.82	-7.70

5.3.2 Determination of binding mode of compounds 1-5 with GCP4 and γ-tubulin complex

Although computationally demanding, we determined the preferential binding mode of compounds **1-5** with GCP4 and γ-tubulin complex by molecular dynamics simulations. Towards this end the complexes obtained after molecular docking were simulated for 10 ns to obtain a total of 10,000 frames. The stability of the system was monitored by means of RMSD of Cα-atoms during the entire duration of simulation as shown in Figure 5.3. The RMSD of all the complexes reaches equilibrium at 4000 ps and after that the RMSDs of atoms oscillated between 2-4 Å. Furthermore, the local protein mobility was analysed by calculating the time averaged RMSF values in free and bound form of GCP4 and γ-tubulin complexes with compounds **1-5**. The RMSF values were plotted against residue numbers based on the 10000 ps trajectory as shown in Figure 5.4.

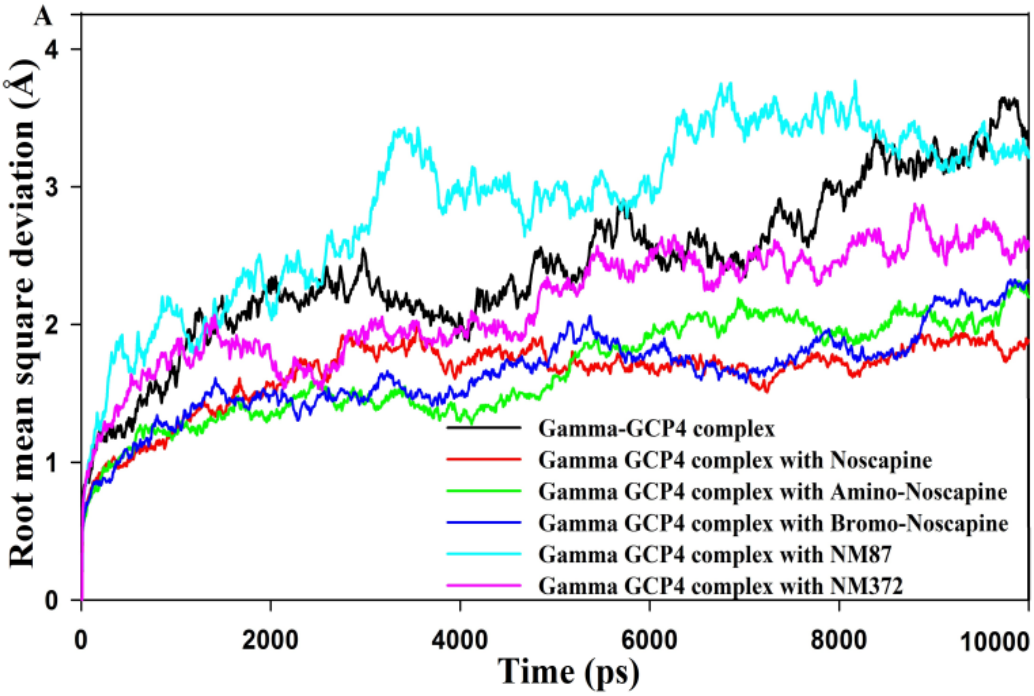

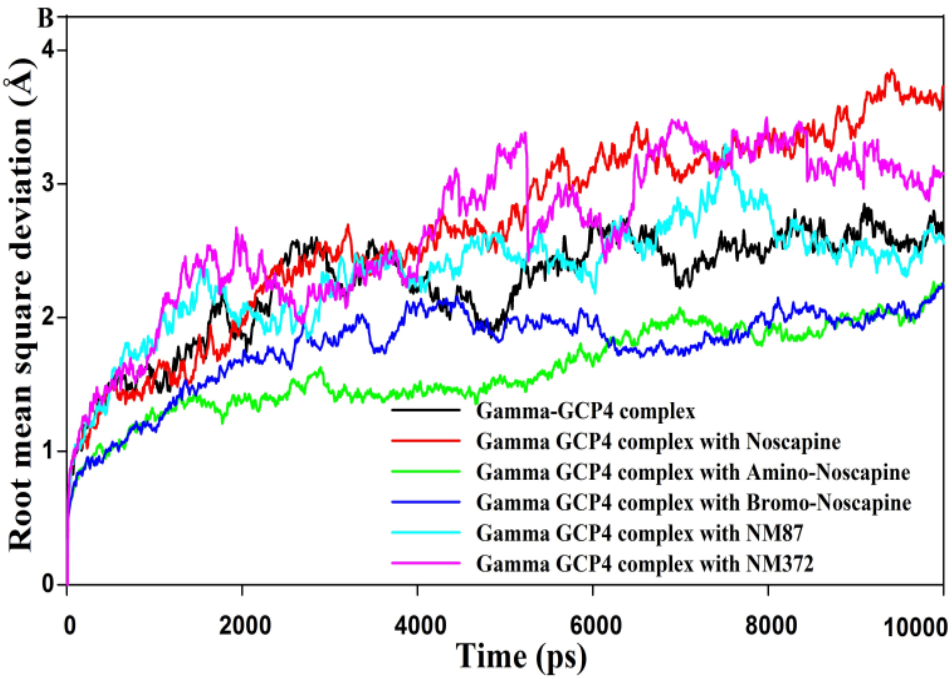

Figure 5.3: Root mean square daviation. The root mean square deviations (RMSD) of Cα atoms in the GCP4 and γ-tubulin complex in dimer 1 (A) and dimer 2 (B) in the free form and bound form with different ligands (noscapine, amino-noscapine, bromo-noscapine, NM87 and NM372) during the entire duration of MD simulation. The relative fluctuation in the RMSD of the Cα atoms is very small after 4000 ps, revealed that each system reaches equilibrium at 4000 ps.

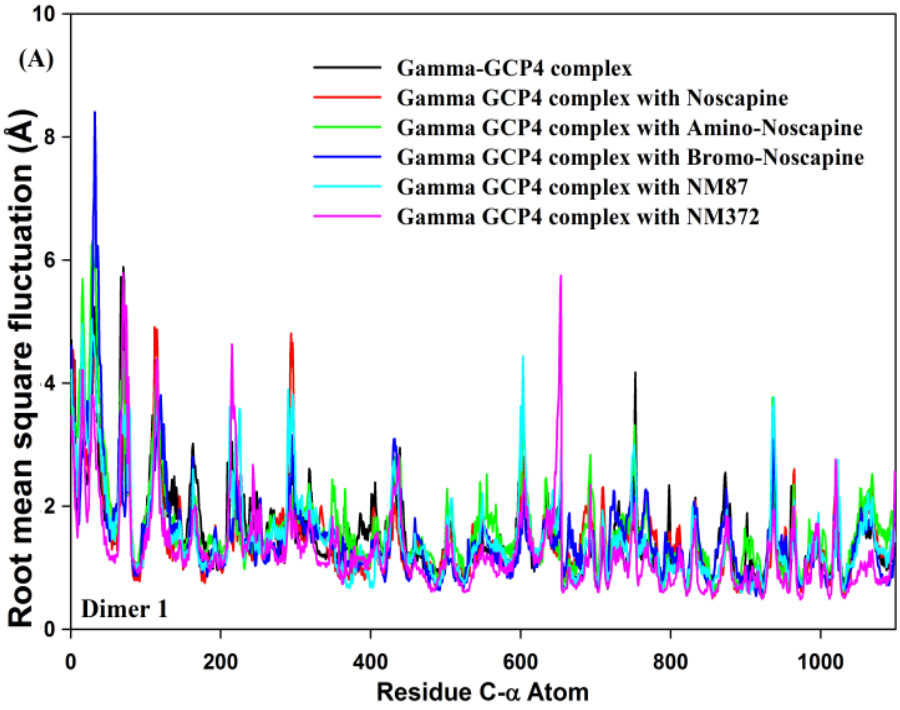

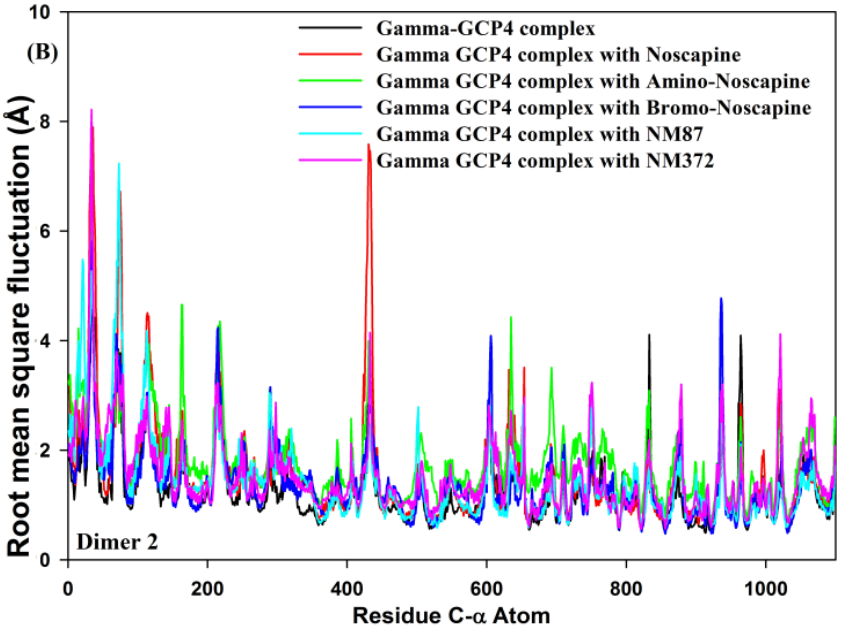

Figure 5.4: Root mean square fluctuation (RMSF) of Cα atoms. RMSF of residues in the complex of GCP4 and γ-tubulin in dimmer 1 (A) and dimmer 2 (B) in the free form and in the bound form with different ligands (noscapine, amino-noscapine, bromo-noscapine, NM87 and NM372) during the entire duration of MD simulation. The residues with higher RMSF tend to show more flexibility. The residues in the bound form show a small degree of flexibility when compared with free GCP4 and γ-tubulin complex.

The profiles of atomic fluctuations were found to be very similar for all the compounds **1-5**. The compounds **1-5** were observed to dock into the GCP4 and γ-tubulin complex throughout the 10 ns simulation. Specifically the MD simulation makes an important contribution to understand the effect of binding of compounds **1-5** on conformational changes of GCP4 and γ-tubulin complex and the stability of protein-ligand system in aqueous solution. The binding mode of **1-5** involves interactions of the compounds with both GCP4 and γ-tubulin at sites reported earlier [20] and are well accomodated inside the binding cavity (Figure 5.5). The binding mode of ligands with the protein complex was represented in two steps: (a) receptor residues that have strong interactions with the ligand, such as a favourable hydrogen-bonding interactions, and (b) receptor residues that are close to the ligand, but whose interactions with the ligand are weak or diffuse, such as hydrophobic interaction. The differential mode of interactions of compounds **1-5** with the residues of GCP4 and γ-tubulin complex are represented in the Ligplot (Figure 5.6). As seen in the figure several hydrogen bonds and hydrophobic interactions are involved in their binding.

5.3.3 Binding affinity between GCP4 and γ-tubulin complexes and drug molecules

Binding free energies of dimer 1 as well as dimer 2 with the noscapinoids (noscapine, amino-noscapine and bromo-noscapine) and the reference molecules (NM372 and NM87)

were calculated using the MM-PBSA and MM-GBSA approach. The predictive binding free energy comes out to be even better for the noscapinoids compared to the reference molecules based on both MM-GBSA and MM-PBSA methods (Figure 5.7). The binding free energy of compounds **1-5** and the respective energy components are include in Table 5. For all complexes, the binding energy was decomposed into its various energy components (the electrostatic, van der Waals and solvation). Both van der Waals ($\mathbf{\Delta E}_{VDW}$) and the electrostatic component ($\mathbf{\Delta E}_{ELE}$) were observed to make very significant contributions to the free energy of binding. However, the net polar contribution ($\Delta G_{(ele,PB/GB)} = \Delta E_{ele} + \Delta G_{(PB/GB)}$) was rendered unfavourable due to very large penalty imposed by the desolvation component ($\Delta G_{PB/GB}$) while the net nonpolar component (ΔE_{vdw}) and ($\Delta G_{sol\text{-}np}$) were observed to make highly favourable contribution to the binding free energy (Figure 5.8). On analysing the energy contribution of each residue in the complex, Tyr247 and Arg361 of γ- tubulin were observed to make significant contribution to the binding of ligands for all the complexes. Ligplot analysis also illustrates strong interaction of Arg361 of γ-tubulin with all the three drug molecules in both the complexes, mostly through H-bond formation (Figure 5.6). It is our hope that the results presented here provide new grounds for further investigations of the therapeutic potential of noscapinoids against microtubule-nucleating γ-tubulin complexes.

The profiles of atomic fluctuations were found to be very similar for all the compounds **1-5**. The compounds **1-5** were observed to docked into the GCP4 and γ-tubulin complex throughout the 10 ns simulation. Specifically the MD simulation makes an important contribution to understand the effect of binding of compounds **1-5** on conformational changes of GCP4 and γ-tubulin complex and the stability of protein-ligand system in aqueous solution. The binding mode of **1-5** involves interactions of the compounds with both GCP4 and γ-tubulin at sites reported earlier [20] and are well accomodated inside the binding cavity (Figure 5.5). The binding mode of ligands with the protein complex was represented in two steps: (a) receptor residues that have strong interactions with the ligand, such as a favourable hydrogen-bonding interactions, and (b) receptor residues that are close to the ligand, but whose interactions with the ligand are weak or diffuse, such as hydrophobic interaction. The differential mode of interactions of compounds **1-5** with the residues of GCP4 and γ-tubulin complex are represented in the Ligplot (Figure 5.6). As seen in the figure several hydrogen bonds and hydrophobic interactions are involved in their binding.

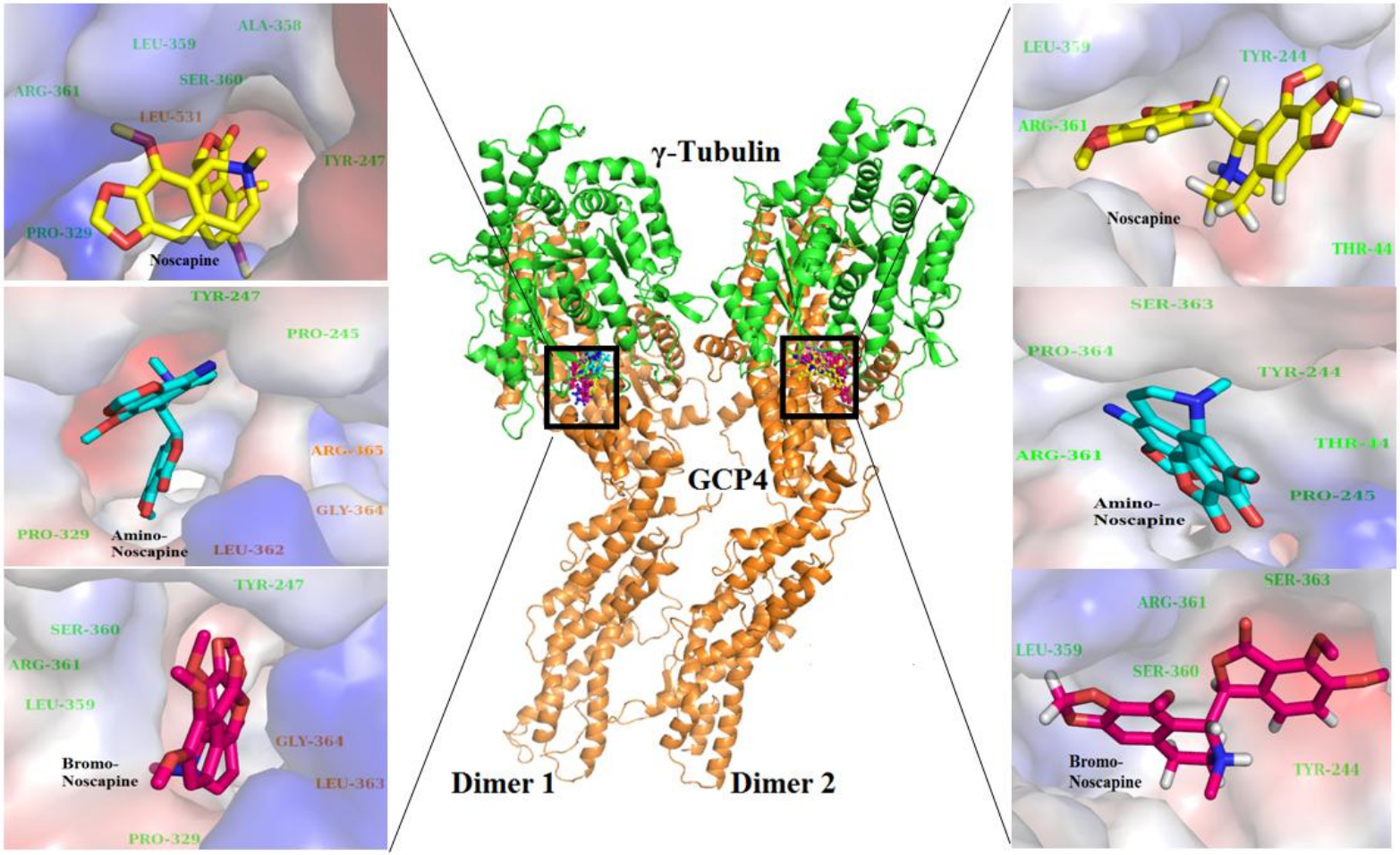

Figure 5.5 A: Binding modes of noscapinoids. Noscapinoids (Noscapine, Amino-Noscapine and Bromo-Noscapine) docked into dimer1 and dimer2. The zoomed views show the binding modes of the noscapinoids alone. The residues which show contribution of more than 1 kcal/mol to the binding affinity are labeled green for γ-tubulin and orange for GCP4.

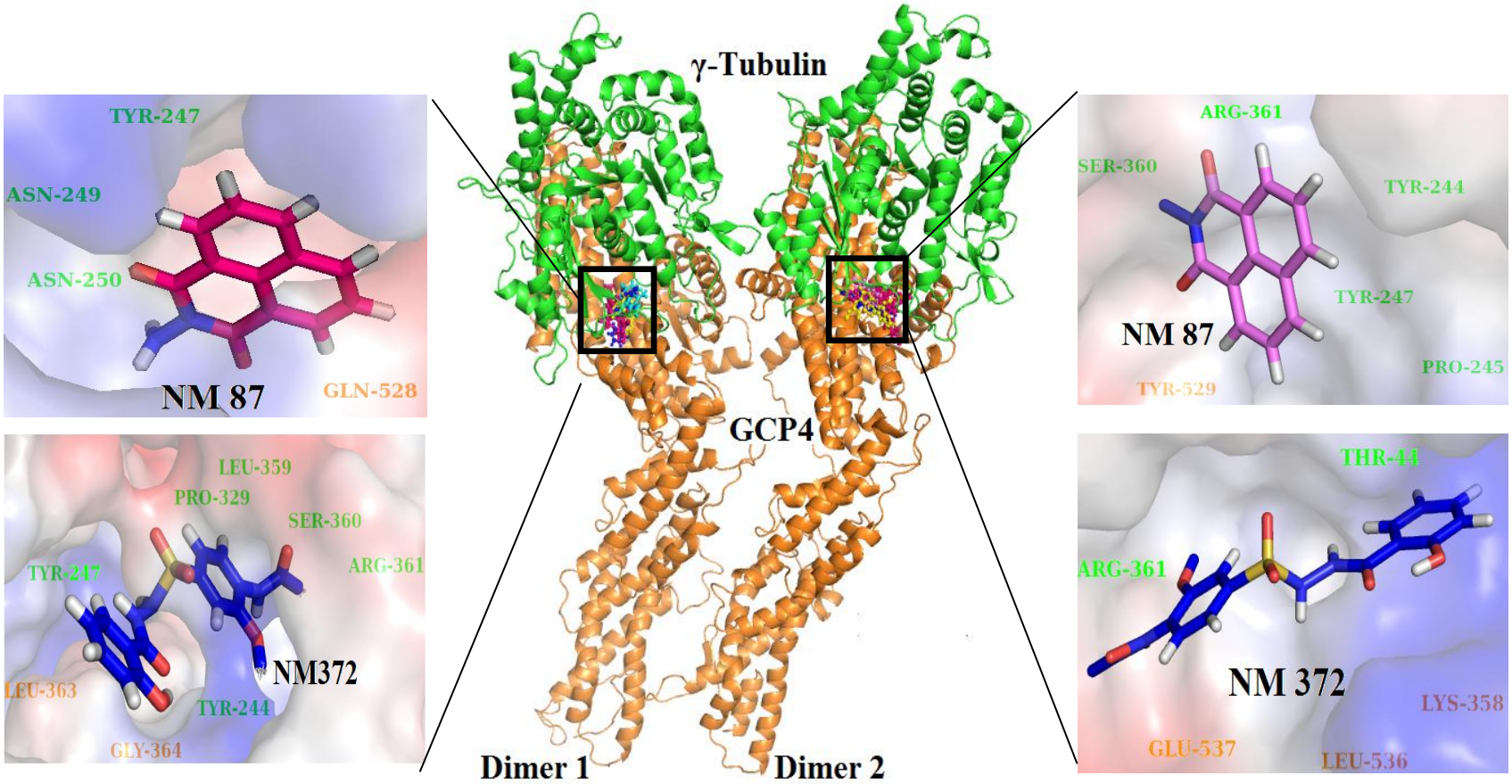

Figure 5.5 B: Binding modes of Reference molecules. Both the reference molecules (NM 87 and NM 372) docked into dimer1 and dimer2. The zoomed views show the binding modes of the reference molecules. The residues which show contribution of more than 1 kcal/mol to the binding affinity are labeled green for γ-tubulin and orange for GCP4.

5.3.4 Binding affinity of drugs with GCP4 and γ tubulin complex

Binding free energies of dimer 1 as well as dimer 2 with the noscapinoids (noscapine, amino-noscapine and bromo-noscapine) and the reference molecules (NM372 and NM87) were calculated using the MM-PBSA and MM-GBSA approach. The predictive binding free energy comes out to be even better for the noscapinoids compared to the reference molecules based on both MM-GBSA and MM-PBSA methods (Figure 5.6). The binding free energy of compounds **1-5** and the respective energy components are include in Table 5.4.

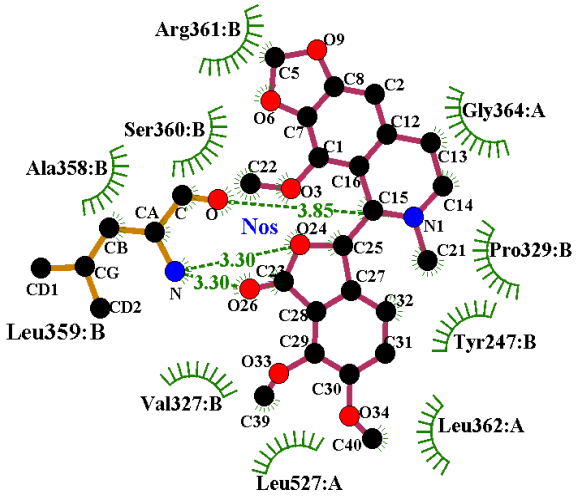

Dimer1-Noscapine

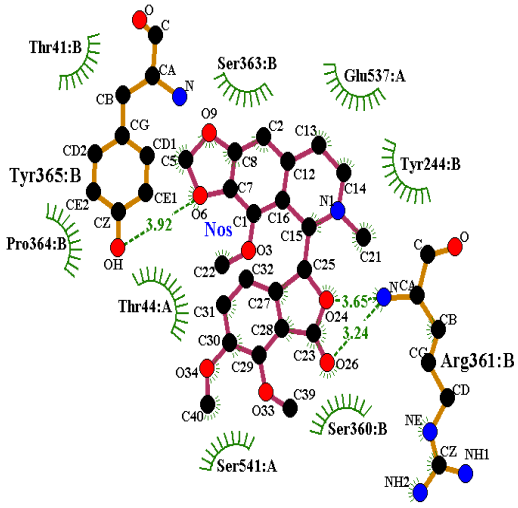

Dimer2-Noscapine

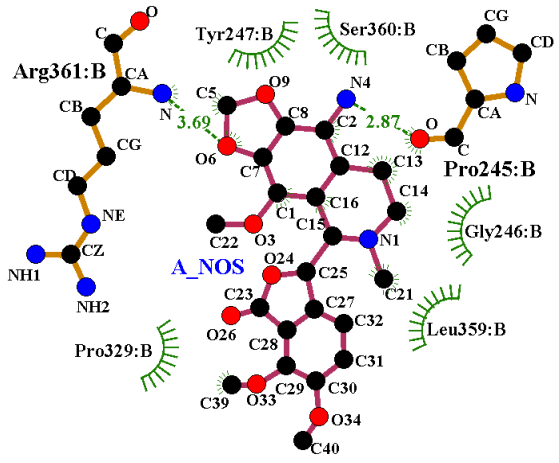

Dimer1-Amino Noscapine

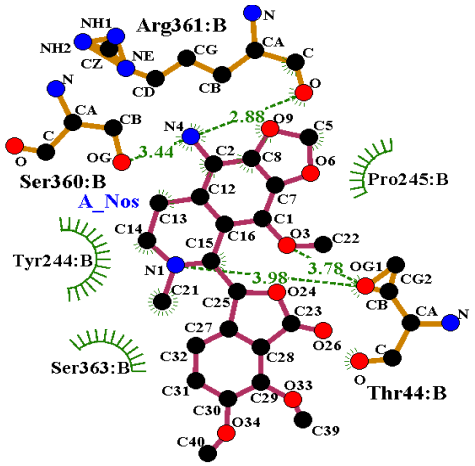

Dimer2-Amino Noscapine

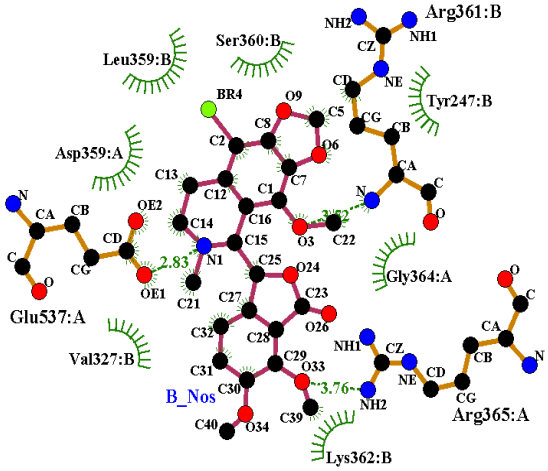

Dimer1-Bromo Noscapine

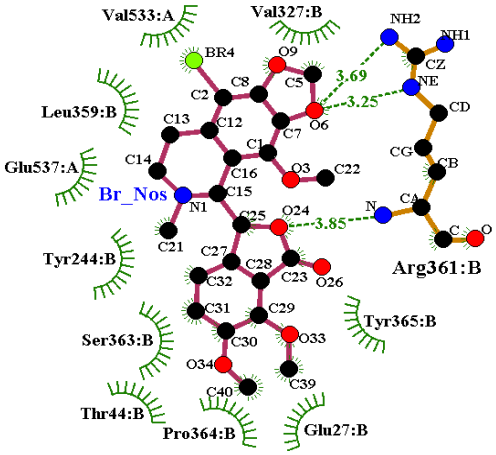

Dimer2-Bromo Noscapine

Figure 5.6 A: 2-D ligplot of noscapinoids: A 2-D representation of the binding mode of noscapinoids (Noscapine, Amino-Noscapine and Bromo-Noscapine) with the complex of GCP4 and γ-tubulin. In the images 'A' denotes the residues of GCP4 and 'B' denotes the residues of γ-tubulin.

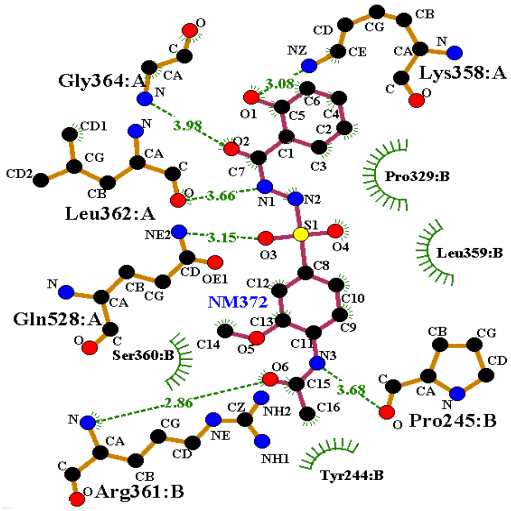

Dimer1-NM372

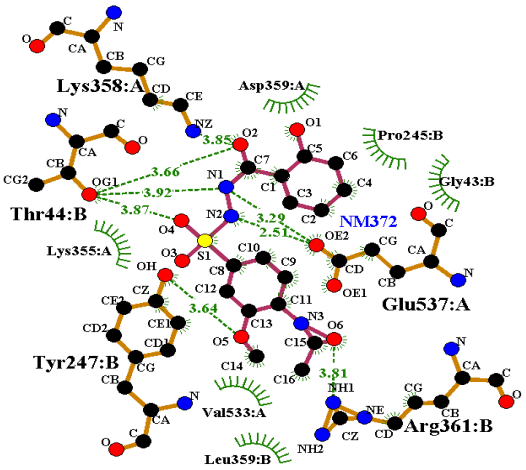

Dimer2-NM372

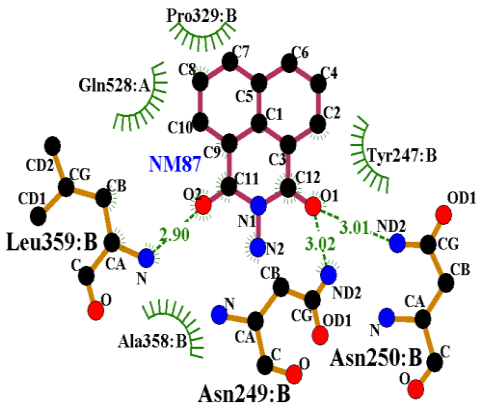

Dimer1-NM87

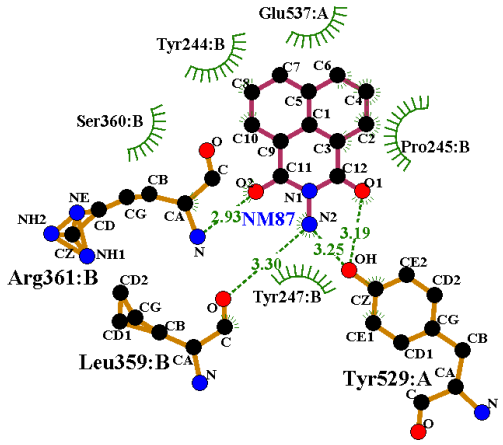

Dimer2-NM87

Figure 5.6 B: 2-D ligplot of reference molecules: A 2-D representation of the binding mode of reference compounds (NM87 and NM372) with the complex of GCP4 and γ-tubulin. In the images 'A' denotes the residues of GCP4 and 'B' denotes the residues of γ-tubulin.

Table 5.5: Binding free energy. Binding affinity of drugs with GCP4 and γ-tubulin complex was calculated using MM-GB/PBSA methods. Binding free energy (kcal/mol) and the respective energy components of noscapinoid drugs binding to GCP4 and γ-tubulin dimers are given in the table below.

Contribution	Noscapine	Amino-Noscapine	Bromo-Noscapine	NM87	NM372
		Dimer1			
ΔE INT	0.00	0.00	0.00	0.00	0.00
ΔE VDW	-52.03	-48.94	-55.48	-24.84	-51.34
ΔE ELE	-220.92	-204.21	-236.13	-18.49	-39.05
ΔE GAS/ ΔE MM	-272.94	-253.12	-291.60	-43.33	2.00
ΔG PB	253.49	236.72	263.75	29.04	70.75
ΔG SOL-NP	-4.15	-4.09	-3.99	-1.67	-3.86
ΔG SOLV,PB	249.35	232.62	259.77	27.37	66.90
ΔG ELE,PB	32.57	32.51	27.62	10.56	31.71
H TOT,PB	-23.60	-20.50	-31.83	-15.95	-23.50
G GB	236.89	223.22	250.54	24.71	59.03
G SOLV,GB	231.25	217.73	244.87	21.56	52.63
G ELE GB	15.97	19.01	14.41	6.22	19.98
H TOT, GB	-41.69	-35.40	-46.73	-21.76	-37.76
		Dimer2			
ΔE INT	0.00	0.00	0.00	0.00	0.00
ΔE VDW	-46.95	-34.61	-52.03	-29.52	-40.22
ΔE ELE	-226.88	-230.12	-234.78	-19.60	-27.18
ΔE GAS/ ΔE MM	-273.81	-264.70	-286.80	-49.12	-67.40
ΔG PB	261.34	247.50	271.30	34.56	48.28
ΔG SOL-NP	-4.02	-2.67	-3.88	-1.92	-3.84
ΔG SOLV,PB	257.32	244.83	267.43	32.64	44.44
ΔG ELE,PB	34.46	17.38	36.52	14.95	21.10
H TOT,PB	-16.50	-19.87	-19.37	-16.49	-22.96
G GB	246.27	246.38	251.66	30.49	42.92
G SOLV,GB	241.00	242.87	246.35	27.06	37.36
G ELE GB	19.39	16.26	16.88	10.89	15.75
H TOT, GB	-32.82	-21.84	-40.45	-22.07	-30.04

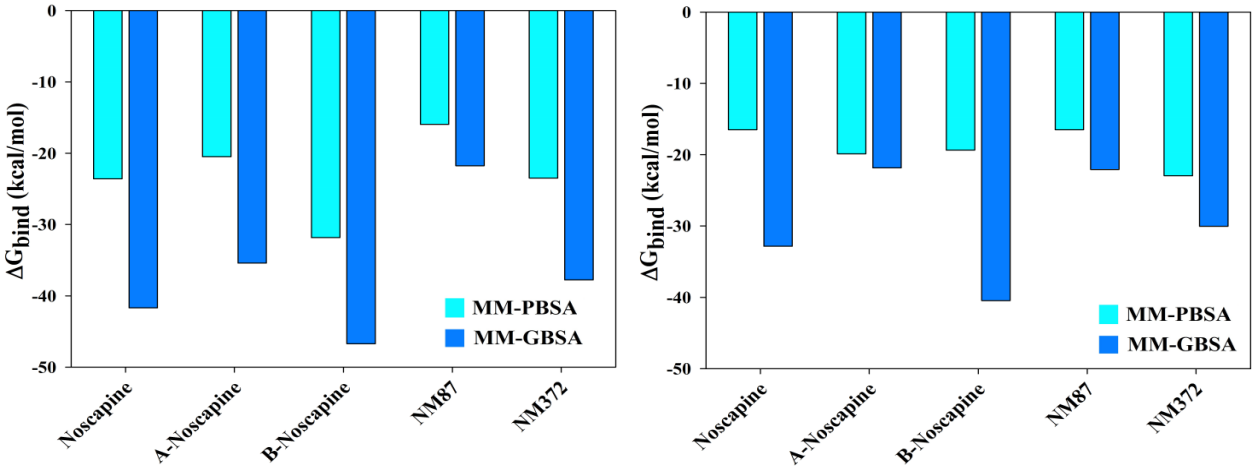

Figure 5.7: Calculated binding free energy. The binding free energy for each of the three drug molecules – Noscapine, Amino-Noscapine, Bromo-Noscapine; and the reference molecules- NM87, NM372; calculated using MM-PBSA and MM_GBSA methods.

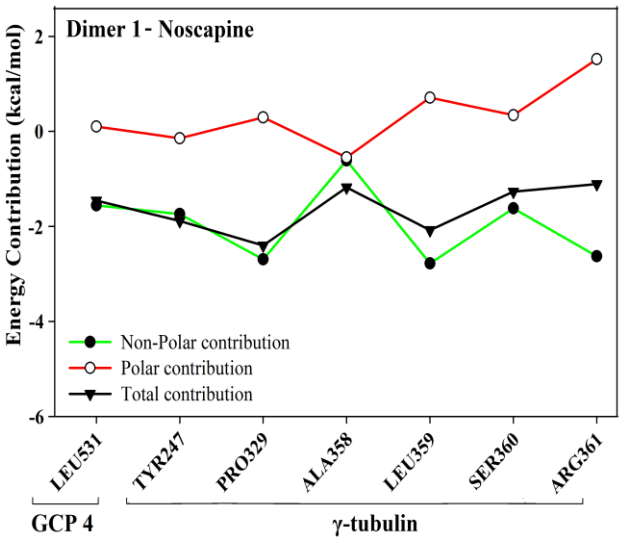
Dimer 1 - Noscapine
Energy Contribution (kcal/mol)
Non-Polar contribution
Polar contribution
Total contribution
LEU531
TYR247
PRO329
ALA358
LEU359
SER360
ARG361
GCP 4
γ-tubulin

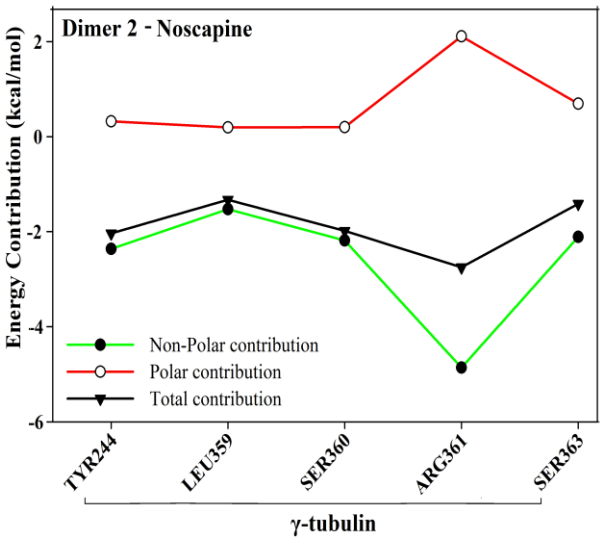
Dimer 2 - Noscapine
Energy Contribution (kcal/mol)
Non-Polar contribution
Polar contribution
Total contribution
TYR244
LEU359
SER360
ARG361
SER363
γ-tubulin

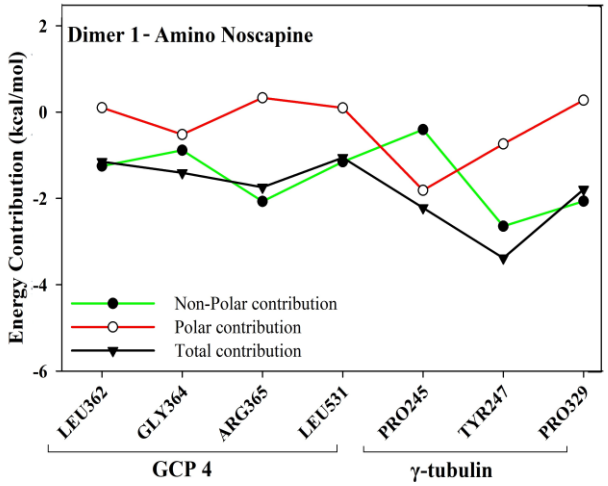
Dimer 1 - Amino Noscapine
Energy Contribution (kcal/mol)
Non-Polar contribution
Polar contribution
Total contribution
LEU362
GLY364
ARG365
LEU531
PRO245
TYR247
PRO329
GCP 4
γ-tubulin

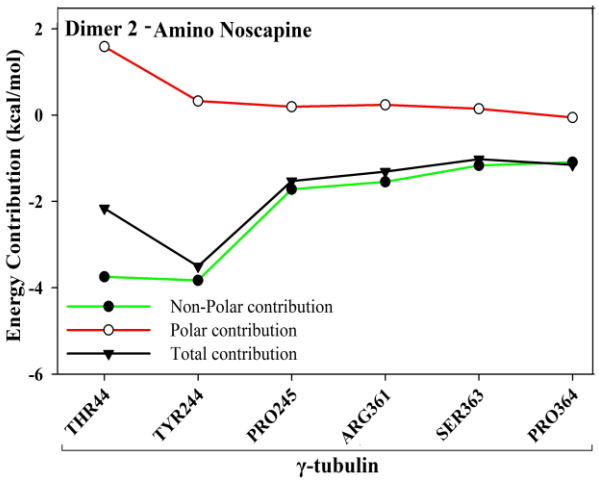
Dimer 2 - Amino Noscapine
Energy Contribution (kcal/mol)
Non-Polar contribution
Polar contribution
Total contribution
THR44
TYR244
PRO245
ARG361
SER363
PRO364
γ-tubulin

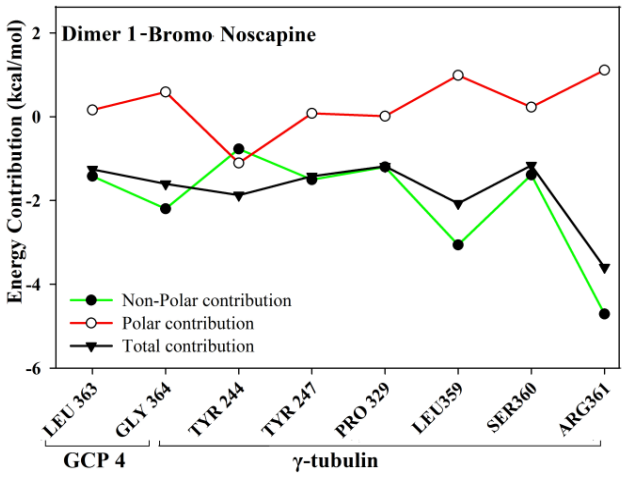
Dimer 1 - Bromo Noscapine
Energy Contribution (kcal/mol)
Non-Polar contribution
Polar contribution
Total contribution
LEU 363
GLY 364
TYR 244
TYR 247
PRO 329
LEU359
SER360
ARG361
GCP 4
γ-tubulin

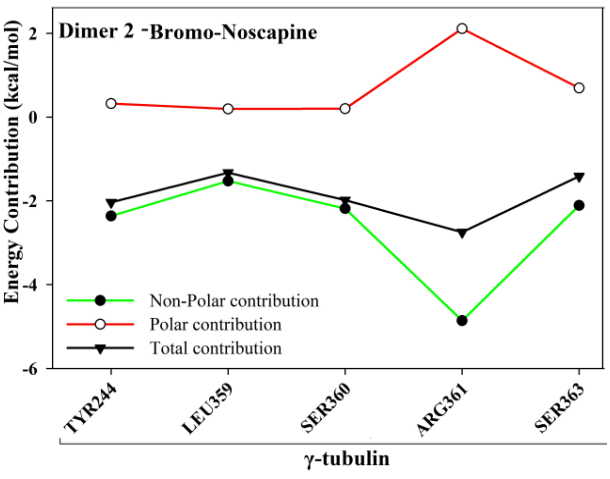
Dimer 2 - Bromo-Noscapine
Energy Contribution (kcal/mol)
Non-Polar contribution
Polar contribution
Total contribution
TYR244
LEU359
SER360
ARG361
SER363
γ-tubulin

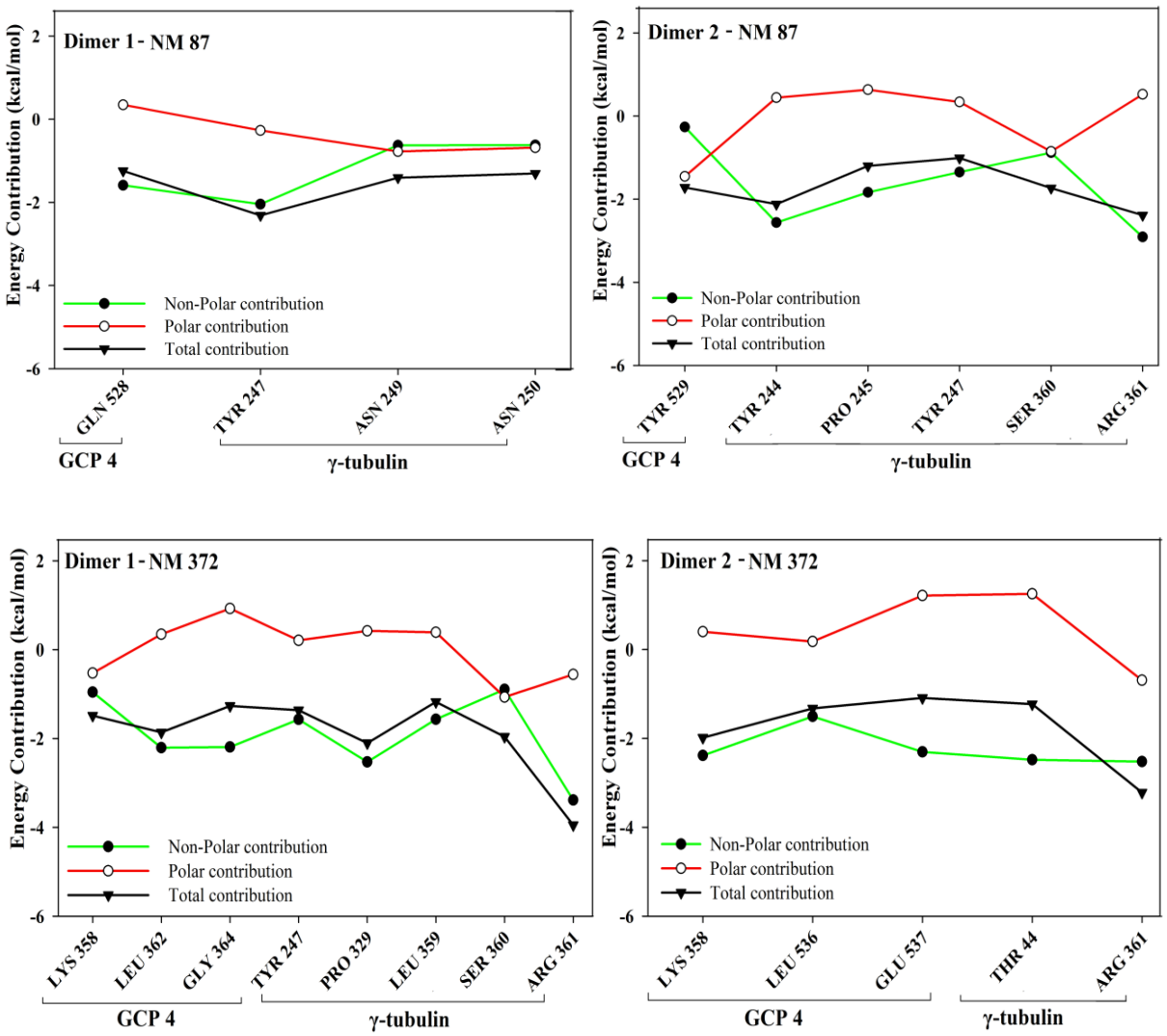

Figure 5.8 : Energy contributions of hotspot amino acids. Non-polar, polar as well as total energy contributions of the amino acid residues that contribute most to the stability of the protein ligand complex. Polar interactions were calculated as sum of electrostatic ($\Delta E_{i,ele}$) and polar solvation ($\Delta G_{i,sol,GB}$) energy components while the non-polar interactions were calculated as sum of van der Waals ($\Delta E_{i,vdw}$) and non-polar solvation component ($\Delta G_{i,sol-np}$).

For all complexes, the binding energy was decomposed into its various energy components (the electrostatic, van der Waals and solvation). Both van der Waals ($\mathbf{\Delta E}_{VDW}$) and the electrostatic component ($\mathbf{\Delta E}_{ELE}$) were observed to make very significant contributions to the free energy of binding. However, the net polar contribution ($\Delta G_{(ele,PB/GB)} = \Delta E_{ele} + \Delta G_{(PB/GB)}$) was rendered unfavourable due to very large penalty imposed by the desolvation component ($\Delta G_{PB/GB}$) while the net nonpolar component (ΔE_{vdw}) and (ΔG_{sol-np}) were observed to make highly favourable contribution to the binding free energy (Figure 5.7). On analysing the energy contribution of each residue in the complex, Tyr247 and Arg361 of γ- tubulin were observed to make significant contribution to the binding of ligands for all the complexes.

Ligplot analysis also illustrates strong interaction of Arg361 of γ-tubulin with all the three drug molecules in both the complexes, mostly through H-bond formation (Figure 5.6). It is our hope that the results presented here provide new grounds for further investigations of the therapeutic potential of noscapinoids against microtubule-nucleating γ-tubulin complexes.

5.4 Conclusion

The binding modes of the three noscapinoids with the GCP4 and γ-tubulin dimers were further illustrated using MD simulation and binding free energy calculations. All three drugs lodged themselves in the pockets located very close to the binding interface of the GCP4 and γ-tubulin. The molecular interaction of all the three drugs are leveraged more towards γ-tubulin. The binding modes of noscapine and bromo-noscapine are quite similar with both the drugs showing strong interaction with Tyr247, Pro329, Leu359, Ser360 and Arg361 of γ-tubulin in dimer 1. Both drugs also displayed similar interactions with Tyr244, Leu359 and Arg361 in dimer 2. Pro329 and Arg361 are also two important identified hotspot amino acids in the interaction of GCP4 and γ-tubulin. We also observe that in almost all complexes the drug makes H-bond with Arg361. Therefore, if these drugs can interfere with a subset of the hotspot amino acids they might be able to perturb some of the interactions between GCP4 and γ-tubulin and further destabilize the γTuRC. Nevertheless, our results offer noscapinoids an important possible chemical framework for the further design of more potent compounds.

REFERENCES

[1] H.C. Joshi, M.J. Palacios, L. McNamara, and D.W. Cleveland, "γ-Tubulin is a centrosomal protein required for cell cycle-dependent microtubule nucleation," *Nature*, vol. 365, pp. 80-83, 1992.

[2] B.R. Oakley, C.E. Oakley, Y. Yoon, and M.K. Jung, "γ-Tubulin is a component of the spindle pole body that is essential for microtubule function in Aspergillus nidulans," *Cell*, vol. 61, (no. 7), pp. 1289-1301, 1990.

[3] M.A. Raynaud-Messina B, "g-Tubulin complexes and microtubule organization," *Current Opinion Cell Biology*, vol. 19, pp. 24–3, 2007.

[4] T. Stearns, L. Evans, and M. Kirschner, "γ-Tubulin is a highly conserved component of the centrosome," *Cell*, vol. 65, (no. 5), pp. 825-836, 1991.

[5] C.D. Katsetos, G. Reddy, E. DrÃ¡berovÃ¡, B. Å mejkalovÃ¡, L. Del Valle, Q. Ashraf, A. Tadevosyan, K. Yelin, T. Maraziotis, and O.P. Mishra, "Altered cellular distribution and subcellular sorting of Î³-tubulin in diffuse astrocytic gliomas and human glioblastoma cell lines," *Journal of Neuropathology & Experimental Neurology*, vol. 65, (no. 5), pp. 465-477, 2006.

[6] H.M. Li Y, Sarkar SH, Eliason J, Li R, Sarkar FH., "Gene expression profiling revealed novel mechanism of action of Taxotere and Furtulon in prostate cancer cells.," *BMC Cancer*, vol. 5, 2005.

[7] T. Liu, Y. Niu, Y. Yu, Y. Liu, and F. Zhang, "Increased Î³-tubulin expression and P16INK4A promoter methylation occur together in preinvasive lesions and carcinomas of the breast," *Annals of oncology*, pp. mdn651, 2009.

[8] C. Montero-Conde, J.M. Martin-Campos, E. Lerma, G. Gimenez, J.L. Martinez-Guitarte, N. Combalia, D. Montaner, X. Matias-Guiu, J. Dopazo, and A. de Leiva, "Molecular profiling related to poor prognosis in thyroid carcinoma. Combining gene expression data and biological information," *Oncogene*, vol. 27, (no. 11), pp. 1554-1561, 2007.

[9] L.T. Niu Y, Tse GM, Sun B, Niu R, Li HM, Wang H, Yang Y, Ye X, Wang Y, Yu Q, Zhang F., "Increased expression of centrosomal a, g-tubulin in atypical ductal hyperplasia and carcinoma of the breast," *Cancer Science*, vol. 100, pp. 580–587, 2009.

[10] B.a. Orsetti, M.l. Nugoli, N. Cervera, L. Lasorsa, P. Chuchana, L. Ursule, C. Nguyen, R. Redon, S. du Manoir, and C. Rodriguez, "Genomic and expression profiling of chromosome 17 in breast cancer reveals complex patterns of alterations and novel candidate genes," *Cancer research*, vol. 64, (no. 18), pp. 6453-6460, 2004.

[11] O. Cala, M.-H.l.n. Remy, V.r. Guillet, A. Merdes, L. Mourey, A. Milon, and G. Czaplicki, "Virtual and Biophysical Screening Targeting the Î³-Tubulin Complexâ€"A New Target for the Inhibition of Microtubule Nucleation," *PloS one*, vol. 8, (no. 5), pp. e63908, 2013.

[12] H. Aldaz, L.M. Rice, T. Stearns, and D.A. Agard, "Insights into microtubule nucleation from the crystal structure of human Î³-tubulin," *Nature*, vol. 435, (no. 7041), pp. 523-527, 2005.

[13] G.M. Alushin, G.C. Lander, E.H. Kellogg, R. Zhang, D. Baker, and E. Nogales, "High-Resolution Microtubule Structures Reveal the Structural Transitions in Î±Î²-Tubulin upon GTP Hydrolysis," *Cell*, vol. 157, (no. 5), pp. 1117-1129, 2014.

[14] J. Lowe, H. Li, K.H. Downing, and E. Nogales, "Refined structure of Î±Î²-tubulin at 3.5 A resolution," *Journal of molecular biology*, vol. 313, (no. 5), pp. 1045-1057, 2001.

[15] R.B.G. Ravelli, B.t. Gigant, P.A. Curmi, I. Jourdain, S. Lachkar, A. Sobel, and M. Knossow, "Insight into tubulin regulation from a complex with colchicine and a stathmin-like domain," *Nature*, vol. 428, (no. 6979), pp. 198-202, 2004.

[16] D.E. Friesen, K.H. Barakat, V. Semenchenko, R. Perezâ€Pineiro, B.W. Fenske, J. Mane, D.S. Wishart, and J.A. Tuszynski, "Discovery of Small Molecule Inhibitors that Interact with Î³â€Tubulin," *Chemical biology & drug design*, vol. 79, (no. 5), pp. 639-652, 2012.

[17] K. Ye, Y. Ke, N. Keshava, J. Shanks, J.A. Kapp, R.R. Tekmal, J. Petros, and H.C. Joshi, "Opium alkaloid noscapine is an antitumor agent that arrests metaphase and induces apoptosis in dividing cells," *Proceedings of the National Academy of Sciences*, vol. 95, (no. 4), pp. 1601-1606, 1998.

[18] P.K. Naik, B.P. Chatterji, S.N. Vangapandu, R. Aneja, R. Chandra, S. Kanteveri, and H.C. Joshi, "Rational design, synthesis and biological evaluations of amino-noscapine: a high affinity tubulin-binding noscapinoid," *Journal of computer-aided molecular design*, vol. 25, (no. 5), pp. 443-454, 2011.

[19] J. Zhou, K. Gupta, J. Yao, K. Ye, D. Panda, P. Giannakakou, and H.C. Joshi, "Paclitaxel-resistant human ovarian cancer cells undergo c-Jun NH2-terminal kinase-mediated apoptosis in response to noscapine," *Journal of Biological Chemistry*, vol. 277, (no. 42), pp. 39777-39785, 2002.

[20] J. Zhou, D. Panda, J.W. Landen, L. Wilson, and H.C. Joshi, "Minor alteration of microtubule dynamics causes loss of tension across kinetochore pairs and activates the spindle checkpoint," *Journal of Biological Chemistry*, vol. 277, (no. 19), pp. 17200-17208, 2002.

[21] R. Aneja, S. Asress, N. Dhiman, A. Awasthi, P.C.G. Rida, S.K. Arora, J. Zhou, J.D. Glass, and H.C. Joshi, "Nonâ€toxic melanoma therapy by a novel tubulinâ€binding agent," *International Journal of Cancer*, vol. 126, (no. 1), pp. 256-265, 2010.

[22] A.D. Becke, “A new mixing of Hartreeâ€“Fock and local densityâ€functional theories,” *The Journal of Chemical Physics*, vol. 98, (no. 2), pp. 1372-1377, 1993.

[23] C. Lee, W. Yang, and R.G. Parr, “Development of the Colle-Salvetti correlation-energy formula into a functional of the electron density,” *Physical Review B*, vol. 37, (no. 2), pp. 785, 1988.

[24] J.S. Binkley, J.A. Pople, and W.J. Hehre, “Self-consistent molecular orbital methods. 21. Small split-valence basis sets for first-row elements,” *Journal of the American Chemical Society*, vol. 102, (no. 3), pp. 939-947, 1980.

[25] M.S. Gordon, J.S. Binkley, J.A. Pople, W.J. Pietro, and W.J. Hehre, “Self-consistent molecular-orbital methods. 22. Small split-valence basis sets for second-row elements,” *Journal of the American Chemical Society*, vol. 104, (no. 10), pp. 2797-2803, 1982.

[26] W.J. Pietro, M.M. Francl, W.J. Hehre, D.J. DeFrees, J.A. Pople, and J.S. Binkley, “Self-consistent molecular orbital methods. 24. Supplemented small split-valence basis sets for second-row elements,” *Journal of the American Chemical Society*, vol. 104, (no. 19), pp. 5039-5048, 1982.

[27] P.K. Naik, S. Santoshi, A. Rai, and H.C. Joshi, “Molecular modelling and competition binding study of Br-noscapine and colchicine provide insight into noscapinoidâ€“tubulin binding site,” *Journal of Molecular Graphics and Modelling*, vol. 29, (no. 7), pp. 947-955, 2011.

[28] R.A. Friesner, J.L. Banks, R.B. Murphy, T.A. Halgren, J.J. Klicic, D.T. Mainz, M.P. Repasky, E.H. Knoll, M. Shelley, and J.K. Perry, “Glide: a new approach for rapid, accurate docking and scoring. 1. Method and assessment of docking accuracy,” *Journal of medicinal chemistry*, vol. 47, (no. 7), pp. 1739-1749, 2004.

[29] T.A. Halgren, R.B. Murphy, R.A. Friesner, H.S. Beard, L.L. Frye, W.T. Pollard, and J.L. Banks, “Glide: a new approach for rapid, accurate docking and scoring. 2. Enrichment factors in database screening,” *Journal of medicinal chemistry*, vol. 47, (no. 7), pp. 1750-1759, 2004.

[30] J. Wang, W. Wang, P.A. Kollman, and D.A. Case, “Automatic atom type and bond type perception in molecular mechanical calculations,” *Journal of molecular graphics and modelling*, vol. 25, (no. 2), pp. 247-260, 2006.

[31] A. Jakalian, D.B. Jack, and C.I. Bayly, "Fast, efficient generation of high-quality atomic charges. AM1-BCC model: II. Parameterization and validation," *Journal of computational chemistry*, vol. 23, (no. 16), pp. 1623-1641, 2002.

[32] W.L. Jorgensen, J. Chandrasekhar, J.D. Madura, R.W. Impey, and M.L. Klein, "Comparison of simple potential functions for simulating liquid water," *The Journal of chemical physics*, vol. 79, (no. 2), pp. 926-935, 1983.

[33] P.A. Kollman, I. Massova, C. Reyes, B. Kuhn, S. Huo, L. Chong, M. Lee, T. Lee, Y. Duan, and W. Wang, "Calculating structures and free energies of complex molecules: combining molecular mechanics and continuum models," *Accounts of chemical research*, vol. 33, (no. 12), pp. 889-897, 2000.

[34] I. Massova and P.A. Kollman, "Combined molecular mechanical and continuum solvent approach (MM-PBSA/GBSA) to predict ligand binding," *Perspectives in Drug Discovery and Design*, vol. 18, (no. 1), pp. 113-135, 2000.

[35] D. Sitkoff, K.A. Sharp, and B. Honig, "Accurate calculation of hydration free energies using macroscopic solvent models," *The Journal of Physical Chemistry*, vol. 98, (no. 7), pp. 1978-1988, 1994.

CHAPTER 6

INTERACTIONS OF γ-TUBULIN WITH MICROTUBULES

Abstract

γ-tubulin is a small globular protein, found to be localised at the microtubule organizing centers which is the centrosome in most eukaryotes. It is experimentally observed to interact with the minus end of microtubules to facilitate the nucleation and organization of mitotic microtubules in dividing cells. The most well accepted hypothesis for the initiation of microtubule polymerization is that αβ-tubulin dimers add onto a γ-tubulin ring complex (γTuRC), in which adjacent γ-tubulin subunits bind to the underlying non-tubulin components of the γTuRC. This template thus determines the resulting microtubule lattice. In this study we use molecular modelling and molecular dynamics simulations, combined with computational MM-PBSA/MM-GBSA methods, to determine the extent of the atomic interaction of γ-tubulin (though one of its horizontal interface) with microtubules. We first prepared the molecular system comprising of γ-tubulin, microtubule represented by αβ-tubulin and GCP4 using protein-protein docking algorithm. We then MD simulated the complex to check its stability through 10 ns of simulation. We calculated the ensemble average of binding free energy of -110.86 kcal/mol by the MM-PBSA method and -120.42 kcal/mol by the MM-GBSA method. These highly favourable binding free energy values imply robust interaction of γ-tubulin with microtubules. Next we identified the hot spot amino acids that play key role in the interactions by computational alanine scanning mutagenesis and free energy decomposition per residue. Experimental mutagenesis validated these hot spot amino acids. The results from the experimental findings were consistent with the theoretical calculations and offer important insights on the mechanism of interaction between the γ-tubulin and microtubules.

6.1 Introduction

'Template model' of nucleation suggests that the γ-tubulins in the γTuRC function as a microtubule template, making lateral contacts with each other around the ring and longitudinal contacts with α-tubulin (minus end of the microtubule). *In vitro*, the γTuRC was shown to interact specifically with microtubule minus ends, at which it functions as a cap to prevent microtubule growth in the minus direction [1]. This was consistent with electron micrograph images showing closed structures at the ends of microtubules, whether nucleated by γTuRCs *in vitro* [1-3] or attached to MTOCs *in vivo* [4]. According to this model γ-tubulin directly interacts, via one of its longitudinal interfaces, with the GCP2, GCP3 or GCP4 and, via its other interface, with the α/β tubulin dimers (Figure 6.1).

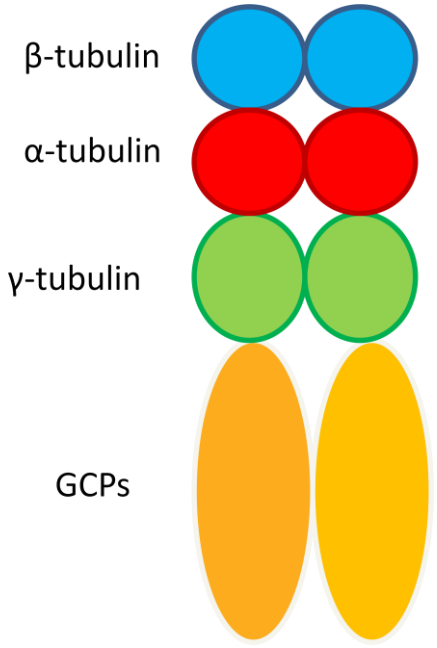

Fig 6.1: Schematic representation of MTOC components along with α/β-tubulin dimer. α, β and γ tubulins are represented as red, blue and green spheres, respectively. GCPs are represented as orange spheres.

A major advance toward the full understanding of γ-tubulin complexes was achieved by the determination of the crystal structure of monomeric human γ-tubulin bound to GTP and to GDP [5, 6] and more recently that of human GCP4 [7]. Also, recent 8 A^0 resolution electron density map of a tetramer sub-complex containing two hetero-dimers of γ-tubulin and GCP4 [7] is a very welcome and timely beginning in the precise understanding of the binding interfaces of γ-tubulin, on its interface with components of the γTuRC.

In this study we use the knowledge of known structures to first obtain a complex of γ with αβ-tubulin and GCP4 using protein-protein docking. We then MD simulated the resultant molecular system for 10 ns. Further binding free energy was calculated elucidate the strength of interaction of γ-tubulin with αβ-tubulin

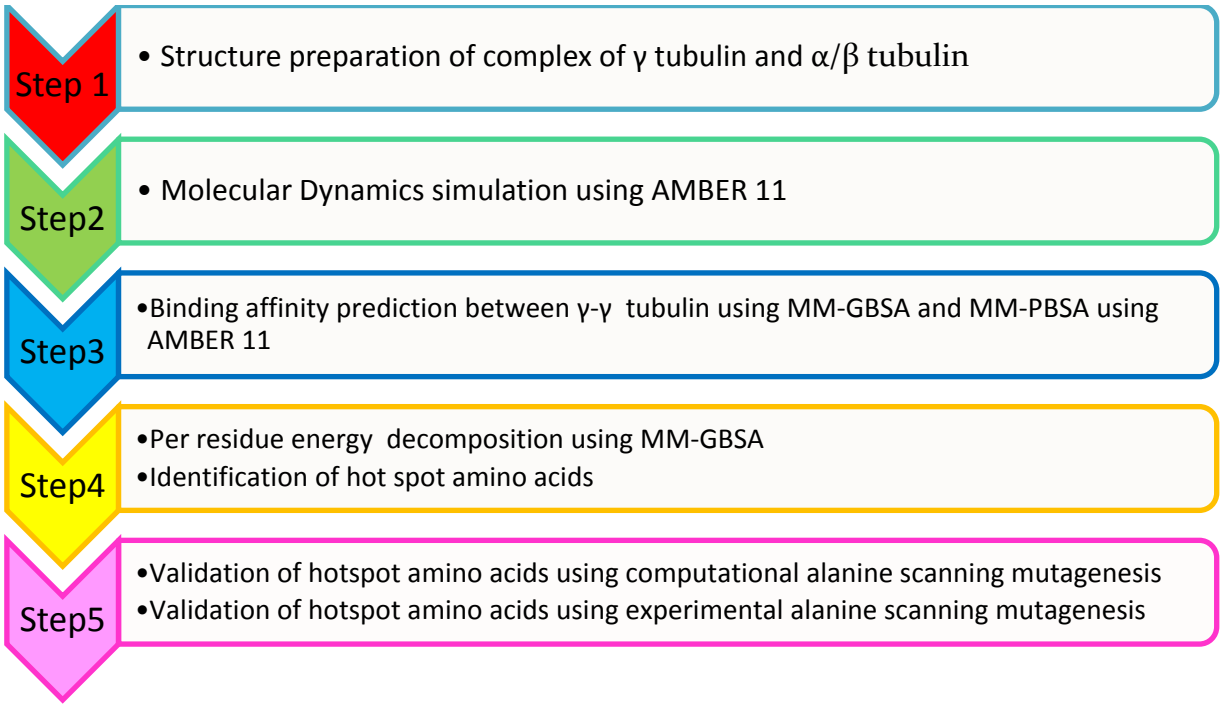

Figure 6.2 : Schematic representation of the overload methodology followed to study the molecular interaction between γ-tubulin and αβ-tubulin.

6.2 Materials and Methods

6.2.1 Molecular system

A pseudo atomic model of the αβ-tubulin tetramer was obtained from supplementary material provided by David B. Wells *et.al*. from University of Illinois, Urbana, Illinois while the coordinated of GCP4 and γ-tubulin tetramer was obtained from Georges Czaplicki, from the Universite´ de Toulouse, UPS, Toulouse, France (Figure 6.3). As γ-tubulin interacts with αβ-tubulin at the minus end, we deleted one of the β-tubulin to obtain the seam conformation. ince no crystal structure of the complete complex (comprising of αβ-tubulin, γ-tubulin and GCPs) is known, we followed a two step process that involved initial protein-protein docking using Zdock (version 2.3) followed by refinement of docked complex using Rdock. Zdock is

a rigid-body docking algorithm based on the principle of pair wise shape complementarity (PSC), electrostatic and desolvation parameters [9].

In step 2, the top scoring poses obtained from Zdock were energy minimized using CHARMM force field. The binding affinity ($\Delta G_{binding}$) between the protein complexes was predicted using Rdock scoring function which is the sum of desolvation and electrostatics contribution.

$$\Delta G_{binding} = \Delta G_{ACE} + \beta \text{ X } \Delta G_{elec}$$

where β is a scaling factor, a value of 0.9 was used in this study. The conformation with least RDock score was then selected for further molecular dynamics studies [10].

6.2.2 Molecular Dynamics Simulation

To further refine the structure, a small run of all atom Molecular Dynamics (MD) simulations was carried out for 1000 ps with a time step of 2 fs on the modelled structure using Gromacs package (Version 4.5.4) [11]. The simulations were set up with Amber99SB [12]force field, in a dodecahedron solvation box at a distance of 12Å from the periphery of the protein with TIP3P water molecules, using periodic boundary conditions [13]. Particle-Mesh-Ewald algorithm was employed to calculate the electrostatic interactions between atoms [14, 15]. The Lenard-Jones and electrostatic interaction cut-off were set at 1.0 nm distance. LINCS algorithm was used to constraint the bond lengths [16]. Prior to the 10 ns MD Simulation the molecular system was neutralized with 36 Na+ ions, energy relaxed using steepest descent algorithm for 1000 steps and then equilibrated for 1000 ps of MD run. An average structure was generated using the last 2000 frames from the total of 10,000 frames generated during MD simulation.

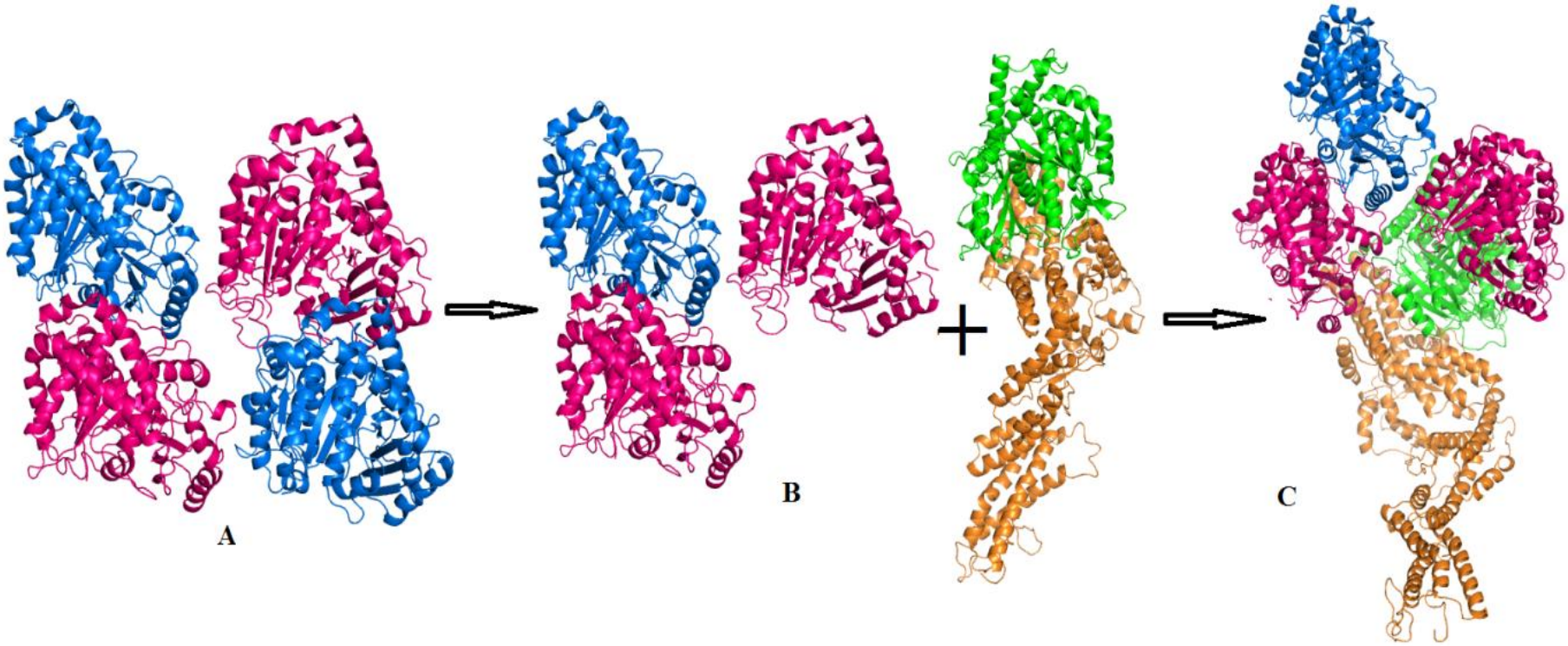

Figure 6.3: Preparation of molecular system. A: The coordinates of 'α/β tubulin tetramer obtained from David B. Wells *et.al*. from University of Illinois. B: Protein complexes for docking. C: The resulting docked complex obtained after Rdock. In the figure α-tubulin is shown as magenta cartoon, β-tubulin as blue cartoon, γ-tubulin as green cartoon and GCP4 as orange cartoon.

6.2.3 Calculation of binding free energy between γ-tubulin and microtubules

The average structure obtained after simulation in gromacs was first minimised, equilibrated for 500 ps followed by 5 ns MD simulation using Amber 11.0 and Ambertools 1.5 [17, 18], keeping the parameters same as described in chapter 2 for γ-tubulin dimer. Binding free energy calculations were carried out using the conventional MM-PBSA and MM-GBSA approaches using Amber 11 [19, 20]. A total of 200 snapshots were extracted, every 10 ps from the 5 ns of the MD trajectory. For each snapshot, the free energy was calculated for each molecular species (complex, protein and ligand). Conceptually the binding free energy can be calculated as :

$$\mathbf{\Delta G_{bind} = \Delta G_{complex} - [\Delta G_{Rec} + \Delta G_{lig}]}$$

$$\mathbf{G = E_{gas} + G_{sol} - TS.}$$

$$\mathbf{E_{gas} = E_{int} + E_{ele} + E_{vdw}}$$

$$\mathbf{G_{sol} = G_{PB(GB)} + G_{sol\text{-}np}}$$

$$\mathbf{G_{sol\text{-}np} = \gamma SAS}$$

Where, **G** is Gibbs free energy, $\mathbf{E_{gas}}$ is the gas phase energy calculated as the sum of internal energy ($\mathbf{E_{int}}$), energy generated as a result of the electrostatic interaction ($\mathbf{E_{ele}}$) and the van der Waals interaction ($\mathbf{E_{vdw}}$). G_{sol} is the solvation free energy calculated as the sum of polar ($\mathbf{G_{PB(GB)}}$) and nonpolar contributions ($\mathbf{G_{sol\text{-}np}}$). Polar interaction contribution ($\mathbf{G_{PB(GB)}}$) was calculated as the summation of electrostatic contribution ($\mathbf{E_{ele}}$) and polar solvation contribution ($\mathbf{G_{PB(GB)}}$). The nonpolar solvation contribution ($G_{sol\text{-}np}$) is approximated as linearly dependent on the solvent accessible surface area (SAS) and γ is the surface tension constant that was set to 0.0072 kcal mol^{-1} $Å^{-2}$ [21].

6.2.4 Per residue energy contribution

Energy decompostion method, implemented in Amber 11, was employed on the 200 frames extracted every 10 ps from 2 ns of simulation using the MM-GBSA method. The residues contributing more than -2 kcal/mol were considered very significant for the binding of GCP4 with γ-tubulin and these residues were designated as hot spot amino acids.

6.2.5 Computational Alanine Scanning Mutagenesis

To further study the energy contribution of these amino acids in the interaction of αβ-tubulin and γ-tubulin, computational alanine scanning was performed. In this method an amino acid of interest is replaced with alanine and absolute binding free energy is recalculated. For our study we also identified those amino acids which contributed significantly to the binding of αβ-tubulin and γ-tubulin and were flanked by two or more polar amino acids. Four such segments were identified as shown in figure 6.4. Corresponding to each segment, four mutant structures were prepared by mutating the polar amino acids in these stretches into alanine. Each of the four mutants were then MD simulated for 5 ns.

6.2.6 Experimental alanine scanning mutation and phenotypes

pALTER-EX1 vector (Promega, Madison, WI) was used to subclone *TUBG1* cDNA into the *NdeI* site downstream from the SP6 promoter to create pTWH101 as described by Hendrickson *et al*.[22]. Based on our findings from the molecular modelling methods, 4 stretches of polar amino acids were identified as shown in figure 6.4. The amino acids in each of the four stretches were mutated to alanine by oligonucleotide-directed mutagenesis using pTWH101 as the template. pALTER-EX1 contains a tetracycline resistance gene and an inactivated ampicillin resistance gene to obtain four mutants. The ampicillin-repair oligonucleotide restores the activity of the inactivated AmpR gene, and the tetracycline knockout oligonucleotide inactivates the TetR gene. This schema, i.e., inactivation of the TetR gene and the activation of the AmpR gene, provided a rapid method for selecting potential alanine-scanning mutants. Because contiguous alanine codons can be used to create a *PstI* site, we used *PstI* digestion to further screen for potential alanine-scanning mutants. We then verified the mutated sequences that represented the only differences between the mutant (*tubg1*) and the wild type (*TUBG1*).

The yeast expression plasmids were constructed by subcloning each of the *tubg1* alleles into pREP1 at the *NdeI* site downstream of the *nmt1+* promoter[23, 24]. Wildtype cells[25] were transformed with either one of the *tubg1*-pREP1 plasmids or the control *TUBG1*-pREP1 and grown in minimal media supplemented with adenine, histidine, and uracil. Transformants were screened at 18 and 36 °C to identify conditional mutants in the presence of endogenous γ-tubulin. The strains were maintained at 30 and 26 °C, respectively. A diploid strain, NC377[26, 27], bearing one endogenous wild-type copy of *S. pombe* γ-tubulin, *gtb1+* and one disrupted copy, *gtb1::ura4+*, was also transformed with the mutant

plasmids. The resulting yeast transformants were randomly sporulated and selected for *ura*+, *leu*+, and the spores were tested for conditional growth.

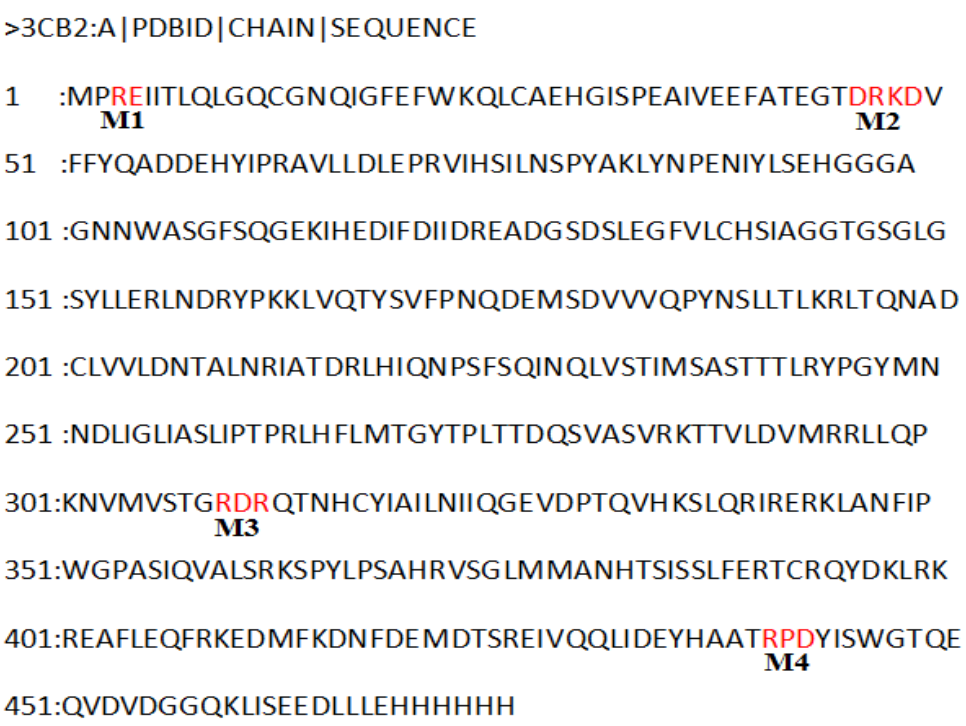

Figure 6.4: Amino acid stretches identified for alanine scanning mutagenesis. A total of seven stretched were identified on the basis of individual amino acid contribution and their participation interaction with α/β tubulin.

6.3 Results and discussions

6.3.1 Preparation of Molecular system

A total of 2,000 conformations, categorized into 100 clusters, were generated after Zdock. On the basis of Zdock score and visual inspection to rule out unfavourable conformations, 132 conformations were selected for Rdock. A total of 79 conformations were found to have favourable Rdock score of which the conformation with least energy was obtained for molecular dynamics (Figure 6.5).

After Rdock, the selected conformation was then simulated for 10 ns in Gromacs. Root mean square deviation (RMSD) analysis reveals a very stable structure throughout 10 ns of simulation (Figure 6.6). An average structure was obtained from the last 2 ns of simulation. The average structure was then minimised and checked for structure quality. The overall quality of the model obtained, stereo-chemical values and non-bonded interactions were tested using PROCHECK, ERRAT and VERIFY3D [28-

31]. The PROCHECK results showed 99.5 % of backbone angles are in allowed regions with G-factors of -0.25. Ramachandran plot analysis revealed only 0.5% residues in the generously allowed region and no residue in the disallowed region. ERRAT is an "overall quality factor" calculator program for non-bonded atomic interactions. The accepted range in ERRAT is 50 and higher scores indicate the precision of the model. For a structure with a resolution between 2.5Å–3Å, the average structure quality is 91%. For the minimized average structure the ERRAT score was 91.43% that is within the range of high quality model. Similarly, VERIFY3D Determines the compatibility of an atomic model (3D) with its own amino acid sequence (1D) by assigned a structural class based on its location and environment (alpha, beta, loop, polar, nonpolar etc) and comparing the results to good structures. The structure passed the VERIFY3D test which implies at least 80% of the amino acids scored >= 0.2 in the 3D/1D profile.

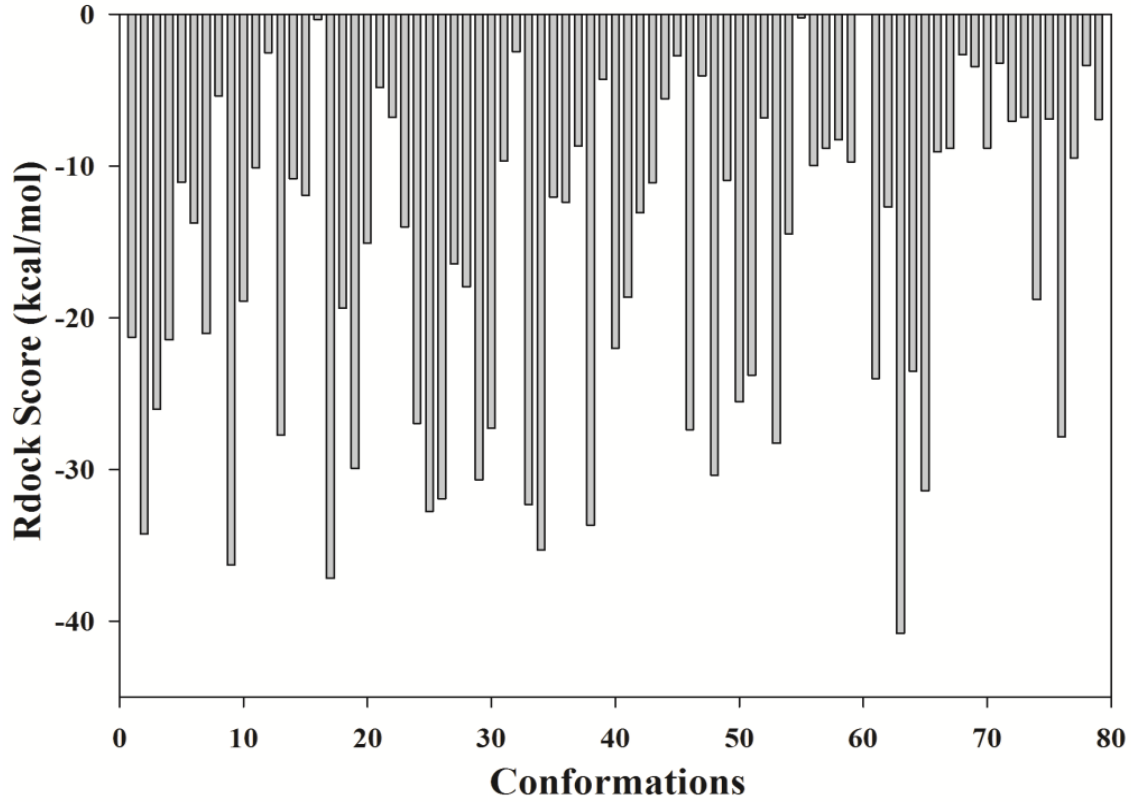

Figure 6.5: Comparison of $\Delta G_{binding}$ energy of different docking complexes between α/β tubulin and γ-tubulin calculated using Rdock.

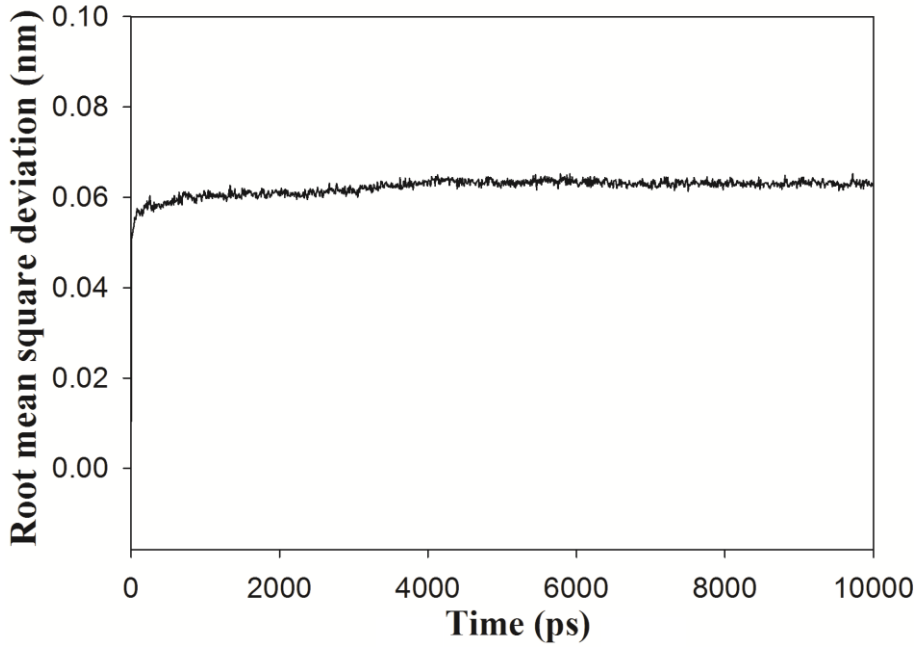

Figure 6.6: Root mean square deviation (RMSD) estimated over 10 ns. The RMSD was very stable around 0.06 nm throughout the simulation.

6.3.2 Molecular Dynamics Simulation

The minimized molecular system was again simulated using Amber11 for 5 ns. Mutant structures were prepared by mutating the identified polar amino acids (as indicated in figure 6.4) into alanine. All four mutants were also MD simulated in amber for 5 ns. Root mean square deviation analysis indicated that all complexes except Mutant 3 stabilized after 2 ns (Figure 6.7). Mutant 3 also showed stability after 3 ns. We also performed root mean square fluctuation (RMSF) of α-β-γ-tubulin complex and the mutants. RMSF of most of the residues was well below 4 Å and only two residues had RMSF > 6 (Figure 6.8). This indicates that the complexes were quite stable throughout the 5 ns simulation.

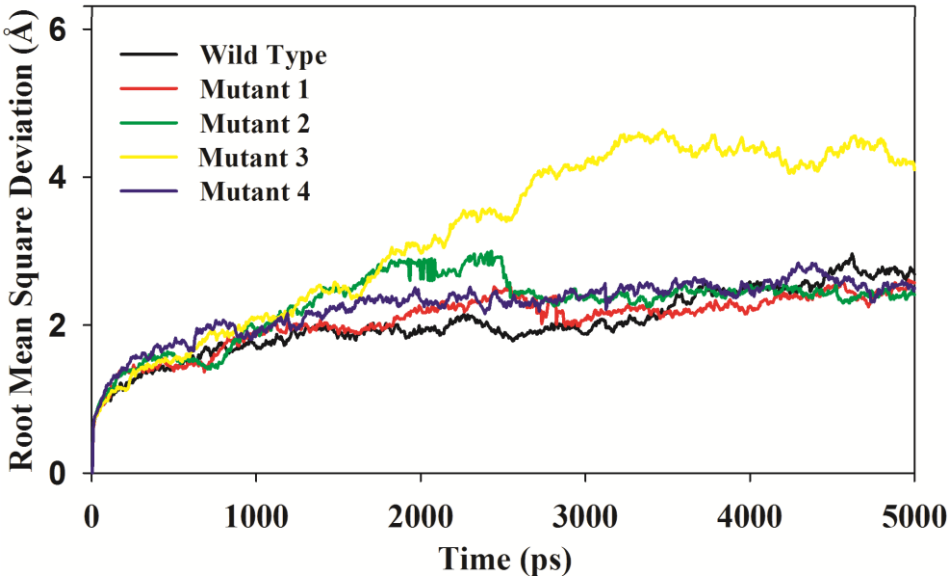

Figure 6.7: Root mean square deviation (RMSD) of α-β-γ-tubulin complex and the mutants estimated over 5 ns. The RMSD was very stable after the initial 2 ns.

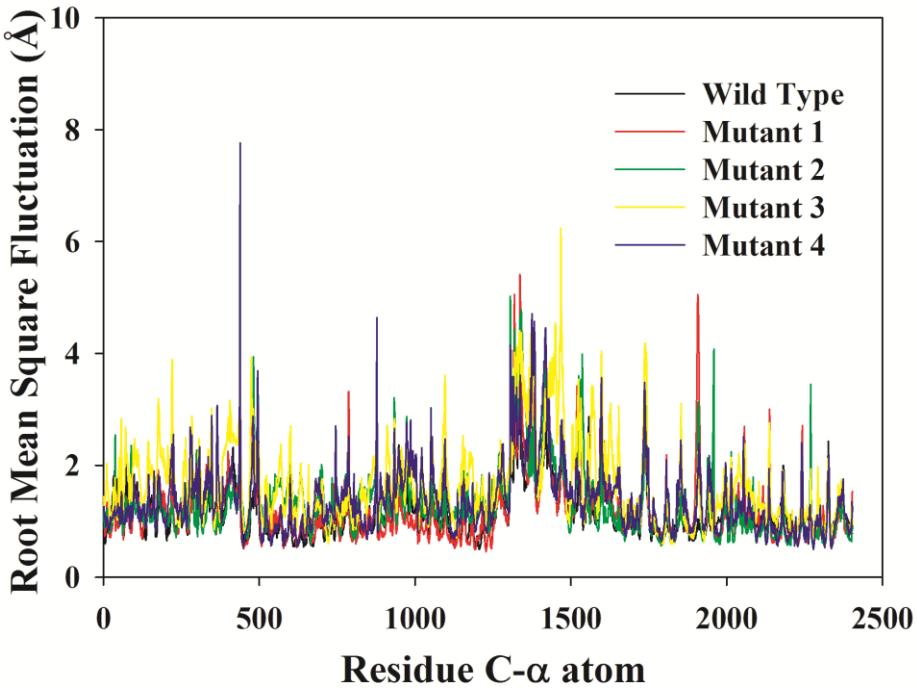

Figure 6.8: Root mean square fluctuation (RMSF) of α-β-γ-tubulin complex and the mutants estimated over 5 ns.

6.3.3 Calculation of binding free energy between γ-tubulin and microtubules

The calculation of binding free energy between the ligand and the complex of GCP4 and γ-tubulin was carried out on 200 frames, obtained every 10 ps from last 2 ns of simulation, using the MM-GBSA and MM-PBSA method. The results are summarized in table 6.1. The ensemble average of binding free energy using MM-

PBSA and MM-GBSA was determined as -110.86 kcal/mol and -120.42kcal/mol. The difference in the values obtained could be attributed to the calculated polar solvation energy which was -1863.37 kcal/mol obtained by MM-GBSA, higher than -1853.81 kcal/mol as obtained using MM-PBSA. All molecular interactions in polar solvent are guided by polar (the polar interaction, $\Delta G_{(ele,PB/GB)} = \Delta E_{ele} + \Delta G_{(PB/GB)}$) and non-polar energy components. The non polar component generally yields a more favourable contribution as compared to the polar component to the molecular interactions as the non-polar residues have the tendency to bury themselves in the hydrophobic pockets allowing the water in the binding site to displace [32]. As observed from Table 6.1, though the desolvation component ($\Delta G_{PB/GB}$) of -1821.50 kcal/mol and -1824.19 kcal/mol calculated by MM-PBSA and MM-GBSA method respectively, is highly favourable to binding, it cannot compensate the large penalty imposed by the Coulombic contributions ΔE_{ele} of 2027.56 kcal/mol. The non-polar components comprising of van der Waals interaction contribution (ΔE_{vdw}) and the non-polar solvation contribution (ΔG_{sol-np}) were estimated to be highly favourable with the values of -284.61 kcal/mol and -32.31 kcal/mol, respectively.

Table 6.1: Calculated binding free energy between α/β tubulin and γ-tubulin. Binding free energy calculated using MM-GBSA and MM-PBSA to ascertain the strength of interaction between α/β tubulin and γ-tubulin. The major energy components like van der Waals, electrostatic, polar solvation and non-polar solvation, contributing to the binding free energy were also estimated.

Contribution	Complex(kcal/mol)
ΔE_{INT}	0.00
ΔE_{VDW}	-284.61
ΔE_{ELE}	2027.56
ΔE_{GAS}	1742.95
ΔG_{PB}	-1821.50
ΔG_{SOL-NP}	-32.31
$\Delta G_{SOLV,PB}$	-1853.81
$\Delta G_{ELE,PB}$	206.06
$H_{TOT,PB}$	-110.86
G_{GB}	-1824.19
$G_{SOLV,GB}$	-1863.37
$G_{ELE\ GB}$	203.37
$H_{TOT,\ GB}$	-120.42

6.3.4 Per-residue energy decomposition

Energy contribution of each residue in the interface between α/β tubulin and γ-tubulin was calculated using the MM-GBSA method to investigate the details of protein-protein interactions at the atomic level (Figure 6.9). We identified 15 hotspot amino acids that have the highest impact (per residue contribution > 2 kcal/mol) on the α/β tubulin and γ-tubulin interaction interface (Table 6.2).

Table 6.2. Decomposition of calculated ΔGbind, GB (kcal/mol) on per residue basis into van der Waals, electrostatic, polar solvation and non-polar solvation energy components. A total of 15 residues with energy contribution of >-2kcal/mol were obtained. The table also includes amino acids with energy contribution > -1 kcal/mol.

Residue	$\Delta E_{i,vdw}$ (kcal/mol)	$\Delta E_{i,ele}$ (kcal/mol)	$\Delta G_{i,sol\ GB}$(kcal/mol)	$\Delta G_{i,sol\text{-}np}$ (kcal/mol)	$\Delta H_{i,tot,GB}$ (kcal/mol)
ARG211	-1.65	214.84	213.64	-0.46	-3.31
ASP215	-1.18	197.66	-197.92	-0.30	-1.74
ARG216	-1.23	250.77	240.94	-0.40	-11.46
HIE218	-5.96	-8.84	10.98	-0.90	-4.72
GLN220	-2.64	-8.92	10.72	-0.82	-1.66
THR276	-3.54	-1.29	2.94	-0.43	-2.32
THR277	-3.17	-1.70	3.92	-0.58	-1.52
ASP278	-1.81	191.34	-191.41	-0.16	-2.05
SER280	-0.52	-2.43	1.87	-0.28	-1.36
GLN298	-1.30	-9.85	9.39	-0.25	-2.01
PRO299	-1.87	-5.26	6.25	-0.24	-1.12
ARG308	-3.58	214.08	216.23	-0.41	-1.83
ARG310	-2.28	269.13	263.88	-0.56	-8.08
GLN311	-4.23	-2.91	5.94	-0.73	-1.93
THR312	-1.59	-0.89	1.25	-0.22	-1.45
ASN313	-0.55	-5.02	4.65	-0.14	-1.07
ARG340	-4.69	198.83	201.26	-0.77	-3.03
PHE347	-3.44	-1.30	0.44	-0.37	-4.68
PRO349	-3.43	-1.92	2.60	-0.48	-3.25
TRP350	-1.31	-1.89	1.67	-0.08	-1.61
PRO352	-2.98	-3.10	3.77	-0.43	-2.73
ALA353	-1.67	-3.49	3.71	-0.28	-1.74
ILE355	-1.17	-0.35	0.46	-0.14	-1.20
ARG389	-0.60	-217.28	212.97	-0.31	-5.22
PRO440	-3.45	-4.69	5.66	-0.58	-3.05
SER444	-1.90	-7.06	7.01	-0.48	-2.44
TRP445	-2.49	161.26	-164.68	-0.60	-6.51

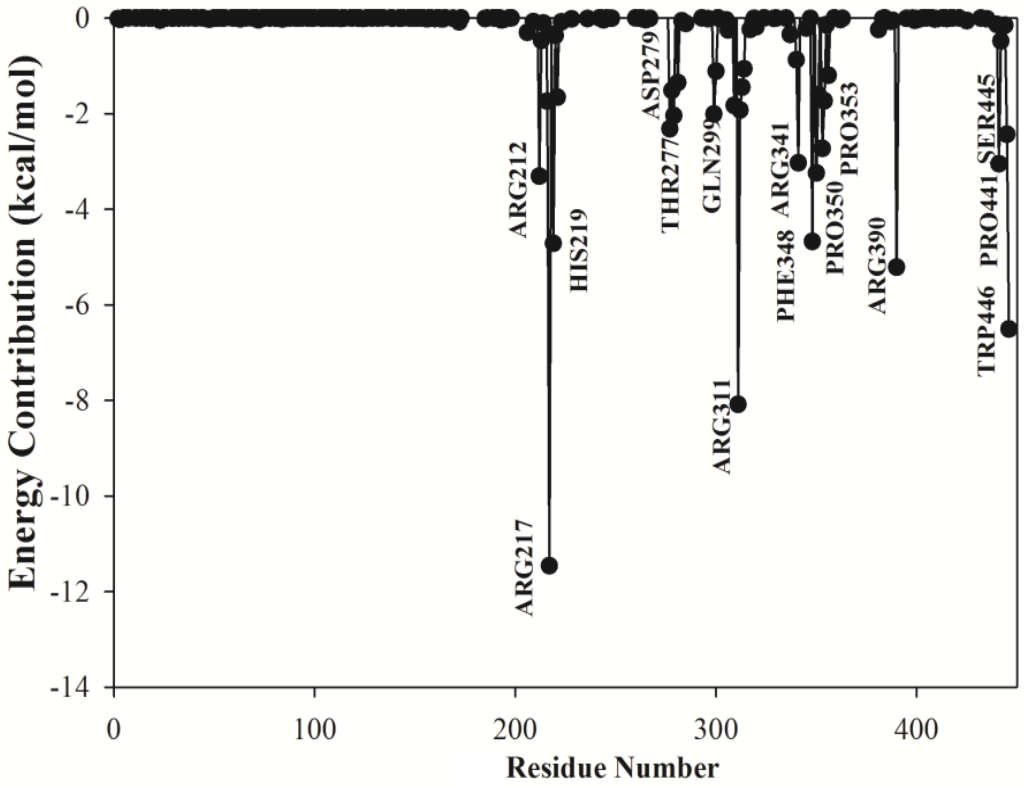

Figure 6.9: **Per residue free energy contribution of residues in the binding process of GCP4 and γ-tubulin.** Free energy contribution of each residue on the surface between α/β tubulin and γ-tubulin calculated based on MM-GBSA. Only the residues contributing free energy of > -2 kcal/mol (designated as hotspot amino acids) are labelled in the figure.

Table 6.3: Ensemble average of binding free energy (kcal/mol) of γ-γ tubulin complex calculated using the MM-GBSA and MM-PBSA methods in Amber

Complex	MM-GBSA (kcal/mol)	MM-PBSA (kcal/mol)
Wild Type	-120.49	-110.86
Mutant 1	-96.51	-65.25
Mutant 2	-90.90	-76.32
Mutant 3	-123.02	-119.95
Mutant 4	-79.24	-82.11

6.3.5 Computational alanine scanning mutagenesis

Each of the prepared mutant was MD simulated in Amber for 5 ns (Figure 6.7). This was followed by calculation of binding free energy (Table 6.3). We observed that except for Mutant 3, there was very significant drop in the calculated binding affinities for Mutant 1, Mutant 2 and Mutant and Mutant 4, using both MM-PBSA and MM-GBSA methods.

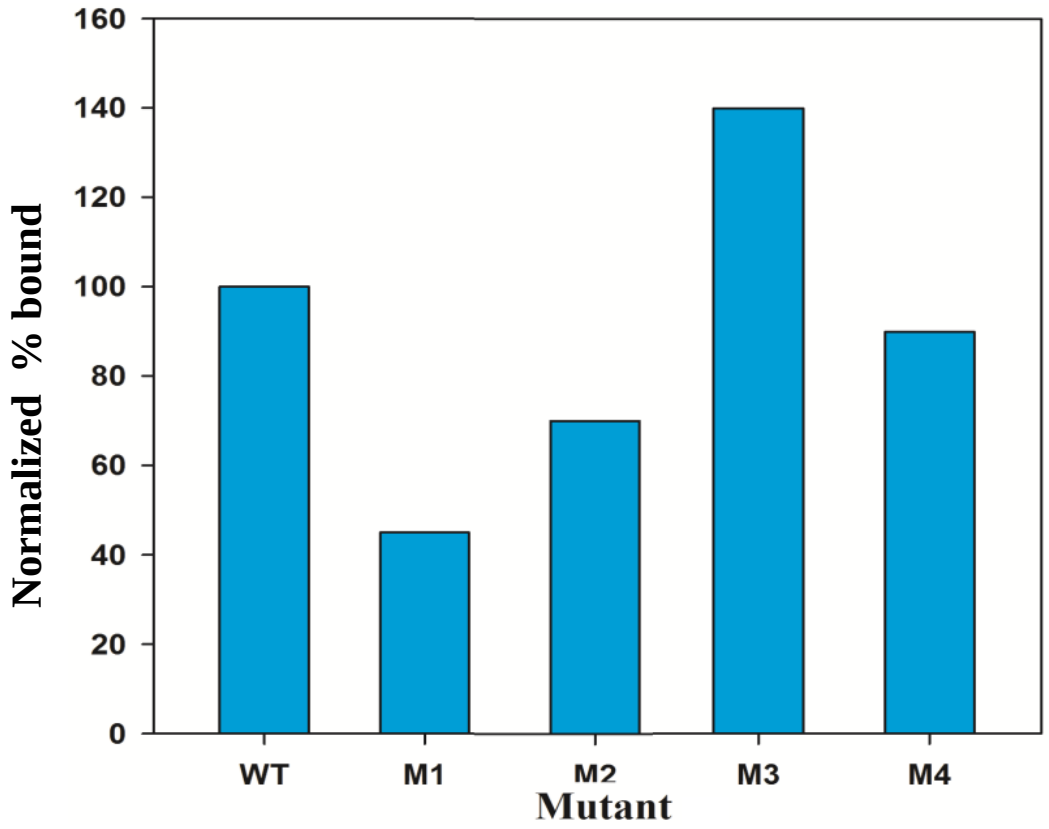

Figure 6.10 : Normalized % bound of αβ-tubulin with γ-tubulin.

6.3.6 Growth of alanine scanning mutant in fission yeast and its phenotype

Since we wished to verify the hot spot amino acids in order to identify evolutionarily conserved features of γ-tubulin, we took advantage of the fact that the human γ-tubulin gene (*TUBG1*) can replace the fission yeast γ-tubulin (*gtb1*). Using alanine-scanning mutagenesis a series of four mutants of γ-tubulin, as described in figure 6.4, which targeted key residues predicted to be involved in protein-protein interactions, were generated. To test the effect of the alanine substitution on protein function haploid yeast cells, wild-type and *gtb1*-, were transformed with the alanine mutants. Wild-type *TUBG1* transformants served as controls. Radiolabeled γ-tubulin was synthesied in vitro using TnT® Coupled Reticulocyte Lysate System (Promega Corp., Madison WI). The radiolabeled γ-tubulin was then purified using Myc antibody. Finally, *In vitro* microtubule binding assay was performed as described by Li and Joshi (1995) with γ-tubulin and its mutant proteins [33]. The % bound of Wild Type was normalized to 100% (Figure 6.10). The % bound of Mutant 1 (M1), Mutant 2 (M2) and Mutant 4 (M4) was less than the Wild type while that of Mutant 3 (M3) was more than the Wild Type. These experimental results corroborate with the computation alanine scanning data.

Conclusion

The binding interface of γ-tubulin with α/β tubulin was identified using molecular modeling calculations. Residues playing crucial role in the interaction were also identified as hot spot amino acids. To further reinforce the hot spots, computational alanine scanning mutagenesis was performed. The results were further verified using the experimental alanine scanning mutagenesis. For three of the mutants- M, M2 and M4 the binding affinity was lesser as compared to the wild type as observed after MM-GBSA analysis (Figure 6.10). Computationally identified interface was well verified by the experimental results.

REFERENCES

[1] C. Wiese and Y. Zheng, "A new function for the γ-tubulin ring complex as a microtubule minus-end cap," *Nature cell biology*, vol. 2, (no. 6), pp. 358-364, 2000.

[2] M. Moritz, M.B. Braunfeld, V. GuÃ©nebaut, J. Heuser, and D.A. Agard, "Structure of the &ggr;-tubulin ring complex: a template for microtubule nucleation," *Nature cell biology*, vol. 2, (no. 6), pp. 365-370, 2000.

[3] T.J. Keating and G.G. Borisy, "Immunostructural evidence for the template mechanism of microtubule nucleation," *Nature cell biology*, vol. 2, (no. 6), pp. 352-357, 2000.

[4] B. Byers, K. Shriver, and L. Goetsch, "The role of spindle pole bodies and modified microtubule ends in the initiation of microtubule assembly in Saccharomyces cerevisiae," *Journal of cell science*, vol. 30, (no. 1), pp. 331-352, 1978.

[5] L.M. Rice, E.A. Montabana, and D.A. Agard, "The lattice as allosteric effector: Structural studies of α/β and γ-tubulin clarify the role of GTP in microtubule assembly," *Proceedings of the National Academy of Sciences*, vol. 105, (no. 14), pp. 5378-5383, 2008.

[6] H. Aldaz, L.M. Rice, T. Stearns, and D.A. Agard, "Insights into microtubule nucleation from the crystal structure of human Î³-tubulin," *Nature*, vol. 435, (no. 7041), pp. 523-527, 2005.

[7] J.M. Kollman, J.K. Polka, A. Zelter, T.N. Davis, and D.A. Agard, "Microtubule nucleating [γ]-TuSC assembles structures with 13-fold microtubule-like symmetry," *Nature*, vol. 466, (no. 7308), pp. 879-882, 2010.

[8] O. Cala, M.-H.l.n. Remy, V.r. Guillet, A. Merdes, L. Mourey, A. Milon, and G. Czaplicki, "Virtual and Biophysical Screening Targeting the γ-Tubulin Complexes "A New Target for the Inhibition of Microtubule Nucleation," *PloS one*, vol. 8, (no. 5), pp. e63908, 2013.

[9] R. Chen, L. Li, and Z. Weng, "ZDOCK: an initialâ€stage proteinâ€docking algorithm," *Proteins: Structure, Function, and Bioinformatics*, vol. 52, (no. 1), pp. 80-87, 2003.

[10] L. Li, R. Chen, and Z. Weng, "RDOCK: Refinement of rigidâ€body protein docking predictions," *Proteins: Structure, Function, and Bioinformatics*, vol. 53, (no. 3), pp. 693-707, 2003.

[11] B. Hess, C. Kutzner, D. Van Der Spoel, and E. Lindahl, "GROMACS 4: Algorithms for highly efficient, load-balanced, and scalable molecular simulation," *Journal of chemical theory and computation*, vol. 4, (no. 3), pp. 435-447, 2008.

[12] W.D. Cornell, P. Cieplak, C.I. Bayly, I.R. Gould, K.M. Merz, D.M. Ferguson, D.C. Spellmeyer, T. Fox, J.W. Caldwell, and P.A. Kollman, "A second generation force field for the simulation of proteins, nucleic acids, and organic molecules," *Journal of the American Chemical Society*, vol. 117, (no. 19), pp. 5179-5197, 1995.

[13] H. Berendsen, J. Postma, W. Van Gunsteren, and J. Hermans, "Intermolecular Forces, ed," *B. Pullman, Reidel, Dordrecht*, vol. 331, 1981.

[14] T. Darden, D. York, and L. Pedersen, "Particle mesh Ewald: An N· log (N) method for Ewald sums in large systems," *The Journal of chemical physics*, vol. 98, (no. 12), pp. 10089-10092, 1993.

[15] U. Essmann, L. Perera, M.L. Berkowitz, T. Darden, H. Lee, and L.G. Pedersen, "A smooth particle mesh Ewald method," *The Journal of Chemical Physics*, vol. 103, (no. 19), pp. 8577-8593, 1995.

[16] J.-P. Ryckaert, G. Ciccotti, and H.J. Berendsen, "Numerical integration of the cartesian equations of motion of a system with constraints: molecular dynamics of< i> n</i>-alkanes," *Journal of Computational Physics*, vol. 23, (no. 3), pp. 327-341, 1977.

[17] D.A. Case, T.E. Cheatham, T. Darden, H. Gohlke, R. Luo, K.M. Merz, A. Onufriev, C. Simmerling, B. Wang, and R.J. Woods, "The Amber biomolecular simulation programs," *Journal of computational chemistry*, vol. 26, (no. 16), pp. 1668-1688, 2005.

[18] D.A. Pearlman, D.A. Case, J.W. Caldwell, W.S. Ross, T.E. Cheatham III, S. DeBolt, D. Ferguson, G. Seibel, and P. Kollman, "AMBER, a package of computer programs for applying molecular mechanics, normal mode analysis, molecular dynamics and free energy calculations to simulate the structural and energetic properties of molecules," *Computer Physics Communications*, vol. 91, (no. 1), pp. 1-41, 1995.

[19] P.A. Kollman, I. Massova, C. Reyes, B. Kuhn, S. Huo, L. Chong, M. Lee, T. Lee, Y. Duan, and W. Wang, "Calculating structures and free energies of complex molecules: combining molecular mechanics and continuum models," *Accounts of chemical research*, vol. 33, (no. 12), pp. 889-897, 2000.

[20] I. Massova and P.A. Kollman, "Combined molecular mechanical and continuum solvent approach (MM-PBSA/GBSA) to predict ligand binding," *Perspectives in Drug Discovery and Design*, vol. 18, (no. 1), pp. 113-135, 2000.

[21] D. Sitkoff, K.A. Sharp, and B. Honig, "Accurate calculation of hydration free energies using macroscopic solvent models," *The Journal of Physical Chemistry*, vol. 98, (no. 7), pp. 1978-1988, 1994.

[22] T.W. Hendrickson, J. Yao, S. Bhadury, A.H. Corbett, and H.C. Joshi, "Conditional mutations in γ-tubulin reveal its involvement in chromosome segregation and cytokinesis," *Molecular biology of the cell*, vol. 12, (no. 8), pp. 2469-2481, 2001.

[23] K. Maundrell, "nmt1 of fission yeast. A highly transcribed gene completely repressed by thiamine," *Journal of Biological Chemistry*, vol. 265, (no. 19), pp. 10857-10864, 1990.

[24] K. Maundrell, "Thiamine-repressible expression vectors pREP and pRIP for fission yeast," *Gene*, vol. 123, (no. 1), pp. 127-130, 1993.

[25] J. Paluh and D. Clayton, "A functional dominant mutation in Schizosaccharomyces pombe RNase MRP RNA affects nuclear RNA processing and requires the mitochondrial-associated nuclear mutation ptp1-1 for viability," *The EMBO journal*, vol. 15, (no. 17), pp. 4723, 1996.

[26] T. Horio, S. Uzawa, M.K. Jung, B.R. Oakley, K. Tanaka, and M. Yanagida, "The fission yeast gamma-tubulin is essential for mitosis and is localized at microtubule organizing centers," *Journal of cell science*, vol. 99, (no. 4), pp. 693-700, 1991.

[27] T. Horio and B.R. Oakley, "Human gamma-tubulin functions in fission yeast," *The Journal of cell biology*, vol. 126, (no. 6), pp. 1465-1473, 1994.

[28] R.A. Laskowski, M.W. MacArthur, D.S. Moss, and J.M. Thornton, "PROCHECK: a program to check the stereochemical quality of protein structures," *Journal of applied crystallography*, vol. 26, (no. 2), pp. 283-291, 1993.

[29] G. Ramachandran, C.t. Ramakrishnan, and V. Sasisekharan, "Stereochemistry of polypeptide chain configurations," *Journal of molecular biology*, vol. 7, (no. 1), pp. 95-99, 1963.

[30] C. Colovos and T.O. Yeates, "Verification of protein structures: patterns of nonbonded atomic interactions," *Protein Science*, vol. 2, (no. 9), pp. 1511-1519, 1993.

[31] D. Eisenberg, R. Lüthy, and J.U. Bowie, "VERIFY3D: assessment of protein models with three-dimensional profiles," *Methods in enzymology*, vol. 277, pp. 396, 1997.

[32] C.J. Tsai and R. Nussinov, "Hydrophobic folding units at protein-protein interfaces: Implications to protein folding and to protein-protein association," *Protein Science*, vol. 6, (no. 7), pp. 1426-1437, 1997.

[33] Q. Li and H.C. Joshi, "gamma-tubulin is a minus end-specific microtubule binding protein," *The Journal of cell biology*, vol. 131, (no. 1), pp. 207-214, 1995.

CONCLUSION AND FUTURE DIRECTION

Microtubule nucleation and organization is thought to be guided by γ-tubulin containing protein complexes at the microtubule organization center (MTOC). It was found to be part of a ~2.2 MDa complex with at least six other proteins: γ-tubulin complex protein 2 (GCP2), GCP3, GCP4, GCP5, GCP6 and NEDD1, which presented as a striking ring shaped complex in electron micrographs. This complex was called γ-tubulin ring complex (γTuRC). The γTuRC dissociates under high salt conditions to yield a stable 300 kDa subcomplex of γ-tubulin associated with GCP2 and GCP3, which is dubbed the γ-tubulin small complex (γTuSC). The most widely accepted model for the mechanism of γTuRC-based nucleation, the 'template model', suggests that the γTuRC acts as a template, presenting a ring of γ-tubulins that make longitudinal contacts with α-tubulin–β-tubulin (αβ-tubulin) at one of the horizontal interface. At the other interface, γ-tubulin interacts directly with the GCP2, GCP3 and GCP4. These interactions make γ-tubulin a key player in the process of nucleation. Therefore we undertook a computational study to understand the interaction of γ-tubulin with the other components of the MTOC and microtubules by using molecular modelling, molecular dynamic simulation and binding affinity analysis.

We first elucidated the protein-protein interactions of γ-tubulin with adjacent γ-tubulin. In this endeavour, we found out the predicted binding affinity between two adjacent γ-tubulin proteins using both MM-PBSA and MM-GBSA methods. We also found the amino acids that contributed most to the stability of GCP4 and γ-tubulin complex. The hot spot amino acids were further verified based on alanine scanning mutagenesis using both experimental and computational methods. The experimental results were well in cognizance with the computational results. We then used molecular modelling and MD simulations, combined with MM-PBSA and MM-GBSA computational methods to understand atomic interactions between γ-tubulin and GCP4. We simulated two conformations of γ-tubulin-GCP4 complex for 10 ns and calculated the binding free energy of -172.7 kcal/mol and -188.5 kcal/mol using MM-PBSA and MM-GBSA method respectively, for dimer1 and -124.6 kcal/mol and -93.58 kcal/mol by MM-PBSA and MM-GBSA methods for dimer 2. These values points to very robust interactions between GCP4 and γ-tubulin. We also identified amino acids crucial for the interaction of γ-tubulin with GCP4, called hot spots, by computational alanine-scanning mutagenesis. In future, it would be very significant to carry

out experimental alanine scanning mutagenesis to further verify our findings. Next we explored the interaction between γ-tubulin and microtubules. We first obtained a molecular system consisting of γ-tubulin, αβ-tubulin and GCP4 using protein-protein docking. We simulated the molecular system for 10 ns and followed it up with binding affinity analysis using MM-GBSA and MM-PBSA approach. We identified the hot spot amino acids which were deemed most critical to the binding of γ-tubulin with the microtubules. These hot spot amino acids were then verified by means of alanine scanning mutagenesis using both experimental as well as the computational methods.

γ-tubulin is known to be absolutely indispensible for the proper nucleation of microtubules. Also, recent studies indicated over-expression of γ-tubulin in many cancer types like pre-invasive lesions, carcinomas of breast and glioblastomas. Moreover, γ-tubulin shows significant structure similarity with β-tubulin as compared with the α-tubulin. Several drugs such as paclitaxel derivatives and vinca alkaloids are now routinely used in chemotherapy of cancer, affecting dynamics of microtubules and thus provoking errors in mitotic spindle assembly and ultimately cause apoptosis. The targets of these inhibitors are α- and β- tubulin. In contrast, so far no chemotherapeutic agents have been developed against γ-tubulin or against any of its associated γ-tubulin complex proteins. Further, the advances in the crystal structures of alpha- beta- and gamma-tubulins yielded a realization that the overall structure of γ-tubulin was more similar to β-tubulin subunit than it is to the α-tubulin subunit. And of the α and β tubulins, β-tubulin has very well characterized drug binding cavities, one straight approach for the future is to explore how well these drug binding cavities are conserved in γ-tubulin structure and whether they can be used to identify additional potential lead compounds that can bind onto them.

In this direction we therefore made an attempt to identify chemical compounds which can disrupt the binding between adjacent γ-tubulins and between γ-tubulin and GCP4. We performed docking studies on γ-tubulin dimer with a promising new class of compounds called noscapinoids which include natural compound called noscapine and two of its derivatives, amino–noscapine and bromo-noscapine. All three ligands showed stable interaction throughout the simulations however, the best binding affinity was calculated for bromo-noscapine. The binding modes of noscapine and bromo-noscapine are quite similar with both the drugs showing strong interaction with Tyr248, Met249, Asn250 of γ-tubulin. Multiple sequence alignment analysis showed the amino acid residues which interact with

noscapinoids were observed to lie in the highly conserved regions. Therefore, if these drugs can interfere with a subset of the hot spot amino acids they might be able to perturb some of the interactions between γ-tubulin units in the γTuRC and further destabilize the γTuRC. Nevertheless, our results offer noscapinoids an important possible chemical framework for the further design of more potent compounds.

We further reported that noscapinoids might fits well in a cavity close to γ-tubulin-GCP4 interface. All noscapinoids displayed stable interaction throughout simulation, however, most robust interaction was observed for bromo-noscapine followed by noscapine and amino-noscapine with binding free energy of -46.73 kcal/mol, -41.69 kcal/mol and -35.40 kcal/mol respectively, using the MM-GBSA method and -31.86 kcal/mol, -23.60 kcal/mol and -20.50 kcal/mol respectively, using the MM-PBSA method with dimer1 of γ-tubulin-GCP4 complex. Similarly with dimer2 of γ-tubulin-GCP4 complex the most robust interaction was observed for bromo-noscapine with the binding affinity of -40 kcal/mol followed by noscapine with -32.82 kcal/mol and -21.84 kcal/mol for amino-noscapine, using MM-GBSA method. This offers a novel chemical scaffold for γ-tubulin binding drugs near γ-tubulin-GCP4 interface.

Since co-crystallization of noscapinoid-γ-tubulin complex has not been successful so far it would worthwhile to try co-crystallization of γ-tubulin with noscapine and its derivatives in order to further explore γ-tubulin as potential anticancer drug target.

LIST OF PUBLICATIONS

1. **Charu Suri,** Triscia W. Hendrickson, Harish C. Joshi, and Pradeep Kumar Naik (2014). "Molecular insight into γ–γ tubulin lateral interactions within the γ-tubulin ring complex (γ-TuRC)." *Journal of computer-aided molecular design*. 1-12**.** [ISSN: 0920-654**X, IF: 3.172]**

2. **Charu Suri,** Harish C. Joshi, and Pradeep Kumar Naik (2014). Molecular modelling reveals binding interface of γ-tubulin with GCP4 and interactions with noscapinoids. *PROTEINS: Structure, Function, and Bioinformatics.* (*Under review*, **IF**: **2.921**)

CONFERENCE PRESENTATIONS

1. **Charu Suri** and Pradeep K. Naik. Refinement of low resolution X-ray crystallographic protein structure utilizing molecular mechanics and molecular dynamics simulation techniques. **Presented** in International conference on "biotechnology advances :omics approaches and way forward (ICBA-2012)"organized by centre of biotechnology (supported by DST-FIST, govt. of India) Siksha 'o' Anusandhan University, Bhubaneswar 20 -22 December, 2012.)